Dynamical Climatology

A 2 × CO_2 climate sensitivity experiment with a global climate model including a simple ocean.

by

C.A. Wilson and J.F.B. Mitchell

DCTN 48

February 1987

Meteorological Office (Met. O. 20)
London Road
Bracknell
Berkshire RG12 2SZ

DYNAMICAL CLIMATOLOGY TECHNICAL NOTE NO. 48

A 2 x CO2 CLIMATE SENSITIVITY EXPERIMENT WITH A GLOBAL CLIMATE MODEL INCLUDING A SIMPLE OCEAN

by

C A Wilson and J F B Mitchell

Submitted for publication in J. Geophys. Res.

Met O 20 (Dynamical
Climatology Branch)
Meteorological Office
London Road
Bracknell
Berkshire, U.K. RG12 2SZ

Note: This paper has not been published. Permission to quote from it should be obtained from the Assistant Director of the above Meteorological Office Branch.

LF/M020

A 2 x CO_2 CLIMATE SENSITIVITY EXPERIMENT WITH A GLOBAL CLIMATE MODEL INCLUDING A SIMPLE OCEAN

BY

C A WILSON and J F B MITCHELL

Abstract

The sensitivity of a global climate model to increased atmospheric CO_2 concentrations is presented, assessed and compared with earlier studies. The ocean is represented by a 50 m slab in which the heat convergence due to oceanic dynamics is prescribed, producing an accurate simulation of sea surface temperatures, sea-ice extents and associated features in the control simulation. Changes in surface temperature are qualitatively similar to those found in earlier studies using models with similar or lower horizontal resolution. The simulated changes in hydrology agree broadly with those in studies made with higher horizontal resolution and prescribed changes in sea surface temperatures, and include a drying over the northern mid-latitude continents. Many of the discrepancies in the responses of different models can be traced to differences in the simulations of present day climate. The choice of convective parametrization appears to influence the sensitivity of the simulated response in the tropics.

A 2 x CO_2 CLIMATE SENSITIVITY EXPERIMENT WITH A GLOBAL CLIMATE MODEL INCLUDING A SIMPLE OCEAN

by

C A Wilson and J F B Mitchell

1. Introduction

Over the last 27 years, concentrations of atmospheric carbon dioxide levels have increased by 8%, and there is evidence that concentrations have risen by 15 to 30% since 1860 (Reichle et al, 1985). There is speculation that CO_2 levels could reach 550 ppm (about twice the estimated pre-industrial level) by the end of the 21st century (Trabalka et al, 1985). Evidence from numerical models suggests that enhanced CO_2 concentrations would lead to significant changes in climate (see for example, Schlesinger and Mitchell, 1985) with potential economic and human consequences.

The investigations of the sensitivity of climate to enhanced carbon dioxide concentrations have produced a variety of estimates of the magnitude and distribution of the expected response (Schlesinger and Mitchell 1985). The calculated global mean surface warming due to doubling carbon dioxide concentrations ranges from about 1.5 to 4.5°C, the higher values occurring in recent simulations with model generated cloud (Schlesinger and Mitchell, 1985; Wetherald and Manabe 1986). Whereas there is some qualitative agreement amongst existing studies on the more detailed aspects of the response, including enhanced warming and precipitation in high latitudes in winter, and a general reduction in upper tropospheric cloud, there are also marked disagreements. For example, Washington and

Meehl (1984) report a general increase in soil moisture in northern and mid-latitudes in summer, whereas studies carried out by Manabe and colleagues (eg Manabe and Wetherald, 1986) and Mitchell (1986) suggest that decreases in soil moisture are more likely.

Schlesinger and Mitchell (1985) show large discrepancies in the simulation of present day climate in three contemporary climate models from different institutions. The response of a model to small perturbations will depend strongly on the simulation of the unperturbed climate, (Spelman and Manabe, 1984; Palmer and Mansfield, 1986; Mitchell et al 1987). Hence a necessary condition for the reliable numerical prediction of climate change is that the models' control simulation is realistic.

Most studies to date have employed a simple representation of the ocean, calculating sea surface temperatures without allowing for oceanic heat transport. On the other hand, Mitchell (1983) and Mitchell and Lupton (1984) used an alternative method. Sea surface temperatures in the control simulation were specified from climatological data, thereby implicitly including the effects of oceanic advection. The changes in sea surface temperature in the anomaly (enhanced CO_2) simulations were then determined to an increasing degree of accuracy in a series of perturbation experiments by assuming that for small perturbations, the changes in surface heating are related linearly to the local changes in sea surface temperature. Whereas in the more usual approach, 10 to 20 years of simulation are required to bring the ocean and atmosphere to equilibrium, the atmosphere equilibrates within a year when the sea surface temperatures are prescribed. Hence Mitchell and his co-workers were able to use higher

horizontal resolution than in other studies, without needing extra computing resources. However, with this approach there is no obvious method of estimating the changes in sea-ice extent, and in high latitudes, non-local effects become imiportant (see Mitchell and Lupton, 1984).

Hansen et al (1984) prescribed the oceanic heat convergence (and mixed layer depth) in a low resolution study of the effect of changes in the solar constant and enhanced CO_2 concentrations. In this paper, we describe results from an experiment in which atmospheric CO_2 concentration is doubled, using a climate model with higher horizontal and vertical resolution, but also using a prescribed oceanic heat convergence. This follows on naturally from earlier experiments carried out within the Meteorological Office: instead of prescribing sea surface temperatures, we prescribe the oceanic heat convergence. However, the present work does not attempt to allow for changes in oceanic heat convergence that might accompany an increase in atmospheric CO_2.

2. The model

The climate model used in the present study comprises an atmospheric general circulation model coupled to a 50 m oceanic mixed layer and an energy-balance sea-ice model.

The atmospheric model is the UK Meteorological Office model described by Slingo (1985), which has been used to investigate the impact of anomalies in sea surface temperature (Palmer and Mansfield, 1986), soil moisture (Cunnington and Rowntree, 1986) and the effect of increased

atmospheric CO_2 (Mitchell et al, 1987). The primitive equations are solved using finite differences on 11 sigma (σ = pressure/surface pressure) layers which are irregularly spaced, being concentrated near the boundary layer and the tropopause. A regular latitude-longitude grid is employed, computational stability and noise being controlled by a multi-point filter near the poles, and by non-linear diffusion. In this version, the horizontal resolution has been degraded to 5° x 7.5° to allow longer simulations with the available computing resources, the timestep has been increased to 20 minutes, and sea level pressure is filtered every 6 hours using a 17-point Shapiro filter.

The treatment of the boundary layer uses the scheme of Richards (1980a,b) which is an extension of the ideas of Clarke (1970). The boundary layer is allowed to occupy up to 3 of the lowest model layers with the top being diagnosed at the position of the lowest inversion. In unstable conditions the turbulent mixing occurs through the lowest 3 layers whilst in stable conditions the mixing is restricted to those layers below the diagnosed boundary layer top. The fluxes of heat, moisture and momentum from the surface are based on Monin-Obukhov similarity theory (Mitchell et al 1985) with evaporation limited, where appropriate, by soil moisture following Manabe (1969). Convection is modelled by a penetrative scheme (Lyne and Rowntree, 1976; Rowntree, 1984) which allows entrainment of environmental air and detrainment from the convective parcel at each level. In the original scheme complete detrainment occurred in the final layer to which convection took place. This was modified to allow some detrainment to the layer above in order to represent the effect of penetration of an inversion by more buoyant plumes in a convective

ensemble. This also provides a mechanism by which the boundary layer and free atmosphere can interact, and improved the prediction of low cloud in the model by reducing the excessive low cloud over tropical oceans. Supersaturation produced either by large scale ascent or following convection is removed by condensation to form precipitation. The convection scheme allows evaporation of the precipitation in the next layer below that in which it formed.

The seasonal and diurnal variations of solar radiation are represented and radiative fluxes depend on temperature, the concentrations of water vapour, carbon dioxide and ozone, and on clouds. Long wave fluxes are calculated using the emissivity approximation in a revised formulation by Slingo and Wilderspin (1986). Over snow-free land the surface albedo is specified to vary geographically with values derived from the global data on land cover and soils compiled by Wilson and Henderson-Sellers (1985). Over snow-covered land albedo increases with snow depth. Albedo is prescribed to be 0.06 over unfrozen sea and 0.7 over land ice. The radiation scheme has provision for three layer clouds (low, medium and high) and a convective tower. The layer clouds are assumed to be one sigma layer thick but convective cloud may occupy more than one sigma layer. The cloud reflectivity is specified as 0.2 for high cloud and 0.6 for other clouds. Clouds are assumed to be black for long-wave calculations except high cloud which has an emissivity of 0.5.

The model was modified to include a cloud prediction scheme for both convective and layer cloud, following Slingo (1980) and Wilson and Mitchell (1986). Convective cloud amount is diagnosed from the maximum parcel size

involved in moist convection, and the base and top determined from the levels between which it occurs, whilst layer cloud amounts are simple functions of the layer relative humidities. In layers where convective cloud is diagnosed the relative humidity of the layer free of convective cloud is used, assuming saturation in the convective cloud fraction. In the case of convection extending more than three layers, the cover in all but the lowest 3 layer is not allowed to exceed 8%, as a crude attempt to represent deep convective towers. Layer cloud may occur in any of the model layers except the top layer. Fractional cloud amount, C, is calculated from a simple quadratic function of relative humidity, R, if it exceeds a threshold value, R_c ie

$$C = (R-R_C)^2/(1-R_C)^2 \qquad R>R_C$$

$$0 \qquad R\leq R_C$$

R_C is 0.9 except for high clouds (the 4 layers next to the top) and for low cloud in the thin bottom layer next to the surface. For these, total cover is predicted if saturation is reached and zero otherwise. This restriction was imposed to limit the overprediction of high cloud found in tuning experiments. The low cloud restriction is more physically reasonable since the bottom layer is thinner and therefore unlikely to contain a cloud with radiative properties similar to those assumed until the depth averaged humidity is close to saturation. The dependence of low cloud on low level stability that was used in the original scheme (Slingo, 1980) was omitted, since the simulated cloud cover was reasonable without it.

The depth of the mixed layers (50 m) was chosen to be sufficient to allow for the seasonal storage of heat in the ocean (Meehl and Washington, 1985) without unduly prolonging the thermal response time of the ocean. The evolution of the mixed layer temperature T at each point is given by

$$\rho h c_p \frac{dT}{dt} = S + C \qquad (1)$$

where ρ, c_p are respectively the density and heat capacity of sea water, S is the heat flux through the surface and C is the prescribed heat convergence due to oceanic processes (advection, convection etc). An effective C for the model was determined by diagnosing S in a four year atmospheric simulation in which the seasonal variation of sea surface temperatures (and so $\frac{dT}{dt}$) were prescribed from climatology, and solving (1) for C as a function of time and space. In the coupled model sea surface temperatures are updated every 5 days based on the net surface heating from the atmosphere and the specified heat convergence.

Sea-ice forms when the ocean temperature falls below the freezing point of sea water, 271.2 K. The surface temperature of sea-ice is updated every atmospheric model timestep so that the effect of the diurnal cycle on both the short and long wave radiation budgets is included (Gordon and Bottomley, 1984). Surface albedo increases linearly from 0.4 at 271.2 K to the land ice value of 0.7 at or below 261.2 K. The decrease in albedo as the temperature increases is intended to represent the presence of melt ponds and inhomogeneous cover over a grid square as the melting point is approached since there is no provision for fractional ice cover of a grid square. Snowfall on top of ice and the diffusive heat flux through the ice are also included. Ice and snow depths and changes in classification are

only updated every 5 days using the accumulated heat budgets and snowfall, which simplifies coding and adequately represents the growth and decay of ice (Gordon and Bottomley, 1984). The temperature of the mixed layer under the ice is kept at freezing point. (If there is ice at a point which was ice-free in the prescribed SST integration the specified heat convergence is either used to reduce the thickness of ice, if positive, or if negative is redistributed evenly over the ice-free points of the hemisphere).

The albedo formulation for sea-ice is similar to that proposed by Robock (1980) and allows ice to melt more easily than would a discontinuous large jump of albedo at the melting point. With increased CO_2 relatively greater ice melt might be expected to occur using a gradual as opposed to a discontinuous change in albedo with temperature, and hence a discontinuous sensitivity for the global surface temperature increase as shown by Washington and Meehl (1986). A disadvantage of our scheme is that the albedo could be seriously underestimated if there is significant snowfall on the ice (Bottomley, personal communication).

3. The experiments

The control integration simulated 20 complete years and at the end of year 7, the anomaly integration was started with an instantaneous doubling of CO_2 amount and ran for 38 years. The time dependence of the global mean sea temperature (Figure 1) and the net heat flux into the mixed layer (Figure 2) show that whilst the control experiment has reached an approximate equilibrium after 10 years, the anomaly has not yet fully

attained its equilibrium after 25 years. Nevertheless the net heating is only of order $^1/_4$ Wm^{-2} and the year to year temperature change is markedly less rapid than the early response. The temperature curve closely follows the exponential law

$$\Delta T(t) = \Delta T_{eq} \, (1 - \exp(-^t/_\tau))$$

with ΔT_{eq} for the slab ocean ~4.5°C and τ ~ 9 years so that by year 25 over 90% of the eventual equilibrium change has been obtained. Also the major differences in circulation and simulation are consistent and similar for the last 15 years of the experiment for which results are presented later.

The initial net heat flux into the surface H_o in the anomaly integration is ~ 3 Wm^{-2} and the difference in net radiation balance at the top of the atmosphere (not shown) is essentially the same. If the model were to adjust to equilibrium like a radiative black body, the heat capacity of 50 m of water would imply an e-folding time of ~ 2 years (the response time $\tau = \rho c_p \Delta T / H_o$ where ρ and c_p are respectively the density and heat capacity of sea water, and ΔT ~ 1.1 K is equilibrium temperature change in the absence of feedbacks). As noted by Hansen et al (1984) feedbacks which magnify the eventual temperature increase also prolong the approach to equilibrium by a similar factor; this is also found here.

4. The control simulation of observed climate

A prerequisite of any climate model used for a climate change simulation such as that due to increased CO_2 is that the model should produce a reasonable simulation of the present climate. Therefore the

behaviour of the coupled model used here with the present level of CO_2 is briefly described and its ability to simulate the present climate and especially its seasonal variation is evaluated. Charts for the means of December, January, February (DJF) and June, July, August (JJA) averaged over the last 15 years of the control integration will mostly be shown although results from other seasons will be mentioned where appropriate.

The mean sea level pressure for DJF (Figure 3a) reproduces fairly well the observed pattern (Figure 3b), in the northern hemisphere. The Siberian and Rockies highs are too weak and displaced southwards and the Aleutian low extends too far over Alaska but the general pattern is reasonable. In the southern hemisphere the most obvious error is the too shallow circumpolar trough (by about 15-20 mb) positioned about 15° too far north. In JJA (Figure 4a) the southern depression belt is again about 12 mb too shallow and displaced to the north of the observed position (Figure 4b). In the northern hemisphere pressure is too high over the pole with a ridge towards the Azores high tending to give easterly flow over Western Europe. The heat lows over the American and Asian continents are reasonably well simulated but there is erroneously low pressure over the north-west tropical Pacific.

Comparison of the precipitation of DJF (Figure 5a) with the observed data of Jaeger (1976), Figure 5b, shows that the main convergence zones are reproduced but the drier areas of the sub-tropical oceans are wetter than observed. At higher latitudes, especially over the northern hemisphere continents, the agreement between the computed and observed amounts is quite close. In JJA (Figure 6a) the rainfall maxima of the ITCZ are near

the observed positions but tend to be excessive over the oceans, especially the Western Pacific and Bay of Bengal. Again both the oceanic sub-tropics and also most areas of north Africa are less dry than observed. Both the Indian and west African monsoons are weaker than observed, whilst the eastern coastal regions of northern continents are too wet.

The zonal mean model temperatures for DJF (Figure 7a) are generally similar to the observed (Figure 7b); the overall pattern is quite well simulated and temperatures are generally within 5°C of observed. The low level inversion at high latitudes in the northern hemisphere is simulated well; however the tropical tropopause is too warm. The model temperatures for JJA (Figure 8a) are again in reasonable agreement with observed (Figure 8b) except that the tropical tropopause is again too warm and upper tropospheric temperatures at high latitudes in the summer hemisphere are 10 to 15°C too low. This is also true in the southern hemisphere in DJF.

The variation with height and latitude of the zonal mean westerly wind for DJF (Figure 7a) and JJA (Figure 8a) is quite similar to the observed (Figures 7b and 8b), with the main features being reproduced. The strength of the southern hemisphere jet in DJF is in excellent agreement although it is positioned about 10° too far north and rather higher than observed. The northern hemisphere jet is about 10 ms^{-1} too weak in both summer and winter and in winter does not show the observed separation from the stratospheric jet. This is also true in the southern hemisphere in winter but given the model's resolution with only 2 layers above 100 mb, it is not too surprising. At low latitudes the observed easterlies are well simulated. However there is a lack of stratospheric summer easterlies. and the low

level westerlies of the southern hemisphere are deficient; this is consistent with the shallow circumpolar trough noted above. The erroneous low level easterly flow at northern hemisphere mid-latitudes in JJA reflects the deficiency in circulation noted above in the discussion of the pressure pattern. Despite these deficiences the overall pattern is reasonably good given the model's horizontal and vertical resolution.

The height-latitude diagrams of mean layer cloud amounts (convective amounts omitted) simulated by the model in the control experiment (Figure 9) show a number of realistic features. Observed estimates of cloud distribution are beset by a number of problems (Crane and Barry, 1984). We use Washington and Meehl's (1984) estimates of zonal clouds derived from the data of London (1957) and Sasamori et al (1972) as a rough guide to the actual cloud distributions in order to evaluate the model's distribution. The high cloud maxima associated with the precipitation zones of the tropics and mid-latitudes are simulated well, as is the low cloud in the tropical convergence zone and the small cloud amounts throughout most of the mid-troposphere in the tropics and sub-tropics. There is too little low cloud generally particularly near 60°N in JJA, 60°S in DJF; however there are appreciable amounts of shallow convective cloud in these regions which are not shown by these diagrams. The excessive low cloud in the northern hemisphere winter at high latitudes occurs in the thin lowest model layer; this is a consequence of the boundary layer collapsing to one layer thick

over the cold land surface and becoming saturated. In summary the model generated cloud amounts generally agree well with the observed estimates and the major patterns are reproduced.

The differences of computed sea surface temperatures from those specified from observations in the integration used to derive the heat convergence have general similarities for both DJF (Figure 10a) and JJA (Figure 10b). Outside the tropics, sea surface temperatures are generally greater than observed and most areas of the tropics are cooler than observed by 1°C or less. The obvious exceptions to this pattern are the eastern tropical oceans which are too warm by up to 1°C. This may be due to a coding error present in the convection scheme during the estimation of the heat convergence, but which was corrected for the coupled simulations. Differences in net heating can also arise from changes in sea ice extents, cloud and circulation.

The sea-ice cover and its seasonal variation are an important influence on temperatures and low cloud at high latitudes. The reduction in sea-ice in the anomaly experiment is also an important factor in determining the size of the eventual equilibrium warming due to doubled CO_2. Therefore it is important that the sea-ice simulation in the control integration is close to observations. Comparison of the mean extents for February, May, August and November (Figure 11) for the model with observations from Alexander and Mobley (1976) show that a good seasonal variation has been obtained. The agreement in the northern hemisphere is especially good with the growth and decay of ice in Hudson Bay, to the east and west of Greenland and in the Sea of Okhotsk reproduced by the model.

The mean depths of perennial ice in the Arctic are around 2 m which also agree well with observations (Maykut and Untersteiner, 1971). The Antarctic sea-ice is also well modelled though there is a very slight tendency for too large an extent in winter and autumn particularly in the Ross Sea area. However the removal of all but the perennial ice in the Ross and Weddell Seas in summer is successfully simulated. The fractional cover for both hemispheres is generally within a few per cent of that specified from observations in the experiment to determine the oceanic heat convergence (Table 1).

The zonally averaged radiation budget (Figure 12) agrees reasonably well with the observations of Stephens et al (1981). The emitted flux generally agrees within 5 to 10 Wm^{-2} except at the north pole in winter where it is 20 Wm^{-2} lower; the size of the equatorial dip is quite well captured although absolute values are a little too high. Albedo agrees very well except at the poles where it is lower than observed estimates (which generally exceed 70%). This is to be expected with maximum albedos in the model for clouds of 60% and ice of 70%. Consequently the net radiation is fairly well simulated except in polar regions.

In summary, the model simulation of the observed climate with the present level of atmospheric CO_2 is fairly good despite the deficiencies noted above. A major strength is the use of a specified oceanic heat convergence which has resulted in a realistic variation of sea-ice and sea-surface temperatures within a degree of observation over most of the ocean; this is a significant improvement on models which do not take oceanic heat transport into account. The model here has

reproduced most of the main features of the observed temperature and precipitation and in broad terms the model simulation of present climate is at least as good as, and often better than that of other models used to study the effects of enhanced CO_2.

5. Model response to doubled CO_2

a. Global annual mean

We now consider the equilibrium climate obtained with double the present level of atmospheric CO_2. Unless otherwise stated results are taken from the means of the last 15 years of the anomaly and control experiments.

The annual mean global average changes are given in Table 2. Sea surface temperature is warmer by 4.1°C and the global surface temperature increase is 5.2°C. Evaporation and precipitation increase by 15% whilst the total atmospheric moisture content increases by 41%. Cloud amount decreases by 4% (of total cover), mostly at medium and high levels, but there is more cloud above $\sigma = .23$. The troposphere warms by 5.7°C and the land surface by 6.4°C. The mean surface warming of 5.2°C is slightly larger than found in similar experiments with climate models incorporating a simple mixed layer ocean performed elsewhere. Hansen et al (1984), obtained global increases of surface air temperature of 4.2°C and 4.8°C with sea-ice cover in the control simulation respectively smaller and larger than observed. Washington and Meehl (1984) obtained a warming of 3.5°C with over-extensive

sea-ice in the control and Wetherald and Manabe (1986) found a warming of 4.0°C. Possible reasons for the warming being greater in the present experiment are discussed later.

b. Zonal mean changes

The zonal mean temperature differences for DJF and JJA averaged over the last 15 years of control and anomaly experiments (Figure 13a, b) show that the top layers of the model atmosphere cools by up to 6°C due to increased radiative cooling to space. The troposphere warms with temperature increases mostly greater than 4°C, except at low latitudes near the surface where they are of order 3.5°C. In the annual mean, the largest increases of 7 to 8°C are in the upper tropical troposphere and are consistent with the tendency of the model's moist processes to adjust the vertical profile towards the moist adiabatic lapse rate; this lapse rate becomes smaller with increasing temperature and so amplifies temperature changes with height. The maximum upper tropospheric warming extends into the summer hemisphere and decreases in altitude. Both this and the large warming of the lower atmosphere and surface at high latitudes in winter are qualitatively similar to the results of Wetherald and Manabe (reported in Schlesinger and Mitchell, 1985), though the changes at low latitudes are bigger here.

The vertical enhancement of temperature increases in the tropics is similar to that found by Hansen et al (1984) who also used a penetrative convection scheme. Wetherald and Manabe (1986) and

Washington and Meehl (1984) employed a moist convective adjustment procedure which gave a less pronounced amplification (see Mitchell et al 1985; Schlesinger and Mitchell, 1985). The warming in the tropics is slightly larger than found by Hansen et al, (1984), perhaps because their model is unable to represent an increase in (high) cloud above $\sigma = .103$. In our model, the increase in high cloud (see Figure 16 for the zonal cloud changes below) reduces long wave emission to space, while the compensating increase in the reflection of solar radiation is small because of the low albedo of high cloud. Part of the reason for the greater warming in the tropics compared to that found by Wetherald and Manabe is probably the greater reduction in tropospheric cloud. This may again be due to use of a penetrative convection scheme rather than moist convective adjustment as similar cloud reductions are also evident in the model used by Hansen et al (1984).

At high latitudes the largest temperature increases are at the surface and in the lower atmosphere of the winter hemisphere. The stable profile results in this large warming being mainly confined to the lower atmosphere. The maximum changes near the surface of 12°C north of 70°N in DJF and near 65°S in JJA are due to temperature albedo feedback and changes in sea-ice. The melting of snow over land due to increased warming decreases the albedo which leads to more warming, further melting of snow and so on. The contribution to the surface warming of reductions in both thickness and extent of sea-ice are discussed in the next section on the geographical response. Here we note that additional warming of the winter lower atmosphere arises from the removal of sea-ice and the resulting enhanced fluxes of both

sensible heat and moisture at high latitudes and possibly through increased convective and layer clouds, particularly high cloud (see Figure 16). The increased cloud has little effect on the solar beam since the insolation is weak but its influence on the longwave radiation will tend to warm the atmosphere by reducing emission to space.

The changes in zonally averaged west to east wind (Figure 14) show stronger westerly flow at upper levels with the strongest increase in low latitudes (though there is a decrease in the northern hemisphere centred around 200 mb here in summer). The changes are largely to be expected given the increased meridional temperature gradient (Figure 13) and assuming geostrophic balance with the implied changes in geopotential gradients. The decrease in meridional gradient through much of the troposphere outside low latitudes results in generally weaker westerly flow. There is increased westerly flow south of 70°S in both seasons, and at low altitudes north of 45°N in winter. There is an increasing reduction in westerly flow with height near 60°S at the latitudes where sea ice is removed during the control winter, as found in the sea-ice anomaly experiment of Mitchell and Hills (1986). The changes, especially the increased westerly flow at upper levels, are generally smaller than those found in the experiments with prescribed sea surface temperature increases and doubled CO_2 with both prescribed cloud (Mitchell et al, 1987) and model generated cloud (Mitchell et al, 1986).

As noted above global precipitation increases by 15%. The zonally averaged precipitation (Figure 15) increases almost everywhere except in the tropics of the winter hemisphere where rainfall is a minimum. The largest increases are in the main regions of convergence, ie the equatorial trough and in middle and high latitudes. The increases at all latitudes are generally much larger than those found in enhanced CO_2 integrations performed at the Meteorological Office using prescribed sea surface temperatures (Mitchell et al, 1987). This might be expected given the global surface temperature increase of 4°C over sea and 6°C over land and consequent increase of atmospheric moisture by 41% whereas Mitchell et al (1987) prescribed sea surface temperature increases of 2°C, land temperature rose by 3°C and the atmospheric moisture content increased by 20%. This is also shown by the much smaller zones of decrease or little change in precipitation in the present experiment compared to the previous experiments. However, the changes in precipitation are less determined by moisture content than by energy balance constraints - see Mitchell et al (1987).

The changes in zonal mean layer cloud (Figure 16) with doubled CO_2 show that there is a general decrease in middle level clouds, increased high level cloud at all latitudes and some increases in low clouds at high latitudes. This pattern is similar to those found in studies at other institutes (see Wetherald and Manabe, 1986), and to the response in the higher resolution model with a uniform 2K increase in sea surface temperatures and 2 x CO_2 (Mitchell et al 1987).

The general reduction in tropospheric cloud is particularly marked in the main precipitation zones of the tropics and mid-latitudes (cf Figure 15) where there are large increases in precipitation. The greater moisture content of the atmosphere and deeper convection contribute to the increased precipitation whilst the raising of the tropopause, increased convection and greater vertical motion into the lower stratosphere lead to a decrease in area-mean relative humidity and cloud amount (Mitchell et al 1986). The cloud reductions are generally greater than those found by Wetherald and Manabe (1986) and Washington and Meehl (1984) but are similar to the results of Hansen et al (1984). As with the amplification of temperature increase with height, this is likely to reflect the use of a penetrative convection scheme rather than a moist convective adjustment procedure.

At high latitudes of the northern hemisphere there is increased cloud at lower levels except in the surface layer. This is to be expected with increased evaporation from the surface and stable stratification tending to restrict convection to lower levels. The largest temperature increases in the layer next to the surface will tend to reduce the strength of the inversion over land and sea-ice in winter and encourage mixing in the boundary layer to a higher level, and so reduce cloud near the surface. Although this feature is absent from the studies of Wetherald and Manabe, and Hansen et al (cloud was not allowed to form in the lowest layer of the model used by

Washington and Meehl, 1984) and there are quantitative differences in the overall response, the pattern of cloud changes is basically similar to those in the other investigations.

c. Geographical response

(i) Temperature

The largest increases in surface temperature (Figure 17), up to 15 to 20°C, are near the sea-ice edge in winter, as was noted in the discussion of the zonal mean temperature differences. The increases in the tropics, over sea at least, are generally between 3 and 4°C. Increases over land are mostly greater than increases over sea at all latitudes, reflecting several different contributions. In northern winter the stable stratification tends to confine the warming to a shallower layer; the removal of snow (not shown) and increased westerly flow into western Eurasia contribute to larger increases; in summer a less cloudy atmosphere allows more solar radiation to heat the surface whilst the general decrease in soil moisture (discussed later) restricts evaporation so that more of the net radiative heating is balanced by increased sensible heat flux and surface temperatures are higher.

The large increases in temperature over sea-ice in winter result from a number of factors which contribute to the sea-ice/temperature feedback. Firstly, melting of sea-ice and

snow during spring allows more heat from the warmer CO_2-enriched atmosphere to be absorbed and stored by the ocean in summer. This leads to a poleward contraction of the ice-edge throughout the year and in these experiments (Table 1) to the almost complete removal of ice during late summer (Figure 18) and autumn. In winter the larger summer heat storage is released and allows greater atmospheric advective heat transport into the regions near the poles. Secondly, the reduced thickness of ice and lesser depth of snow (a more effective insulator than ice) allows greater heat flux through the ice to maintain a higher surface temperature (although a greater flux will then tend to increase ice thickness). Furthermore, the reduction in the temperature dependent albedo for temperatures above 261.2 K allows more absorption of solar radiation at the surface. Given the weak insolation in winter the last factor is likely to be least effective. This is clear from the change in surface absorption of solar radiation (Figure 19) which shows large increases in summer where the ice has contracted polewards (see Figure 18) and the effect of decreased snow cover in northern winter but little change over the poles. In the Arctic in summer, where all the sea-ice is removed in the 2 x CO_2 experiment, the temperature change is only 2°C because of the large heat capacity of 50 m of water and since in the control the ice is at or close to melting point. The same applies to the Ross and Weddell Seas in summer, where most of the sea-ice is removed.

Comparing the changes with results obtained elsewhere with similar models, the tropical temperature increases are larger than those found by Wetherald and Manabe (1986) and by Washington and Meehl (1984) and similar to those in the study by Hansen et al (1984), (see also Schlesinger and Mitchell, 1985); outside the tropics the response is most similar to that obtained by Wetherald and Manabe in both seasons. Although Hansen et al found changes in the northern hemisphere in winter which are qualitatively quite similar, during summer they found land temperature increases only of about 2 to 4°C, much less than in this experiment and in the study by Wetherald and Manabe. This is related to the reduction in soil moisture content (see Section 5c(iii)) found in both the latter investigations but less evident in the former.

In summary temperature increases range from 2°C over the summer pole to 20°C over the sea-ice of the winter pole; temperatures increase by less than 4°C in the tropics but are 8 to 10°C higher over much of the land in the northern hemisphere in winter and 6 to 8°C in summer. In the appendix the statistical significance of the changes is assessed against the interannual variability of the model; over most of the globe the changes are significant at least at the 5% level and over a very large region at the 1% level.

ii. Surface pressure

During December to February, there is a reduction in surface pressure (Figure 20a) over the Arctic, especially over Baffin Bay, the Norwegian Sea and off Kamchatka where there is substantially less sea ice than in the control simulation (Figure 18a). Mitchell and Hills (1986) also found significant reductions in surface pressure where sea-ice was removed in a prescribed anomaly experiment. To the south, there are increases over much of the North Atlantic and southern Europe, giving enhanced westerly flow into northern Europe and Asia. Increased westerly flow over Europe (and also northern Canada) in winter and spring was also evident in previous CO_2 studies with prescribed sea surface temperature increases using a different model (Mitchell, 1983; Mitchell and Lupton, 1984).

There are substantial reductions in the subtropics in southern hemisphere summer and a similar but more pronounced response in the northern hemisphere during June to August (Figure 20b). These changes may be larger in northern hemisphere because of the greater atmospheric warming (compare Figures 13a, b), particularly near 30 to 40° of latitude in the summer hemisphere. Note also the increases in surface pressure over the western tropical Pacific and the extreme south east of Asia which is associated with a northward shift of the models' ITCZ, discussed in the next sub-section.

Pressure increases in southern high latitudes in winter (Figure 20b), probably due to mass displaced from the northern hemisphere. Note that the rises are a minimum along the new sea-ice edge (figure 18b), consistent with the findings of Mitchell and Hills (1986).

(iii) Precipitation and soil moisture

Precipitation is greater at high latitudes in both seasons (Figure 21); the largest increases are along the depression tracks and are consistent with increased moisture convergence due to a higher atmospheric moisture content. In winter at high latitudes this increased precipitation occurs as snow and increases the snow depth over Asia in particular (not shown). In northern summer (Figure 21b), the precipitation is greater along the ITCZ over the central and east Pacific, the Atlantic and into west Africa. The Asian monsoon is strengthened and there are decreases over the west Pacific, south-east Asia and the Indian Ocean, north of the equator. There is decreased rainfall in the already dry north African region and extensive reductions over southern Europe, and mid-latitudes of Asia. In DJF (Figure 21a) the pattern of changes shows a general shift southwards of rainbelts in the tropics and southern hemisphere with increases over central South America, central southern Africa, the Indian Ocean, northern Australia and the south-west and central southern Pacific with decreased precipitation generally to the north of

the rainbelt. Elsewhere in the tropics the pattern is less clear eg there are increases in the east Pacific north of the equator in the main precipitation band (cf Figure 5a) but decreases over Mexico and nearby and over the east Atlantic north of the equator. Along the equator in the eastern Pacific, which was a rainfall minimum in the control (Figure 5a) there is increased precipitation. In JJA the pattern of changes shows some shifts northwards of the main rainbelts with the strengthening of the Asian monsoon the most noticeable, but the pattern is generally less consistent than the southward shift in DJF. Such a northward movement could be due to increased heating over land in summer (see Figures 19b and 23c) because of reduced cloud.

Although the other studies with similar models were all in agreement with the increases at high latitudes, there were considerable discrepancies in the tropics and over land in mid-latitudes in JJA. In this respect, our results with the decreases over Europe and much of Asia, and the increased monsoon circulation are most like those obtained by Wetherald and Manabe (see Schlesinger and Mitchell, 1985). They are also similar to our results with higher resolution models with prescribed cloud (Mitchell and Lupton, 1984; Mitchell et al, 1987) and model-generated cloud (Mitchell et al, 1986), although there are differences, for example over the tropical oceans during DJF.

Soil moisture increases over much of northern Europe, north-west and central Asia, the western USA and Canada in DJF (Figure 22a, cf control simulation Figure 22c). In the southern hemisphere there are increases near 15°S. In JJA (Figure 22b, cf control Figure 22d) soil moisture decreases over most areas except India and southern Asia, west Africa and northern Mexico where there is increased precipitation from monsoon circulations. The drying of the land in the northern hemisphere is similar to the results of the Meteorological Office experiments with higher resolution (for example, Mitchell 1984, 1986) and those with GFDL models (see Manabe and Wetherald, 1986; Schlesinger and Mitchell, 1985). The mechanism for the drying in this experiment is similar to that found by Manabe et al (1981). At latitudes north of 45°N the spring snowmelt and runoff start and end earlier in the warmer climate (Figures 23 a, b) so both the summer drying season is longer, and more solar radiation is absorbed and available to increase evaporation due to the earlier removal of highly reflective snowcover (Figure 23c). To the south of this region the reductions in precipitation and cloud enhance the winter to summer seasonal drying. There is a corresponding increase in absorption of solar radiation between 30 and 55°S from November to March (Figure 23c) because of the large reductions in cloud (see Figure 16a). The zonal mean changes of soil moisture through the year (Figure 24) show a pronounced drying in summer centred near 50°N. The pattern of changes is very much like that obtained by Manabe and Wetherald (1986) although there is a pronounced drying along the equator in our

experiment whereas there is little change in soil moisture here in their model; the model used by Hansen et al (1984) produced increases both near 60°N and the equator (see Schlesinger and Mitchell, 1985). Another difference from these two studies is the band of increase in summer and autumn near 20°N (see Figure 24); this reflects the increases in monsoon areas, which despite generally larger changes in precipitation in the Wetherald and Manabe (1986) study (see Schlesinger and Mitchell, 1985) are not in general accompanied by increased soil moisture.

6. Summary and Conclusions

The sensitivity of global climate to doubled atmospheric CO_2 has been investigated using a global general circulation model coupled to a simple mixed layer ocean model and a thermodynamic sea-ice model. The depth of the ocean was sufficient to model the seasonal storage and release of heat. Transport of heat by the oceans was allowed for by specifying a seasonally varying heat convergence.

A control integration of 20 years with the present level of CO_2 reached a state reasonably close to equilibrium after 7 years and simulated well many features of the observed climate. The prescribed heat convergence in the ocean ensured that both sea surface temperatures and the seasonal variation of ice were in close agreement with observations. The zonally meaned distribution of clouds generated by the model is

qualitatively similar to observed estimates. Overall the simulation of present climate is at least as good as in the published results from other models used to study the sensitivity to enhanced CO_2.

The anomaly integration, with 2 x CO_2, attained a state in reasonable equilibrium by year 38. No attempt was made to accelerate the approach to equilibrium. The global mean surface temperature increased by 5.2°C, slightly larger than in recent similar studies elsewhere. As discussed above the main reasons for a larger warming are probably the use of a penetrative convection scheme rather than a moist convective adjustment procedure and the larger cloud temperature feedback due to not restricting the formation of cloud at high levels. Zonal mean tropospheric temperatures are warmer by 4°C or more nearly everywhere with increases of up to 8°C in the upper tropical troposphere. The tendency of the model to adjust the vertical profile towards the moist adiabatic lapse rate leads to the vertical amplification of the warming, which is probably larger owing to the use of the penetrative convection scheme rather than a moist convective adjustment procedure used in some other models. At higher latitudes in winter the stable profile mainly confines the largest warming to the surface and lower troposphere. Zonal mean westerly wind is stronger at upper levels in the tropics and generally decreased outside low latitudes which is consistent with the respectively increased and decreased meridional temperature gradients.

The global mean moisture content of the atmosphere increases by 41% and precipitation by 15%. Zonally averaged precipitation increases almost everywhere except in the sub-tropics during winter, with largest increases

in the main convergence zones of the equatorial trough and middle and high latitudes. The broad pattern of zonal mean cloud changes is similar to that found in the Meteorological Office model at higher resolution with prescribed sea-surface temperatures (Mitchell et al, 1986) and to that found elsewhere (see Wetherald and Manabe, 1986); there is a general decrease in middle level clouds, increased high cloud at all latitudes and some increases in low cloud at high latitudes. The decrease in relative humidity in the mid-troposphere and increase above is consistent with a raised tropopause and deeper convection.

The surface temperature increase varies geographically from less than 2°C where sea-ice has melted in the Arctic in summer, and from 3 to 4°C over tropical oceans to 15 to 20°C over winter sea-ice. Over northern hemisphere land increases are mostly 6 to 8°C in summer and 8 to 10°C in winter. At high latitudes the thinner ice and reduction in snow contribute to the warming as does the release of greater heat stored in the ice-free ocean during the previous summer. The reduction in snow and increased westerly flow into Europe contribute to the winter warming whilst the reduction in soil moisture and cloud give the large warming over much of northern hemisphere land in summer. Here, spring snowmelt and runoff start and end earlier so that the drying season is longer and, with reductions in cloud and precipitation in some areas, more pronounced, so drying out much of the land. Similar reductions in soil moisture have been found in previous Meteorological Office experiments and are broadly in agreement with the results of Manabe and Wetherald (1986).

In broad terms there is a fair amount of agreement between our results and the similar studies of Hansen et al (1984), Washington and Meehl (1984) and Wetherald and Manabe (1986), especially with respect to zonal mean changes. However there are some important differences some of which may be due to the different treatments of convection and the land surface or to differences in the control climate simulations (Mitchell et al, 1987). All the studies obtain warmings of 4 or 5°C with reduction in cloud probably being the major reason for enhanced warming compared to earlier studies with fixed clouds.

We have described the time averaged response of a three dimensional climate model to a doubling of atmospheric CO_2 concentrations. Detailed analyses of both the changes in cloud cover and in temporal variability will form the subject of future papers. An additional experiment in which CO_2 was doubled and sea ice extents were prescribed as in the control simulation will be reported later.

Finally, in order to identify topics which are a priority for future work, it is instructive to consider the limitations of the present work and other similar studies.

1. The representation of cloud is extremely crude, and studies to date take no account of possible changes in cloud optical properties. Somerville and Remer (1984) have revived speculation that cloud water and hence cloud reflectivities would increase in warmer, moister atmosphere, providing a significant negative feedback which would

reduce the sensitivity of climate to increased atmospheric CO_2. A parametrisation of cloud water has been developed (Smith, 1985) and will be used in future studies of enhanced CO_2.

2. The dynamics of sea-ice and changes in ocean dynamics are not taken into account. Numerical simulations indicate that the inclusion of ice dynamics would enhance the seasonal variation in sea-ice cover (Hibler, 1984). Nevertheless the present model produces an accurate simulation of the seasonal amplitude of ice extent variations, although this was found to be sensitive to the specification of the surface albedo. It is possible that temperature albedo feedback over sea-ice is excessive, compensating for the lack of sea-ice dynamics to give a realistic annual variation, but producing an unrealistically large response in the enhanced CO_2 integration. The neglect of changes in ocean circulation may not lead to serious errors as experiments with an idealised coupled ocean atmosphere (Manabe and Bryan, 1985) suggest that the strength of the oceanic meridional circulation changes little on increasing atmospheric CO_2. However, a more detailed model of the ocean than that used here will be needed to estimate the time dependent response of climate to the observed gradual increase in CO_2 and other trace gases. A version of the Meteorological Office 11-layer atmospheric model has been coupled to a dynamical model of the ocean for use in further studies of the equilibrium and transient response to enhanced CO_2 concentrations.

3. The horizontal resolution used in this study and elsewhere does not represent adequately the weak baroclinic disturbances characteristic of northern mid-latitudes in summer. The present work needs to be repeated at higher resolution to ensure that features such as the drying of the northern mid-latitude continents in summer are not artifacts of the low resolution used.

4. Although the parametrization of some physical processes (for example radiation) can be validated against detailed theoretical models, others (including convection and the representation of cloud and land surface) contain arbitrary assumptions and constants which cannot be verified directly against theory or measurement. We have seen that models using a penetrative convection scheme produce a much larger warming in the upper tropical troposphere with increased atmospheric CO_2 than models using moist convective adjustment. An investigation of the effect of changes in the earth's orbital parameters currently in progress in the Meteorological Office indicates that the simulated changes in precpitation over the subtropical continents are sensitive to the prescription of evaporation. We plan to repeat the present study using a revised parametrization of the land surface to determine it the response of the present model is sensitive to such model changes in formulation.

It is clear that we are still some way from predicting the magnitude and distribution of climate change due to increased atmospheric CO_2 with the accuracy required for climatic impact studies. Experiments such as that described above should be regarded as sensitivity studies and not as

forecasts. These sensitivity studies indicate the mechanisms which are likely to be important as climate changes, and identify those processes which must be modelled accurately. There is still much work to do in this direction.

Table 1 Mean sea-ice cover as a fraction of global area or area between specified latitudes

Experiment	Period	Globe	90°N-30°N	90°S-30°S
Prescribed sea-ice and SST for derivation of heat convergence	Annual	.046	.081	.101
	DJF	.040	.101	.057
	MAM	.040	.098	.060
	JJA	.051	.064	.135
	SON	.053	.059	.151
Control	Annual	.045	.076	.102
	DJF	.043	.095	.075
	MAM	.039	.100	.055
	JJA	.048	.061	.127
	SON	.050	.047	.149
Anomaly 2 x CO_2	Annual	.019	.042	.032
	DJF	.018	.056	.014
	MAM	.022	.077	.007
	JJA	.016	.027	.037
	SON	.019	.008	.067

Table 2 Changes due to doubled CO_2 (Global 15 year means)

Surface Temperature (°C)			Tropospheric Temperature (°C)
All Points	Sea	Land	
5.2	4.1	6.4	5.7

Atmospheric Moisture Content (%)	Evaporation (%)	Precipitation (%)	Cloud Cover (%)
41	15	15	4

NB: (i) The sea temperature change does not include sea-ice points.

(ii) The troposphere is taken as the first 8 levels of the model up to $\sigma = 0.23$.

Appendix

Statistical significance of changes in surface pressure, surface temperature, precipitation and soil moisture

Climate simulations made with 3-dimensional models exhibit random fluctuations from year to year in a similar way to the observed climate. Some of the differences between the anomaly and control integrations described above may therefore have arisen by chance. A simple significance test has been used to determine those changes unlikely to occur by chance and which are probably due to increased CO_2.

A 2-tailed Student's t-test was carried out on the DJF and JJA seasonal means from the last 15 years of control and anomaly for each of the changes in surface pressure, surface temperature, precipitation and soil moisture. The limitations of such a test applied to meteorological variables which are correlated in space and which may not be sampled from a normal population (especially true of precipitation (Reed 1986)) have been noted by Mitchell et al (1987). The tests should be viewed as confirming those aspects of the model response for which a physical explanation can be given.

Charts of the t-statistic show that the increase in pressure over the north Atlantic and Europe in DJF (Figure 25a) and the decreases over the North Pole and in the sub-tropics in the southern hemisphere are significant at least at the 90% level of confidence. In JJA (Figure 25b) the general fall in pressure over the northern hemisphere is mostly

significant at the 95% level and in much of the region at the 99% level, as is the increase in pressure over south-east Asia and the west tropical Pacific.

The surface temperature increase is significant at the 99% level of confidence almost everywhere in both DJF and JJA (not shown) as might be expected from the large warming compared to interannual seasonal variability. Precipitation is inherently more variable spatially and so one might expect a smaller total area of significant changes and a less coherent pattern. However the increases at high latitudes in both seasons (Figure 26) are mostly significant at the 95% level or higher as is the southward shift of the main precipitation bands in DJF and also the northward shift and strengthening of the monsoon rainfall in JJA. The decreases in the winter sub-tropics and over southern Europe and Asia in JJA are also significant in many areas.

The t-statistic for changes in soil moisture, which tends to have a large interannual variability, even so shows that the major changes such as a wetter surface over parts of Canada, northern Europe and Asia in DJF, and the drying of northern hemisphere land in summer are mostly significant at the 90% level of confidence or higher (Figure 27).

The greater length of the integrations compared to previous studies with prescribed sea surface temperatures has enabled tests with more degrees of freedom to be performed. The high level of significance of many of the changes here, which are similar to previous results, encourages the belief that the model's true response to enhanced CO_2 has been identified.

REFERENCES

Alexander R C and Mobley R L 1976 Monthly average sea surface temperatures and ice pack limits on a 1° global grid. Mon. Wea. Rev. 104, 143-148.

Clarke R H 1970 Recommended methods for the treatment of the boundary layer in numerical models. Australian Met. Mag. 18, 51-73.

Crane R G and Barry R G 1984 The influence of clouds on climate with a focus on high latitude interactions. J. Climatol. 4, 71-93.

Cunnington W M and Rowntree P R 1986 Simulations of the Saharan atmosphere-dependence on moisture and albedo . Quart. J. R. Met. Soc. 112, 971-999.

Gordon C and Bottomley M 1984 A scheme for incorporating the thermodynamic sea-ice model into a coupled ocean-atmosphere model. Met O 20 DCTN No. 1., Meteorological Office, Bracknell, Berkshire RG12 2SZ, UK.

Hansen J; Lacis A; Rind D; Russell G; Stone P; Fung I; Ruedy R and Lerner J 1984 Climate Sensitivity and Analysis of Feedback Mechanisms. In Climate Processes and Climate Sensitivity (ed. J. Hansen and T Takahashi) Geophysical Monograph 29, 130-163. American Geophysical Union, Washington DC.

Hibler W D 1984 The role of sea ice dynamics in modelling CO_2 increases. Ibid. P 238-253.

Jaeger L 1976 Monatskarten des Niederschlags fuer die Ganze Erde. Ber. Deutsche. Wet. 18, No. 139 38 pp.

London J 1957 A study of the atmospheric heat balance. Final Report AFCRC Contract No. AF19(122)-165. New York University, 99 pp. DDC AD 117227.

Lyne W H and Rowntree P R 1976 Development of a convective parametrization using GATE data. Met O 20 Tech. Note II/70, Meteorological Office, Bracknell, Berkshire RG12 2SZ, UK.

Manabe S 1969 Climate and the ocean circulation I. The atmospheric circulation and the hydrology of the earth's surface. Month. Weath. Rev., 97, 739-774.

Manabe S and Wetherald R T 1986 Reduction in summer soil wetness induced by an increase in atmospheric carbon dioxide. Science 232, 626-628.

Manabe S, Wetherald R T and Stouffer R J 1981 Summer dryness due to an increase of atmospheric CO_2 concentration. Climate Change 3, 347-386.

Manabe S and Bryan K 1985 CO_2-induced change in a coupled ocean-atmosphere model and its paleoclimatic implications. J. Geogphys. Res. 90, 11689-11707.

Maykut G A and Untersteiner N 1971 Some results from a time-dependent thermodynamic model of sea-ice. J. Geophys. Res. 76, 1550.

Meehl G A and Washington W M 1985 Sea surface temperatures computed by a simple ocean mixed layer coupled to an atmospheric GCM. J. Phys. Oceanogr. 15, 92-104.

Mitchell J F B 1983 The seasonal response of a general circulation model to changes in CO_2 and sea surface temperature. Q.J.R. Met. Soc., 109, 113-152.

Mitchell J F B 1986 On changes in soil moisture in CO_2 climate studies. Proc. ISLSCP Conference, Rome, 2-6 Dec 1985. ESA SP-248, 171-173.

Mitchell J F B and Hills T S 1986 Sea-ice and the Antarctic winter circulation: a numerical experiment. Quart. J. R. Met. Soc., 112, 953-969.

Mitchell J F B and Lupton G 1984 A 4 x CO_2 experiment with prescribed changes in sea temperatures. Progress in Biometeorology 3, 353-374.

Mitchell J F B, Wilson C A and Cunnington W M 1987 CO_2 climate sensitivity and model dependence of results. Quart. J.R. Met. Soc., 113, 293-322

Mitchell J F B, Wilson C A, Ingram W J and Cunnington W M 1986 Numerical studies of the effect of increased atmospheric carbon dioxide on climate. Final report of CEC Contract CL-114-UK(H). (Unpublished).

Mitchell J F B, Wilson C A and Price C M 1985 On the specification of surface fluxes in coupled atmosphere ocean general circulation models. In "Coupled Ocean-Atmosphere Models" (ed. J C J Nihoul) Elsevier Oceanography Series 40, 249-262.

Palmer T N and Mansfield D A 1986 Wintertime circulation Antartics during past El Nino events, using a High Resolution General Circulation Model. I Influence of model climatology. Quart. J. R. Met. Soc.112, 613-638.

Reed D N 1986 Simulation of time series of temperature and precipitation over eastern England by an atmospheric general circulation model. J. Climatol. 6, 233-253.

Reichle D E, Trabalka J R and Solomon A M Approaches to studying the global carbon cycle. In "Atmospheric carbon dioxide and the global carbon cycle". (ed. Trabalka) US Dept. of Energy Report DOE/ER-0239, Washington DC 15-24.

Richards P J R 1980a An objective assessment of specifications of boundary-layer eddy diffusion coefficients. Met O 20 Tech. Note II/140, Meteorological Office, Bracknell, Berkshire, RG12 2SZ, UK.

Richards P J R 1980b The parametrization of boundary layer processes in general circulation models. Ph.D. thesis, Department of Meteorology, University of Reading, England.

Robock A 1980 The seasonal cycle of snow cover, sea-ice and surface albedo. Mon. Wea. Rev. 108, 267-285.

Rowntree P R 1984 Sensitivity of global simulations to the evaporation of convective condensates. Workshop on convection in large scale numerical models, 28 November-1 December 1983, ECMWF. Also appears as Met O 20 Tech. Note II/226, Meteorological Office, Bracknell.

Sasamori T, London J, and Hoyt D V 1972 Radiation budget of the southern hemisphere. Meteorol. Monogr. 13, 9-23.

Schlesinger M E and Mitchell J F B 1985 Model projections of equilibrium climatic response to increased CO_2 concentration. In 'Projecting the climatic effects of increasing carbon dioxide', (ed. M C MacCracken and F M Luther) US Dept. of Energy Report DOE/ER-0237 Washington DC 81-148.

Slingo A (Editor) 1985 Handbook of the Meteorological Office 11-layer Atmospheric General Circulation Model. Met O 20 DCTN 29. Meteorological Office, Bracknell, Berkshire RG12 2SZ, UK.

Slingo J M 1980 A cloud parametrization scheme derived from GATE dat for use with a numerical model. Quart. J. R. Met. Soc. 106, 747-770.

Slingo A and Wilderspin R C 1986 Development of a revised long wave radiation scheme for an atmospheric general circulation model. Quart. J.R. Met. Soc. 112, 371-386.

Smith R N B 1985 An integrated approach to the representations of cloud processes. In proceedings of workshop on cloud cover parametrization in numerical models, 26-28 November 1984, ECMWF. Also Met O 20 DCTN23. Meteorological Office, Bracknell, Berkshire RG12 2SZ.

Somerville R C J and Remer L A 1984 Cloud Optical Thickness Feedbacks in the CO_2 Climate Problem. J. Geophys. Res. 89, 9668-9672.

Spelman M J and Manabe S 1984 Influence of oceanic heat transport upon the sensitivity of a model climate. J. Geophys. Res. 89, 571-586.

Stephens G L, Campbell G G and Vonder Haar T H 1981 Earth radiation budgets. J. Geophys. Res. 86, 9739-9760.

Trabalka J R, Edmonds J A, Reilly J M, Gardner R H and Voorhees L D 1985 Human alterations of the global carbon cycle and the projected future. In "Atmospheric carbon dioxide and the global carbon cycle". US Dept of Energy Report DOE/ER-0239, 247-287.

Washington W M and Meehl G A 1984 Seasonal cycle experiment on the climate sensitivity due to a doubling of CO_2 with an atmospheric general circulation model coupled to a simple mixed layer ocean model. J. Geophys. Res. 89, 9475-9503.

Wetherald R T and Manabe S 1986 An investigation of cloud cover change in in response to thermal forcing. Climate change, 8, 5-24.

Wilson M F and Henderson-Sellers A 1985 A global archive of land cover and soils data for use in general circulation climate models. J. Climatol., 5, 119-143.

Wilson C A and Mitchell J F B 1986 Diurnal variation and cloud in a general circulation model. Quart. J. R. Met. Soc. 112, 347-369.

Figures

Figure 1. Evolution of global mean annual mean slab ocean temperature (°C) for the control (solid line) and doubled CO_2 (dashed line) experiments.

Figure 2. Evolution of the global mean annual mean net heat flux into the slab ocean (Wm^{-2}) for the control experiment (solid line) and the doubled CO_2 experiment (dashed line). This is calculated from the radiative, sensible and latent fluxes from the atmospheric model, the prescribed oceanic heat convergence and the heat required to melt snow falling into the sea, and multiplied by the fraction of the globe covered by sea, to give a mean net downward heat flux per total global area.

Figure 3. Pressure reduced to mean sea level (a) for a mean of 15 northern winters (December to February, DJF) of the control experiment and (b) Observed (mean of 3 winters 1983/1984 to 1985/1986 derived from Meteorological Office operational analyses). Contour interval 4 mb.

Figure 4. Pressure reduced to mean sea level (a) for a mean of 15 northern summers (June to August, JJA) of the control experiment and (b) observed (mean of 3 summers 1983 to 1985 derived from Meteorological Office operational analyses). Contour interval is 4 mb.

Figure 5. Precipitation in northern winter (DJF) (a) from a 15 year mean of the control experiment and (b) from the climatology of Jaeger (1976). Contours at 0.1, 1, 2, 5, 10, 20 and 40 mm/day, shaded above 5 mm/day.

Figure 6. As Figure 5, but for JJA.

Figure 7. As Figure 3 but for zonally averaged zonal winds (full lines ms^{-1}) and temperatures (dashed, K) as a function of log (pressure). Easterly (negative) winds shaded. Contour intervals 5 ms^{-1} and 10 K.

Figure 8. As Figure 7, but for JJA.

Figure 9. (a) Log (sigma)-latitude cross-section of zonal-mean layer cloud cover meaned over 15 Northern winters (DJF) of the control experiment. Contour interval 5% of total cover, stippled above 15%. (b) As (a) but for a mean of 15 northern summers (JJA).

Figure 10. Differences of sea surface temperatures simulated by the control experiment from those prescribed from observations for the experiment from which the heat convergence was calculated, meaned over 15 seasons (a) DJF, (b) JJA. Contour interval 1 K, negative values (cooling) stippled.

Figure 11. Mean sea ice extents in the control experiment for (a) February, (b) May, (c) August and (d) November. A point is counted as sea ice in the mean if it was sea ice for more than half of the time during the 15 months meaned.

Figure 12. Zonal means of infra-red radiation emitted at the top of the atmosphere (Wm^{-2}), net downward radiation at the top of the atmosphere (Wm^{-2}) and planetary albedo (%) for a 15 year mean of the control experiment and from observations of Stephens et al (1981). (a) DJF, (b) JJA.

Figure 13. Log (pressure) - latitude cross-sections of difference of zonal-mean temperature (2 x Co_2 - control, 15 year means), for (a) DJF and (b) JJA. Negative anomalies stippled, contour interval 1 K.

Figure 14. As Figure 16, but for westerly wind with contour interval 1 ms^{-1}.

Figure 15. Zonal-mean precipitation (mm/day) for control and doubled CO_2 experiments meaned over 15 years and their difference, for (a) DJF and (b) JJA.

Figure 16. Log (sigma) - latitude cross-section of difference of zonal-mean layer cloud cover (2 x CO_2 - control, 15 year means), for (a) DJF and (b) JJA. Contours at 1% of total cover, decreases stippled.

Figure 17. Differences in surface temperature (2 x CO_2 - control, 15 year means) with contours at multiples of 2 K up to 10 K, and then at multiples of 5 K. Increases over 4 K stippled.

Figure 18. Sea ice extents in (a) February and (b) August for 15 year means of the control experiment (x) and the doubled CO_2 experiment (O). Means defined as for Figure 11.

Figure 19. Differences in solar radiation absorbed at the surface (2 x CO_2 - control, 15 year means) with contours at 0 and multiples of ± 15 Wm^{-2} and decreases stippled for a) DJF and b) JJA.

Figure 20. Differences of pressure reduced to mean sea level (2 x Co_2 - control, 15 year means), for (a) DJF and (b) JJA. Contours at $\pm$ 1 mb, $\pm$ 2 mb and multiples of 4 mb, decreases stippled.

Figure 21. Precipitation changes (2 x CO_2 - control, 15 year means), with contours at 0, ± 1 and ± 2 mm/day and decreases stippled for a) DJF, b) JJA.

Figure 22. (a), (b) as Figure 20, but for soil moisture content, with contours at 0, ± 1, ± 2, ± 5 and ± 10 cm, and decreases shaded. Soil moisture for control (c) DJF, (d) JJA, with contours at 0.3, 1.25, 2.5, 5, 10 and 14.5 cm and shaded below 5 cm.

Figure 23. Time-latitude diagrams of difference of zonal mean over land of (a) snowmelt, (b) runoff (both with contour interval 0.05 cm/day, and decreases stippled) and (c) surface absorption of solar radiation (contour interval 10 Wm^{-2}, decreases stippled) in the doubled CO_2 experiment from the control experiment.

Figure 24. As Figure 23, but for soil moisture content, with contour interval 0.5 cm and decreases stippled.

Figure 25. Student's t-statistic for changes in pressure reduced to mean sea level between doubled CO_2 and control experiments in (a) DJF and (b) JJA, contoured at 10%, 5% and 1% significance levels for two-tailed tests, with changes significant at the 10% level stippled, light for decreases and dark for increases.

Figure 26. As Figure 25, but for precipitation.

Figure 27. As Figure 25, but for soil moisture content.

Annual Mean Global Average

Temperature of Slab Ocean (Depth 50m)

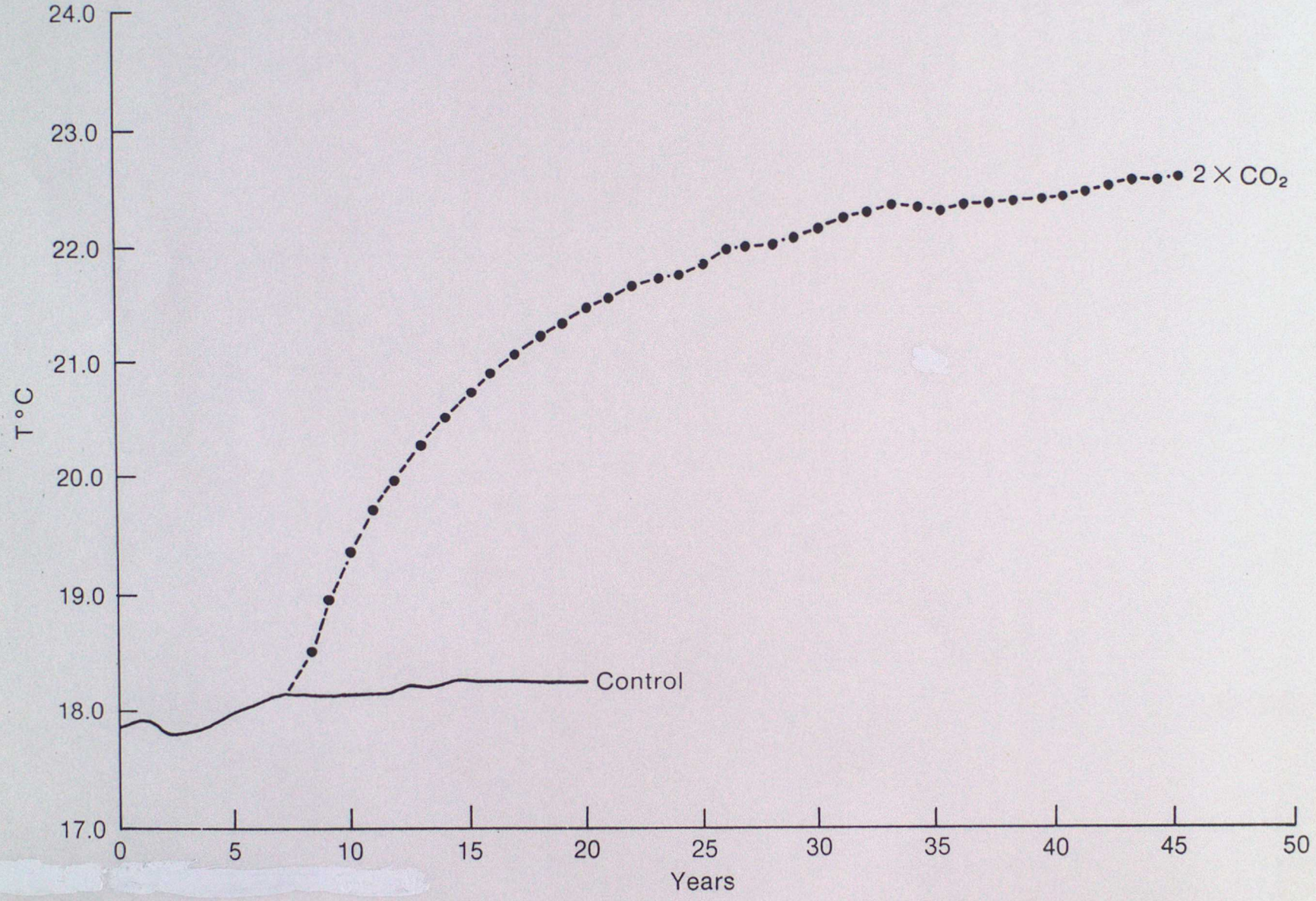

Figure 1

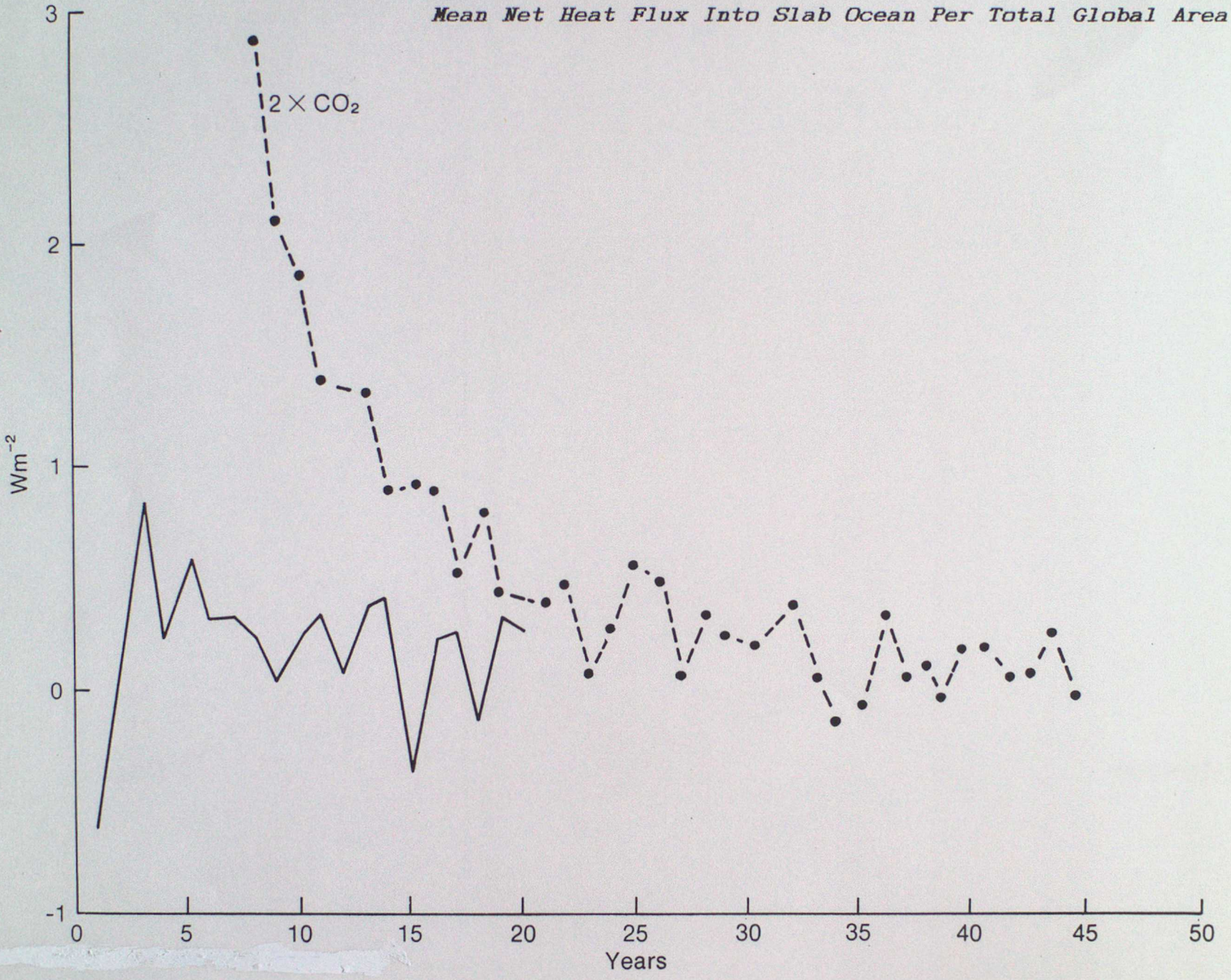
Mean Net Heat Flux Into Slab Ocean Per Total Global Area
2 × CO2
Wm-2
3
2
1
0
-1
0
5
10
15
20
25
30
35
40
45
50
Years

Figure 2

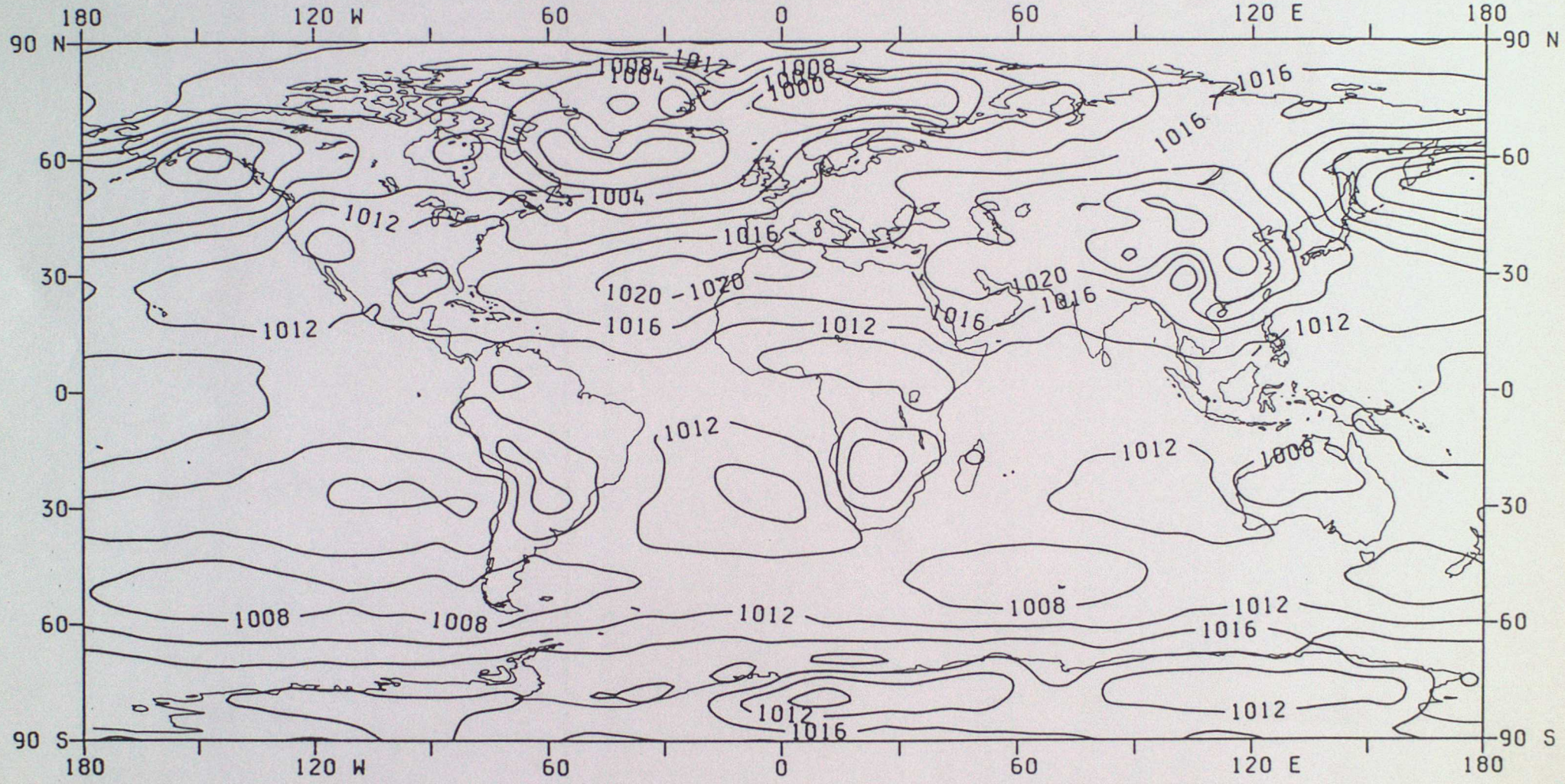
180
120 W
60
0
60
120 E
180
90 N
60
30
0
30
60
90 S
1008
1004
1012
1000
1016
1020

Figure 3(a)

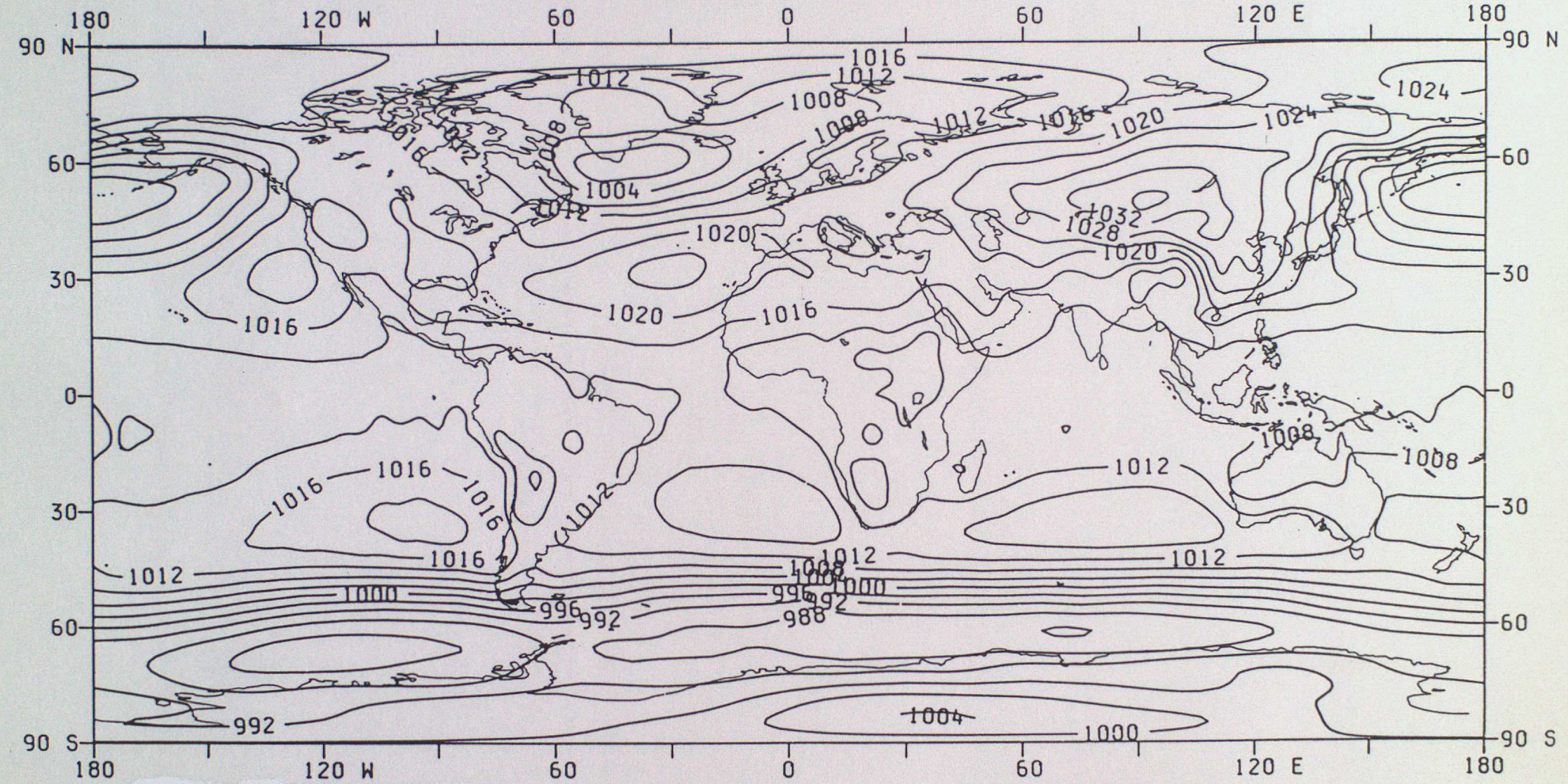
180
120 W
60
0
60
120 E
180
90 N
60
30
0
30
60
90 S
1016
1012
1008
1004
1000
996
992
988
1020
1024
1028
1032

Figure 3(b)

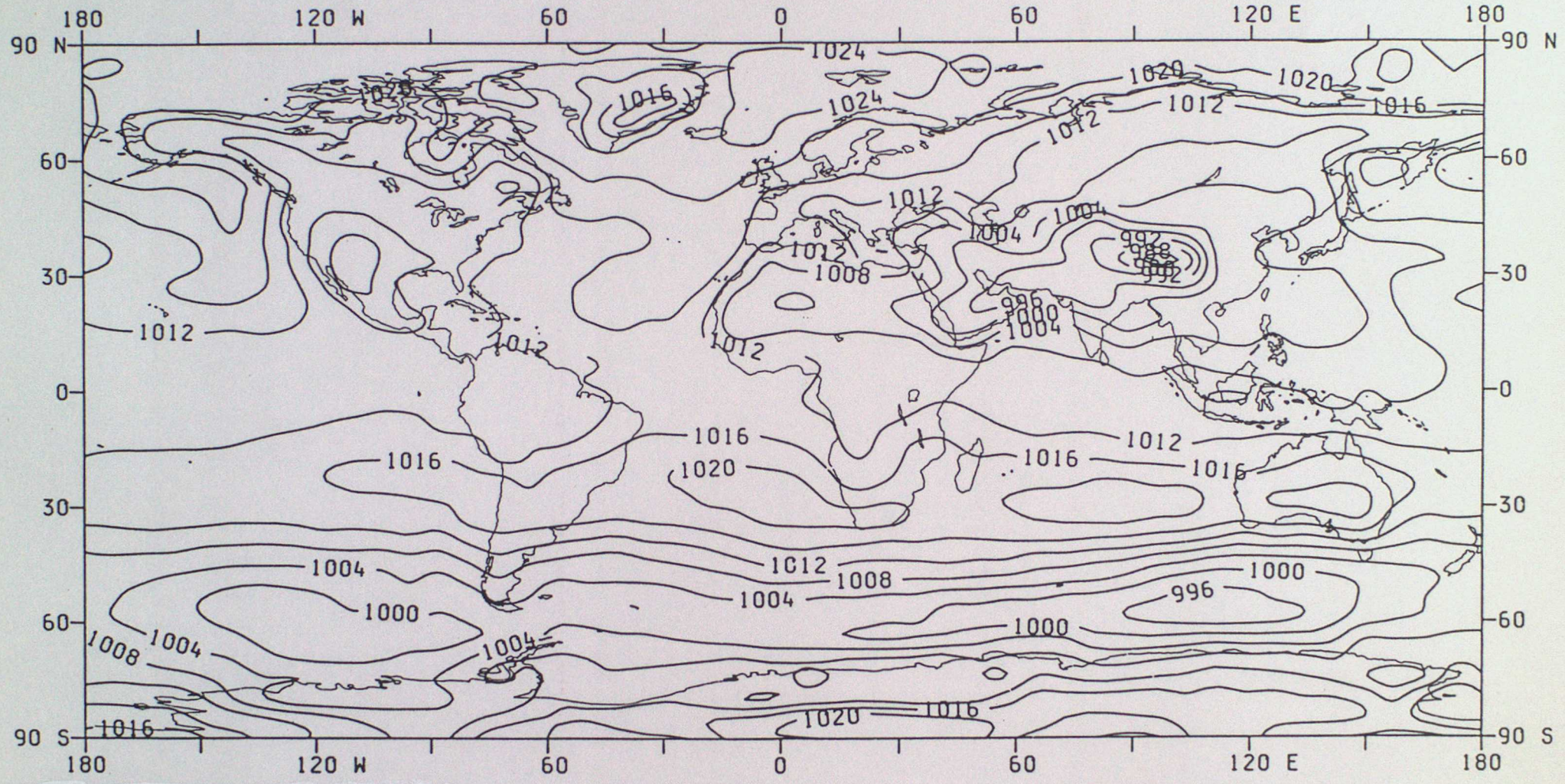
180
120 W
60
0
60
120 E
180
90 N
90 S
60
30
0
30
60
1024
1020
1016
1012
1008
1004
1000
996
992
988

Figure 4(a)

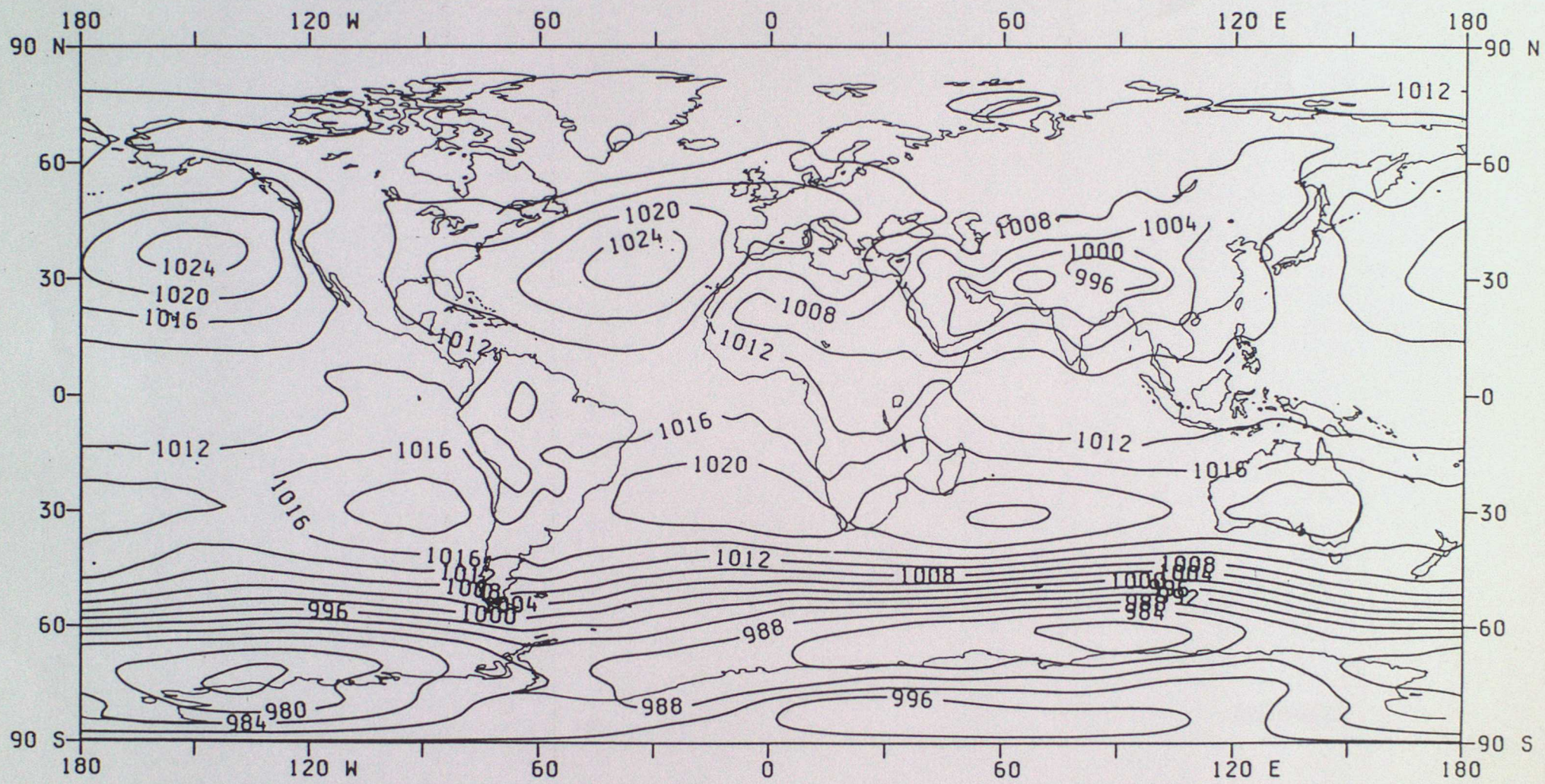
180
120 W
60
0
60
120 E
180
90 N
60
30
0
30
60
90 S
1012
1020
1024
1008
1004
1000
996
1016
988
984
980

Figure 4(b)

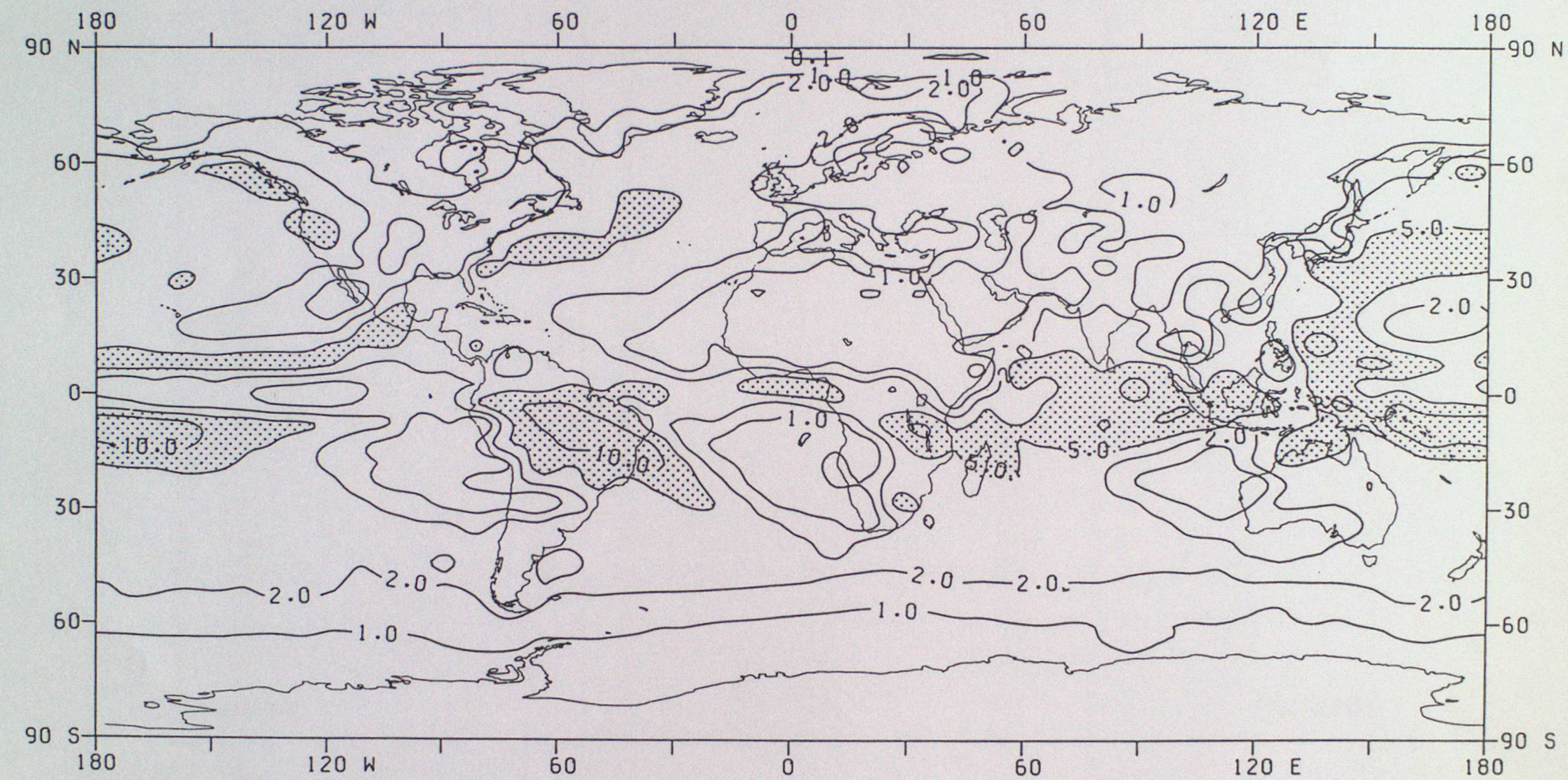

Figure 5(a)

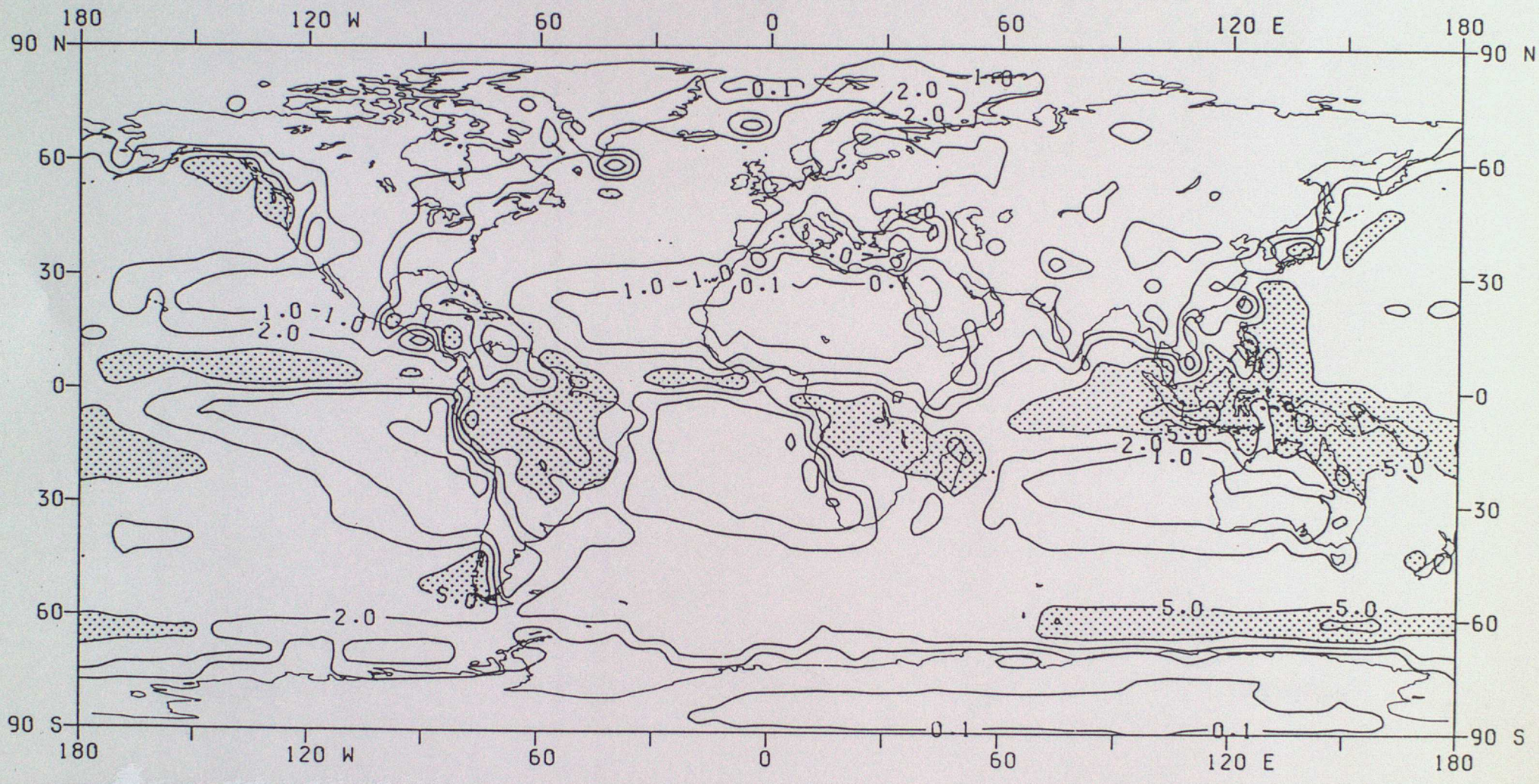

Figure 5(b)

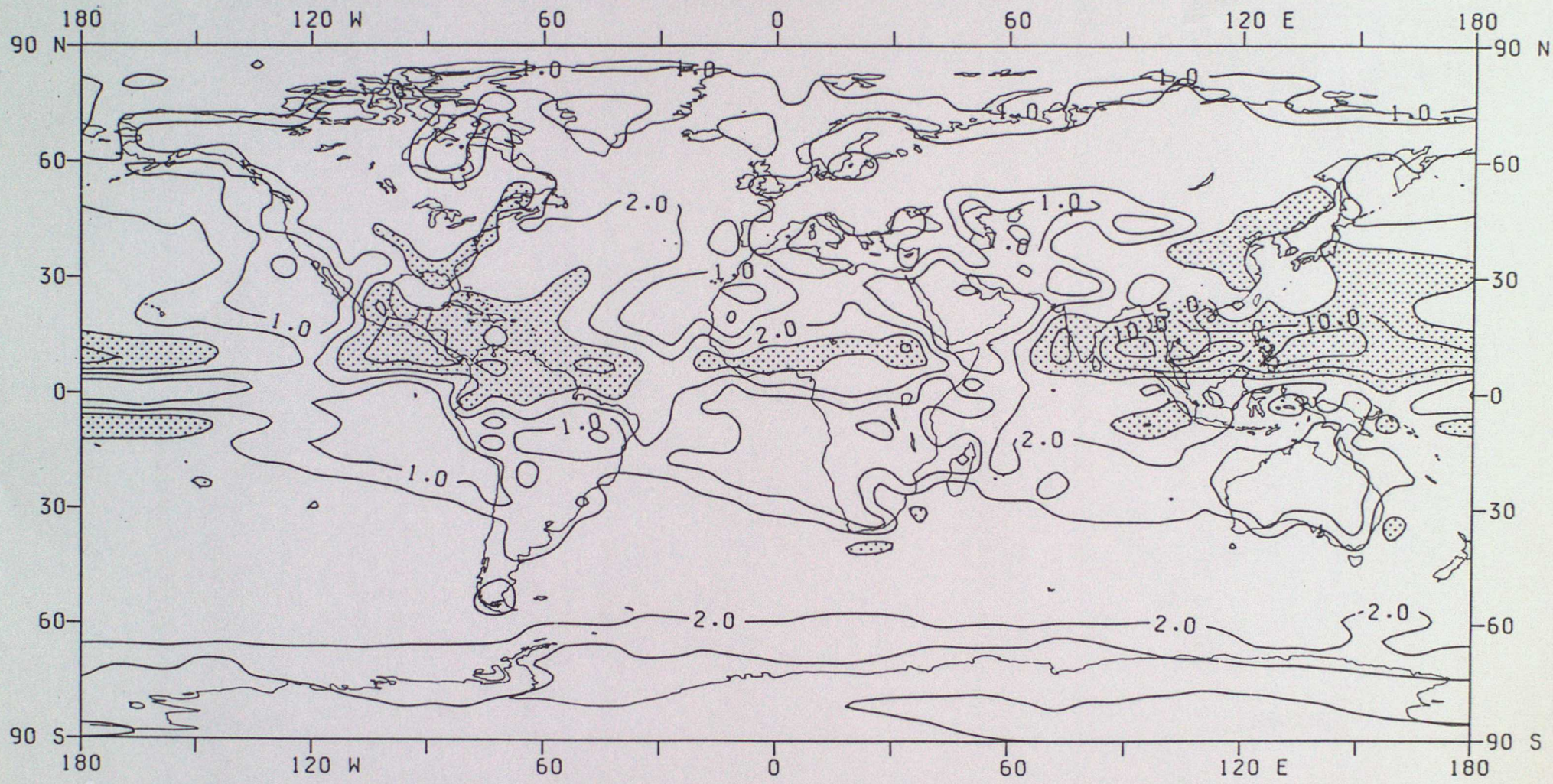

Figure 6(a)

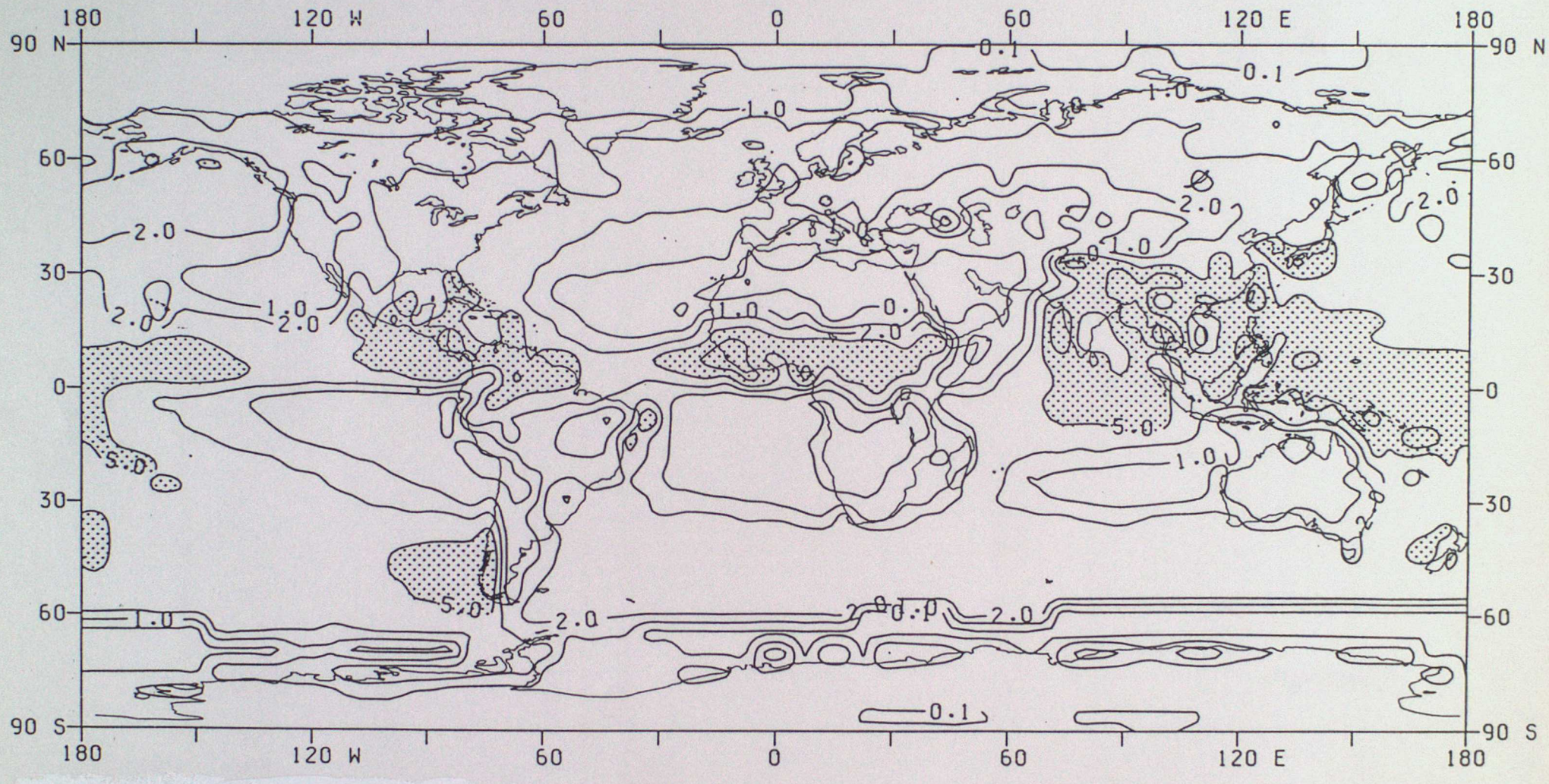

Figure 6(b)

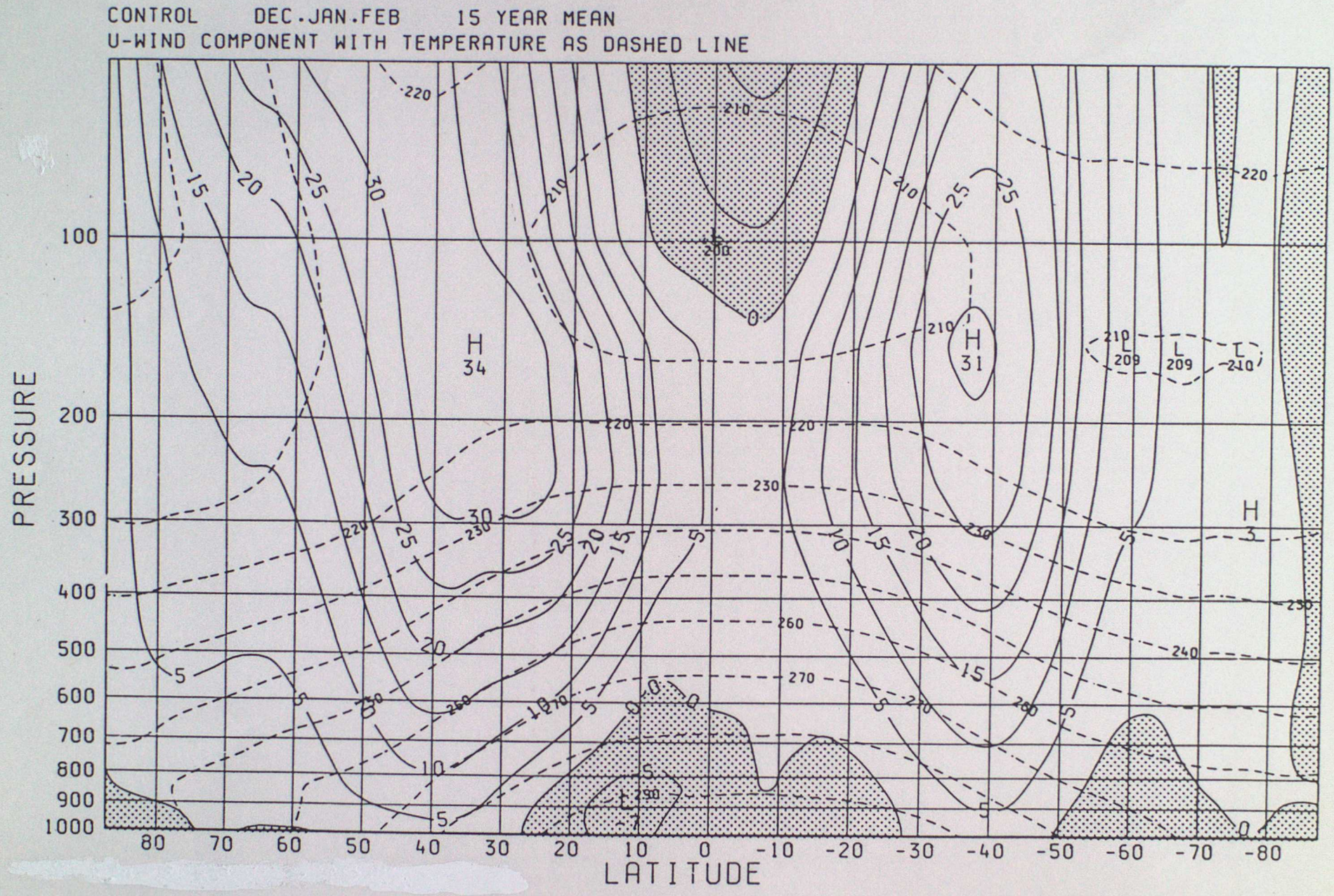
CONTROL DEC.JAN.FEB 15 YEAR MEAN
U-WIND COMPONENT WITH TEMPERATURE AS DASHED LINE
PRESSURE
100
200
300
400
500
600
700
800
900
1000
80 70 60 50 40 30 20 10 0 -10 -20 -30 -40 -50 -60 -70 -80
LATITUDE
H 34
H 31
L 209
L 209
L 210
H 3

Figure 7(a)

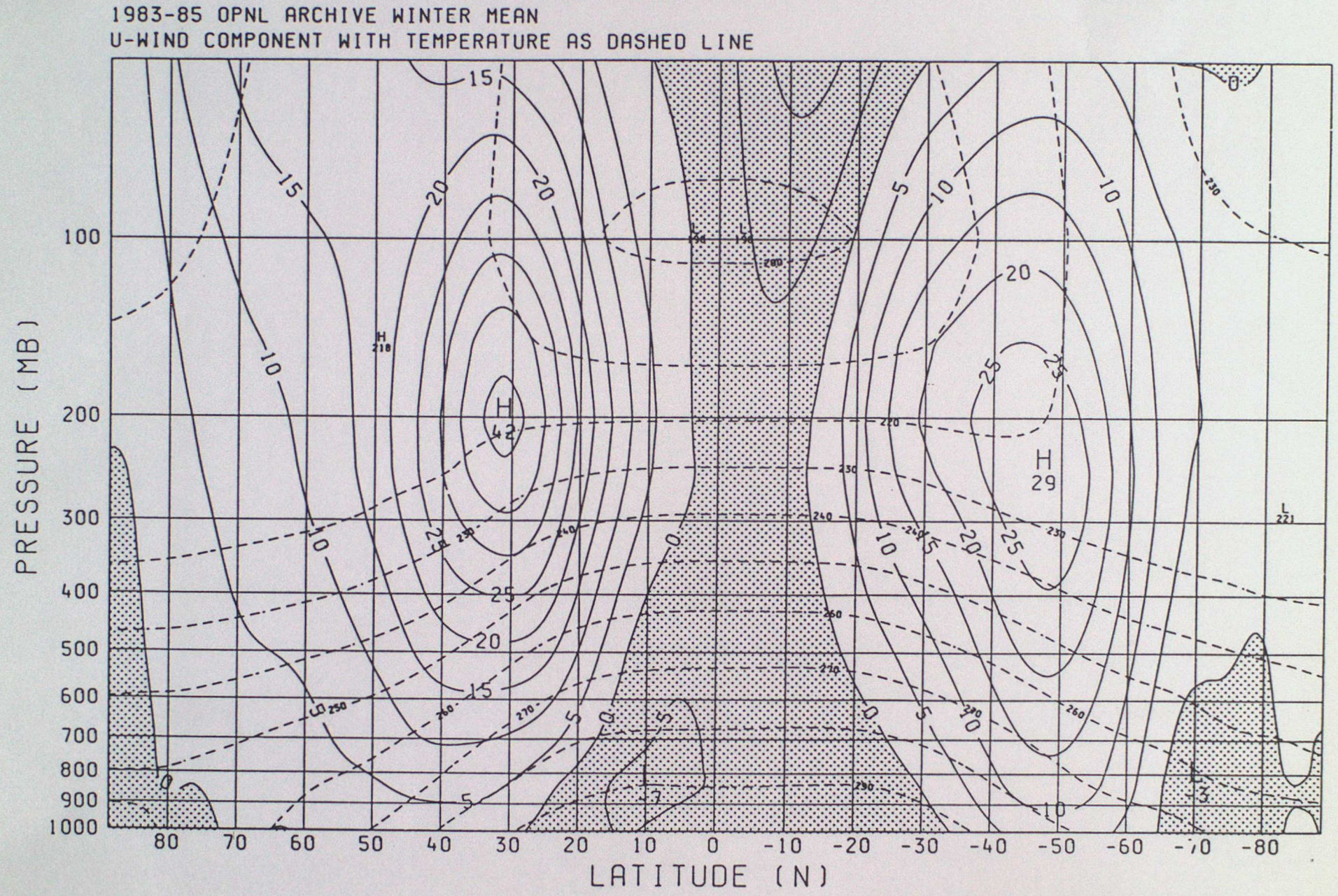
1983-85 OPNL ARCHIVE WINTER MEAN
U-WIND COMPONENT WITH TEMPERATURE AS DASHED LINE
PRESSURE (MB)
100
200
300
400
500
600
700
800
900
1000
80
70
60
50
40
30
20
10
0
-10
-20
-30
-40
-50
-60
-70
-80
LATITUDE (N)

Figure 7(b)

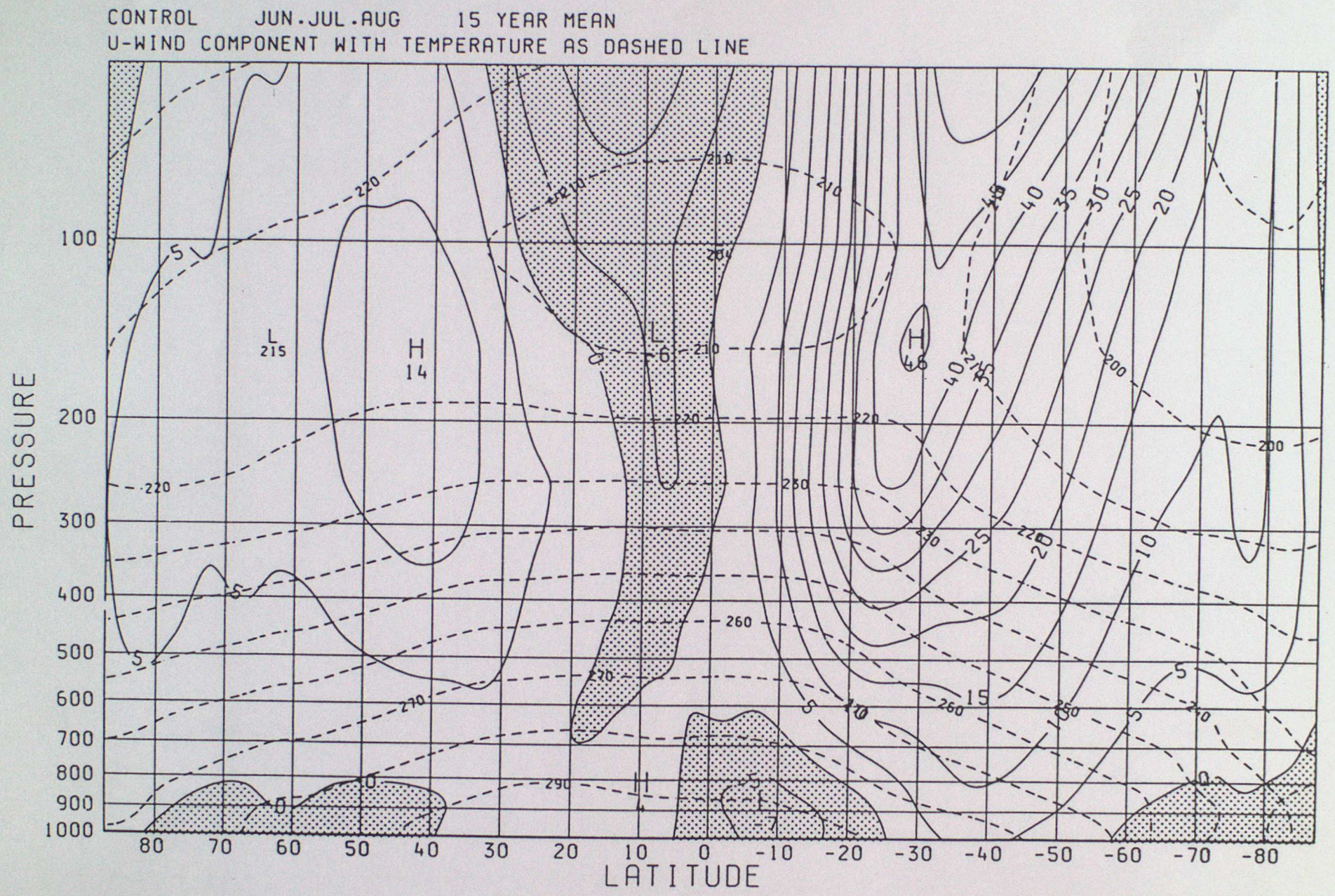
CONTROL JUN.JUL.AUG 15 YEAR MEAN
U-WIND COMPONENT WITH TEMPERATURE AS DASHED LINE
PRESSURE
100
200
300
400
500
600
700
800
900
1000
80 70 60 50 40 30 20 10 0 -10 -20 -30 -40 -50 -60 -70 -80
LATITUDE
L 215
H 14
L 6
H 45

Figure 8(a)

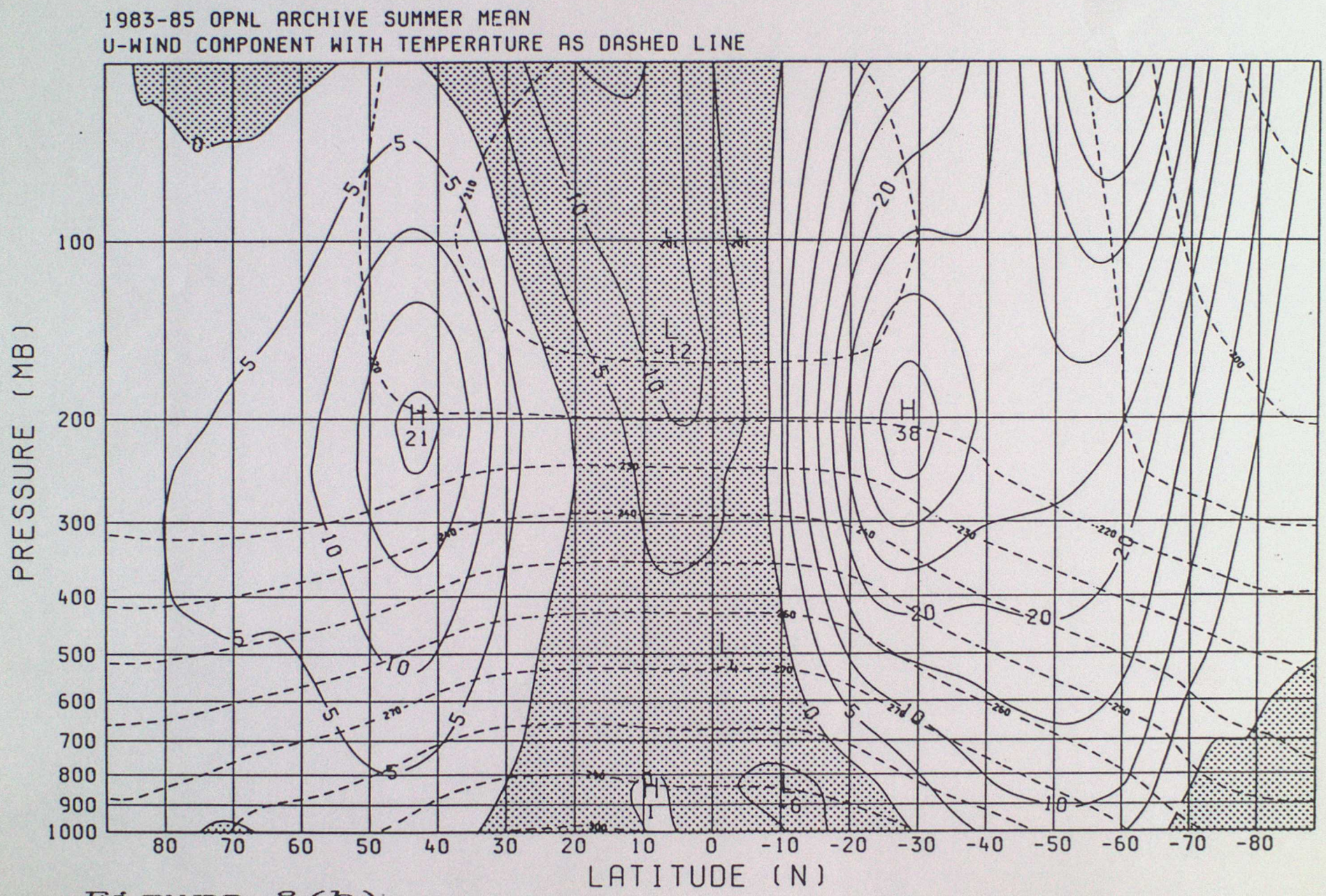
1983-85 OPNL ARCHIVE SUMMER MEAN
U-WIND COMPONENT WITH TEMPERATURE AS DASHED LINE
PRESSURE (MB)
100
200
300
400
500
600
700
800
900
1000
80 70 60 50 40 30 20 10 0 -10 -20 -30 -40 -50 -60 -70 -80
LATITUDE (N)

Figure 8(b)

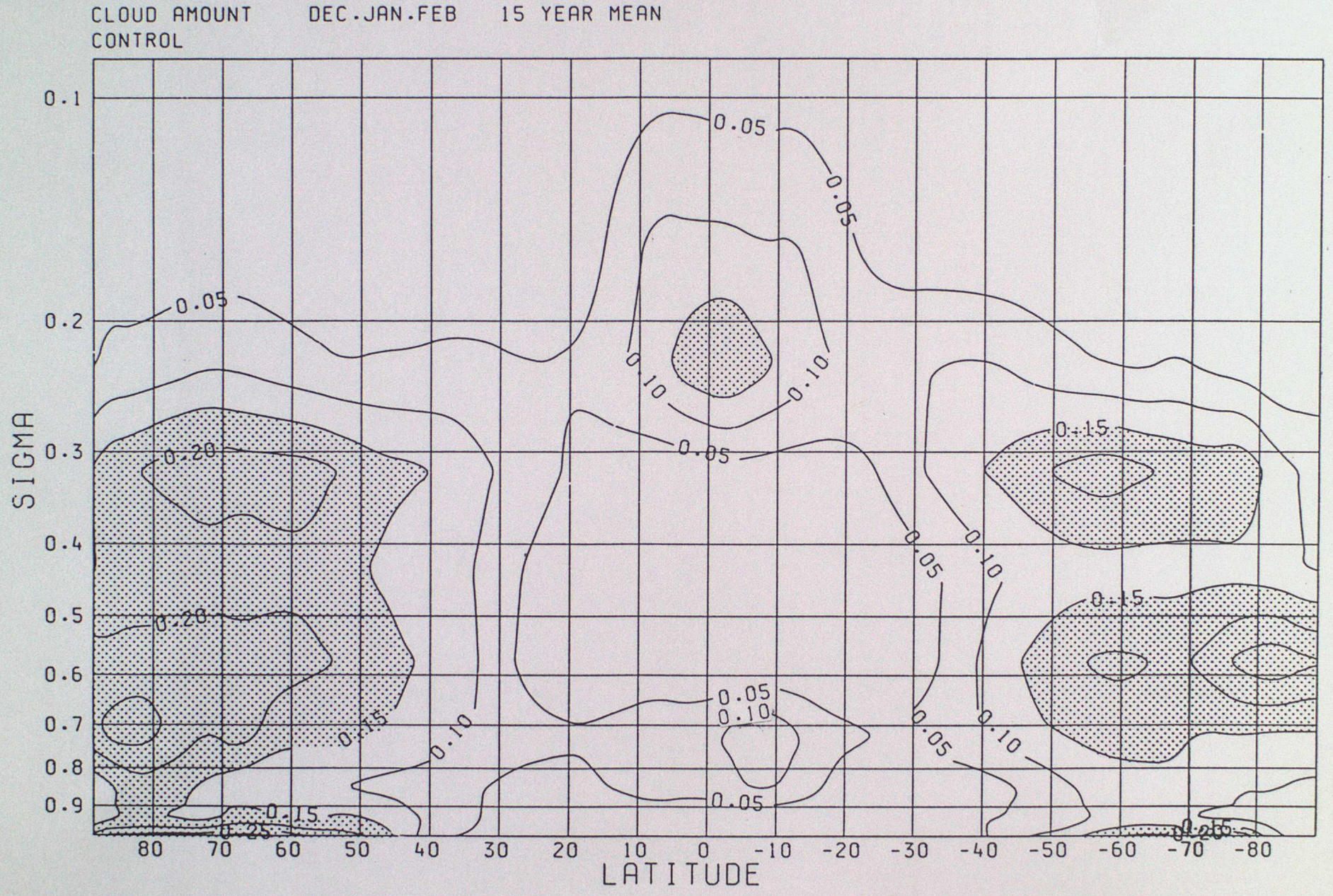
CLOUD AMOUNT DEC.JAN.FEB 15 YEAR MEAN
CONTROL
SIGMA
0.1
0.2
0.3
0.4
0.5
0.6
0.7
0.8
0.9
0.05
0.10
0.15
0.20
0.25
80 70 60 50 40 30 20 10 0 -10 -20 -30 -40 -50 -60 -70 -80
LATITUDE

Figure 9(a)

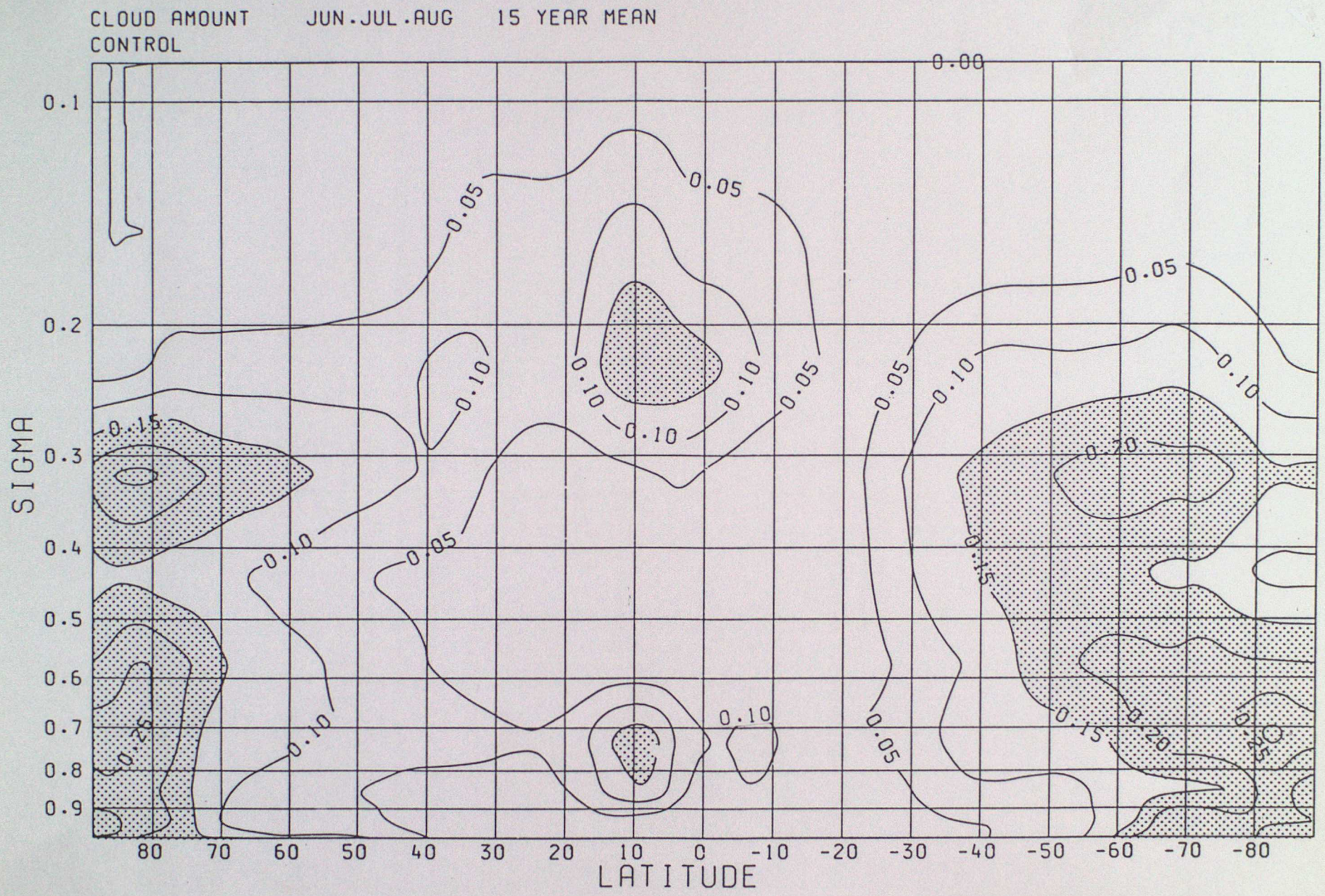
CLOUD AMOUNT JUN.JUL.AUG 15 YEAR MEAN
CONTROL
SIGMA
0.1
0.2
0.3
0.4
0.5
0.6
0.7
0.8
0.9
80 70 60 50 40 30 20 10 0 -10 -20 -30 -40 -50 -60 -70 -80
LATITUDE
0.00
0.05
0.10
0.15
0.20
0.25

Figure 9(b)

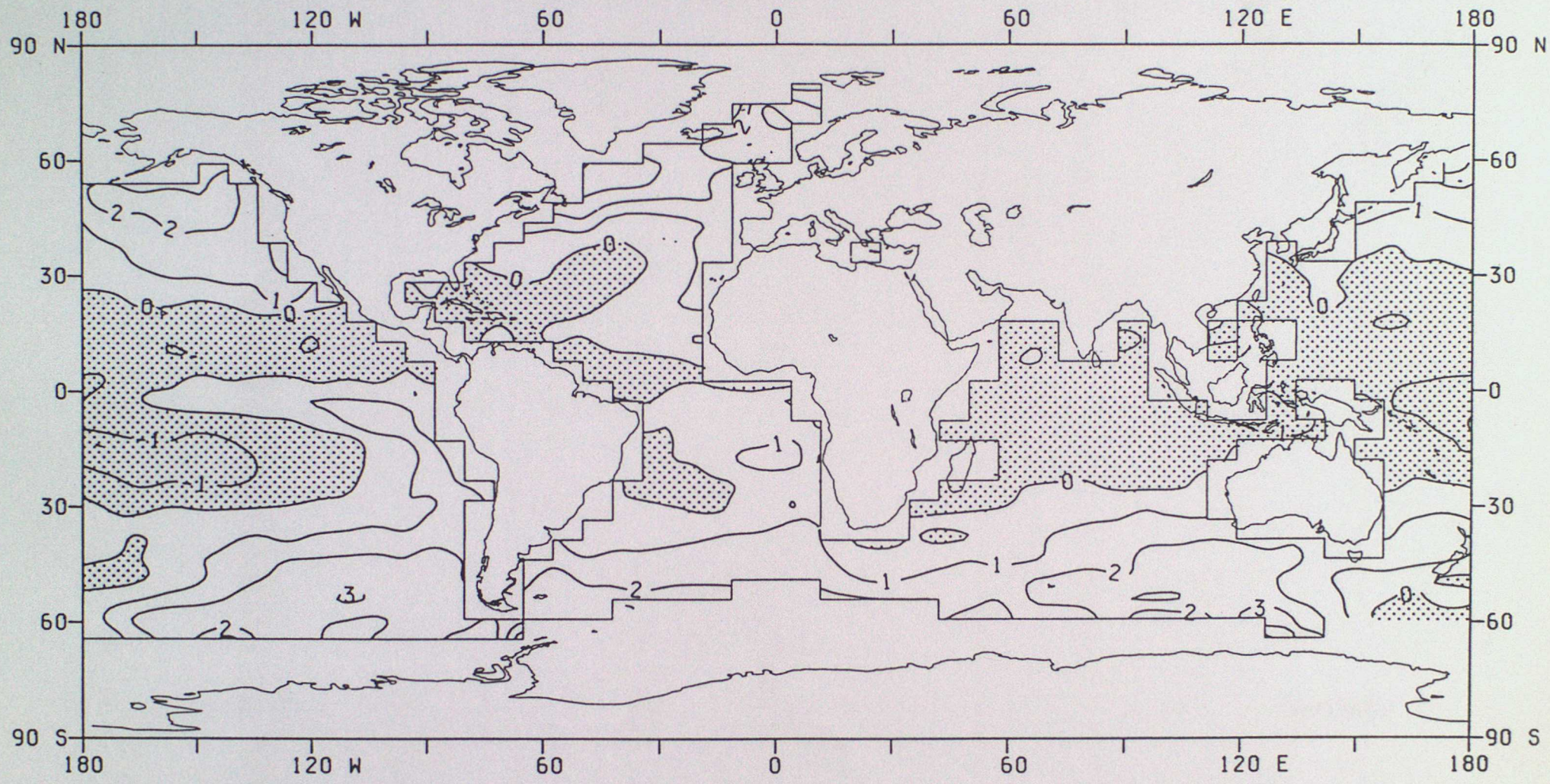

Figure 10(a)

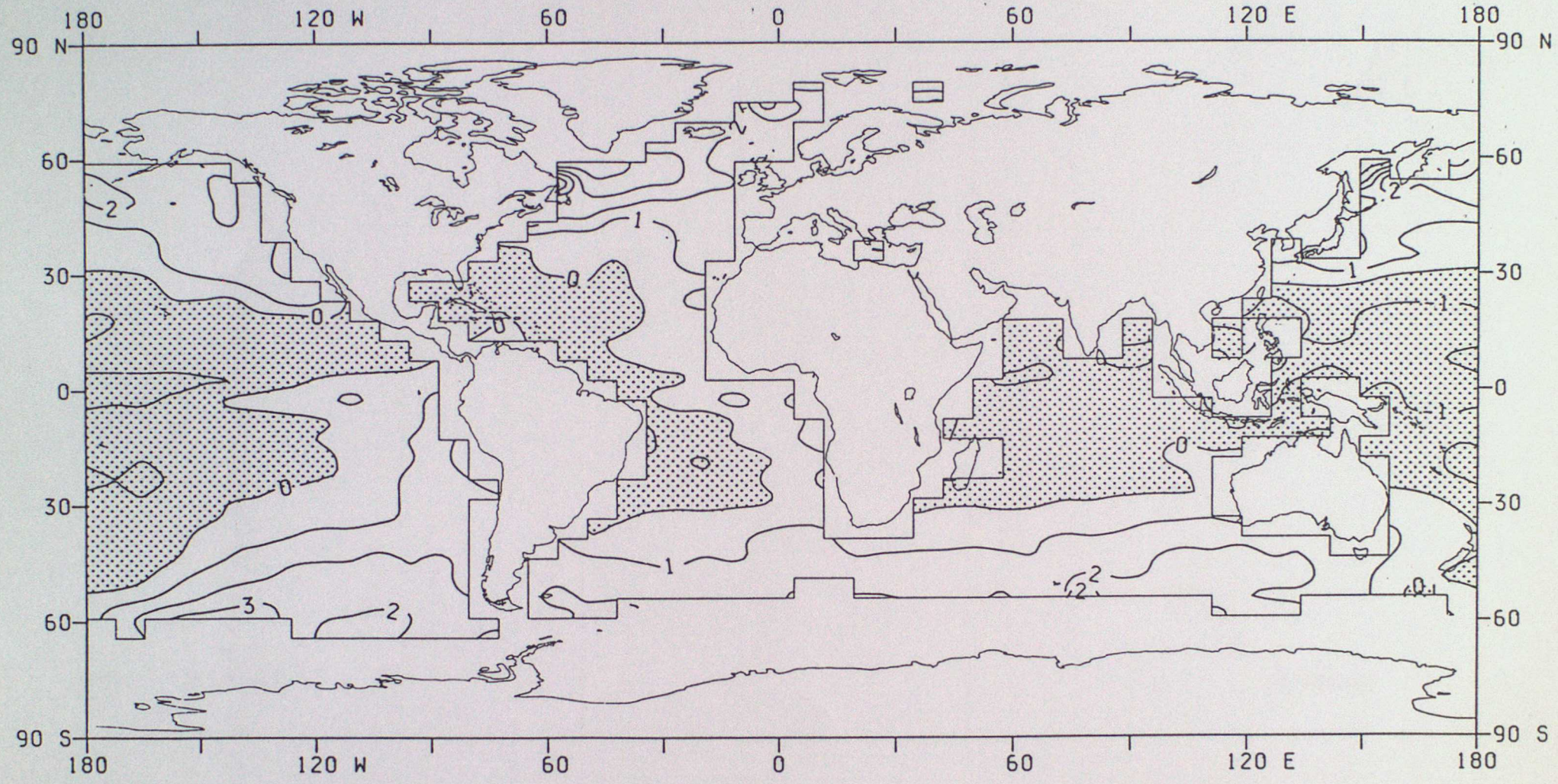

Figure 10(b)

SEA-ICE FEB 15 YEAR MEAN CONTROL

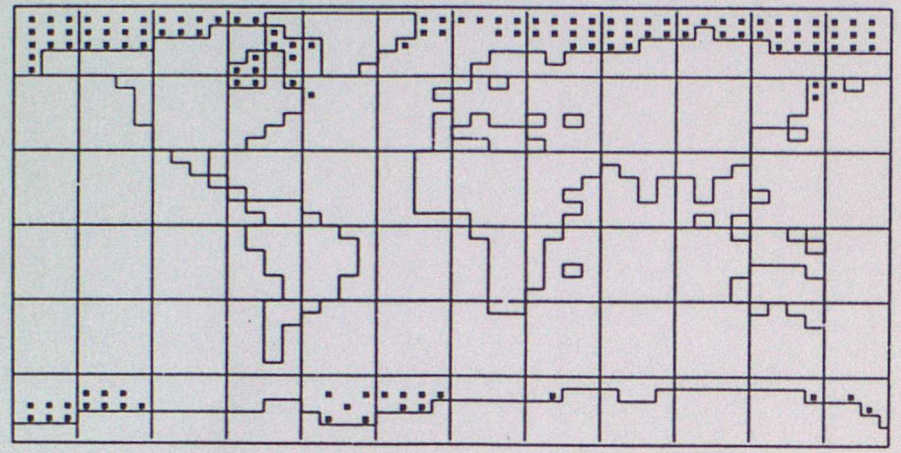

(a)

SEA-ICE AUG 15 YEAR MEAN CONTROL

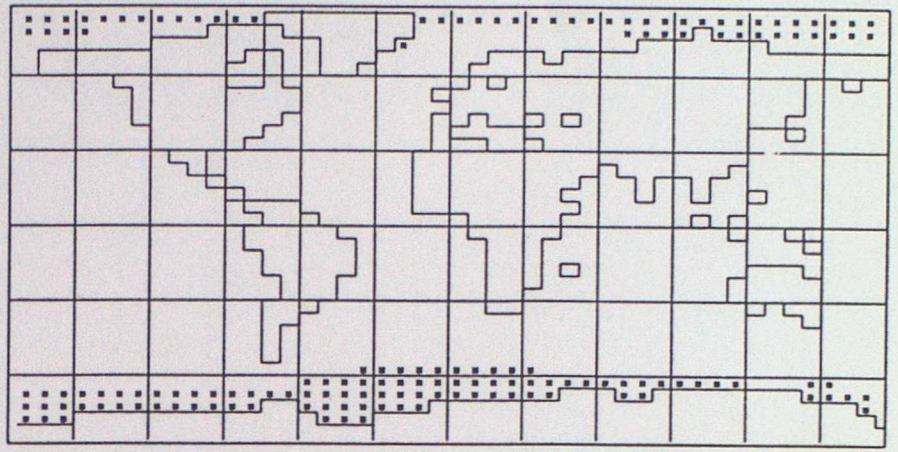

(c)

SEA-ICE MAY 15 YEAR MEAN CONTROL

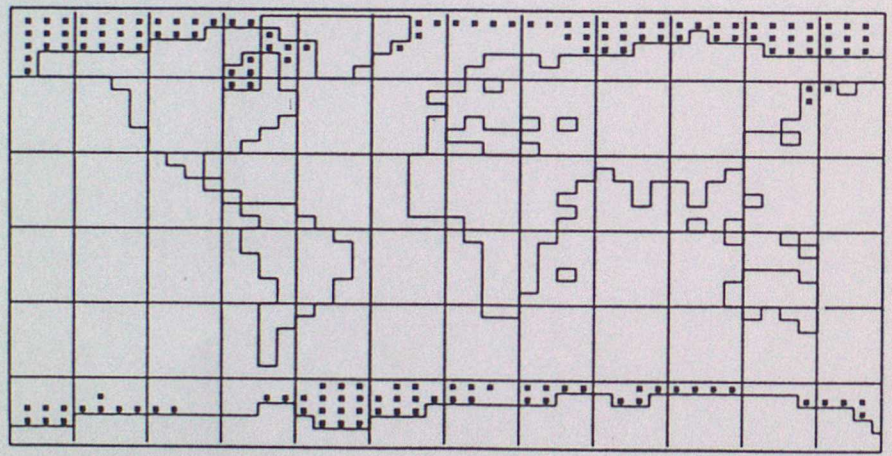

(b)

SEA-ICE NOV 15 YEAR MEAN CONTROL

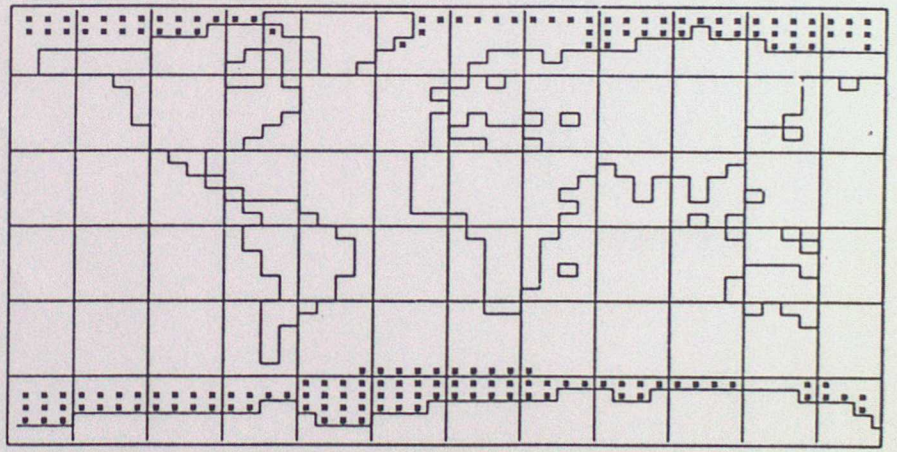

(d)

Figure 11

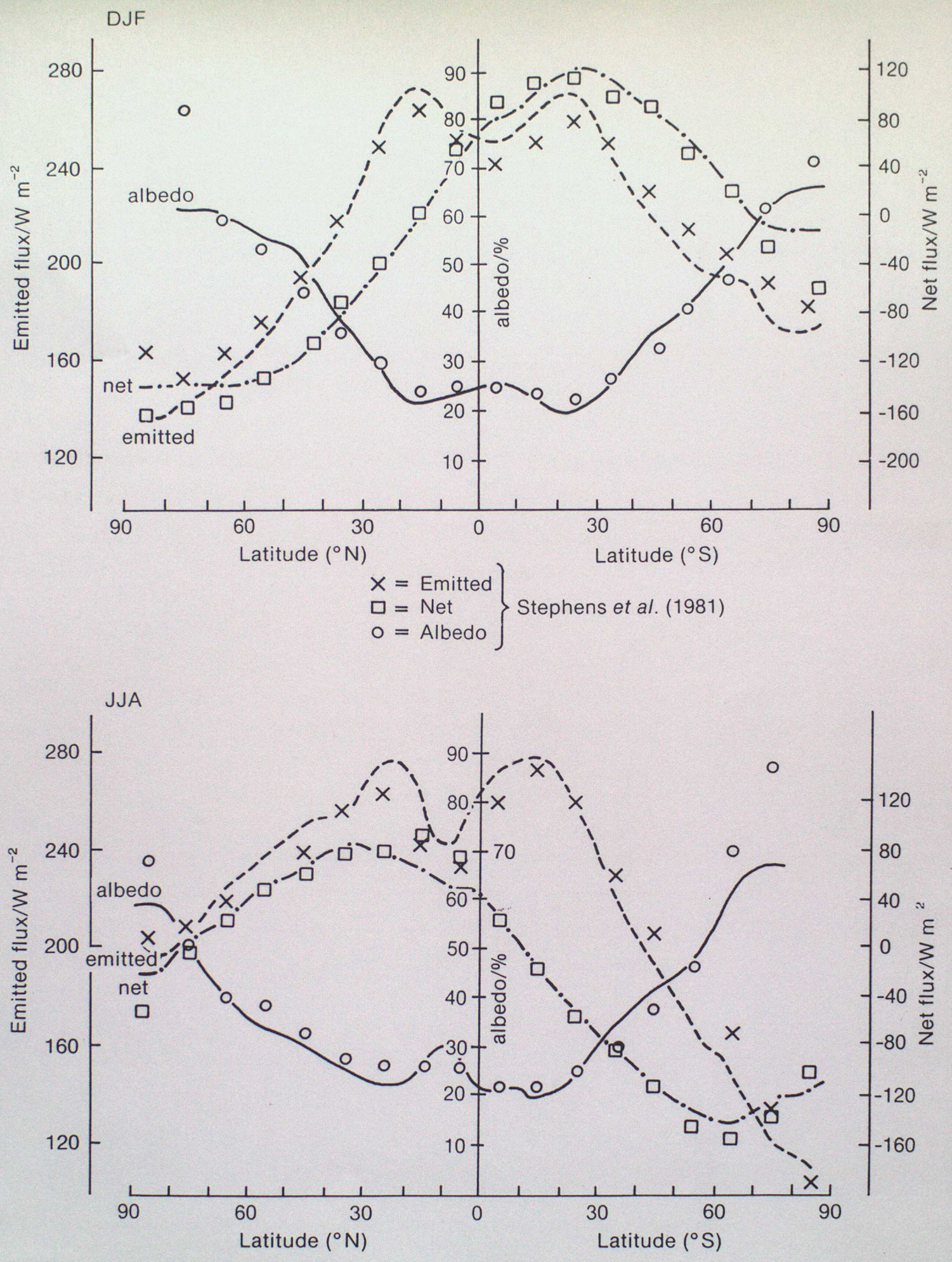
DJF
Emitted flux/W m^{-2}
albedo/%
Net flux/W m^{-2}
albedo
net
emitted
Latitude (°N)
Latitude (°S)
× = Emitted
□ = Net
○ = Albedo
Stephens *et al.* (1981)
JJA
Emitted flux/W m^{-2}
albedo/%
Net flux/W m^{-2}
albedo
emitted
net
Latitude (°N)
Latitude (°S)

Figure 12

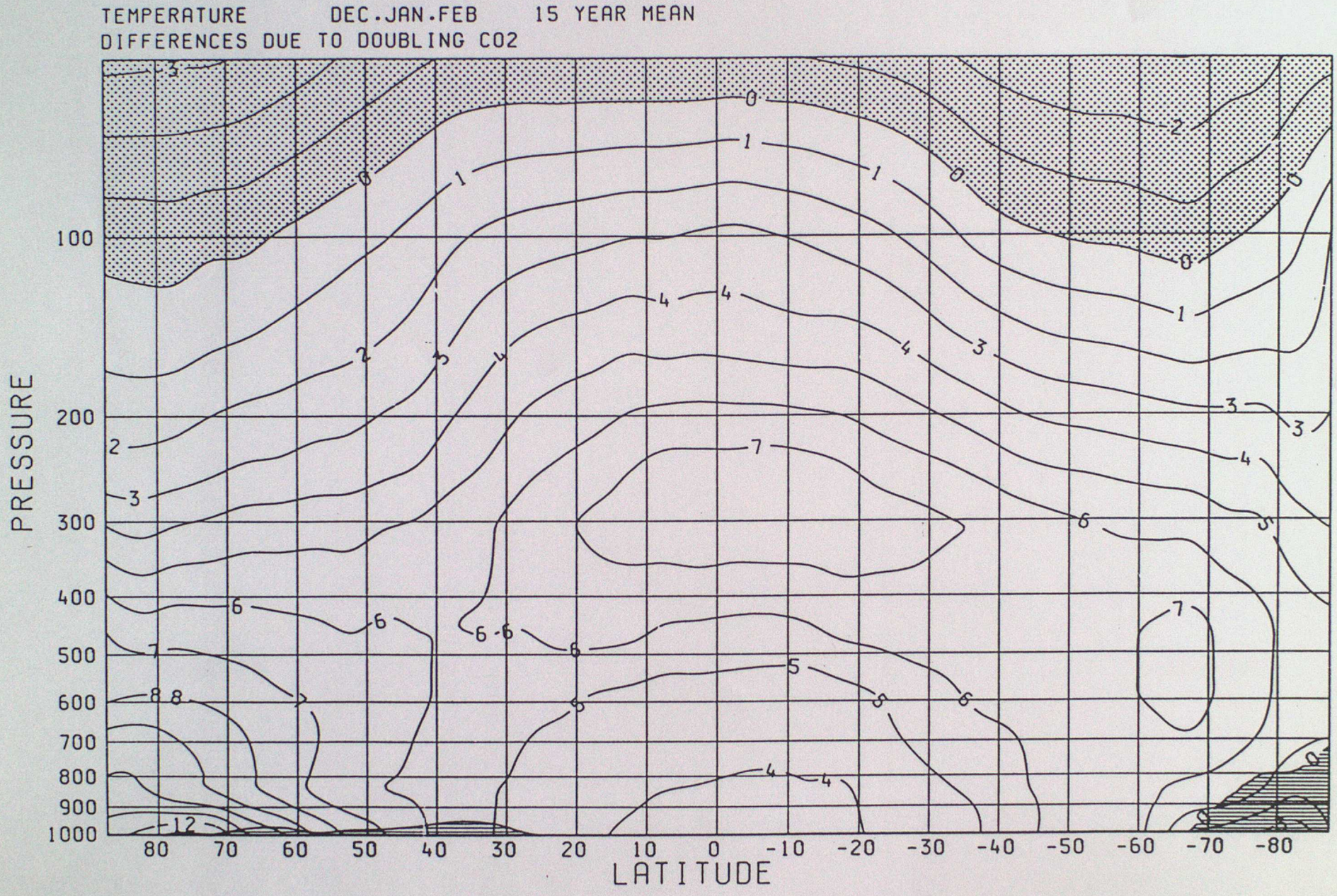
TEMPERATURE DEC.JAN.FEB 15 YEAR MEAN
DIFFERENCES DUE TO DOUBLING CO2
PRESSURE
100
200
300
400
500
600
700
800
900
1000
80 70 60 50 40 30 20 10 0 -10 -20 -30 -40 -50 -60 -70 -80
LATITUDE

Figure 13(a)

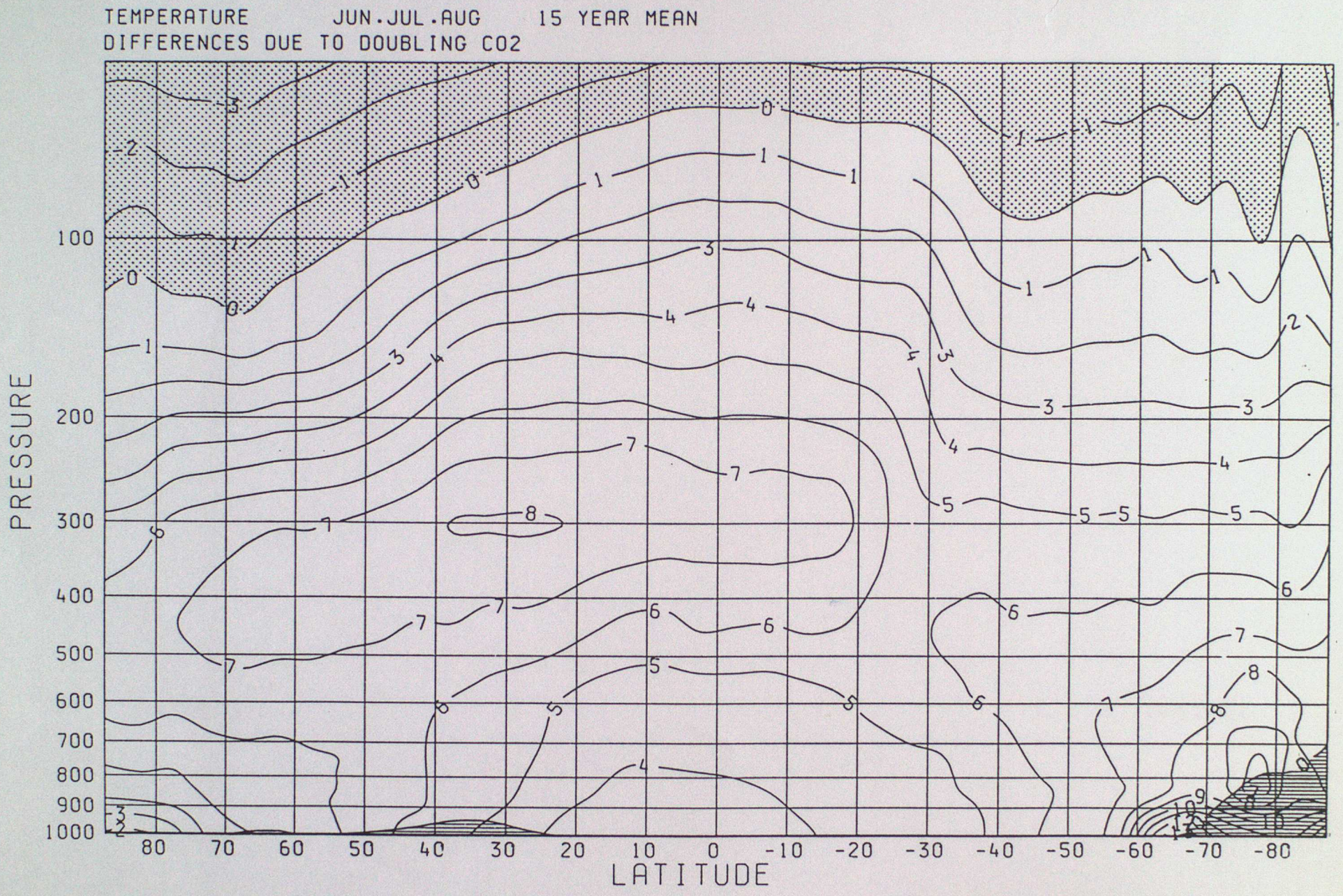
TEMPERATURE JUN.JUL.AUG 15 YEAR MEAN
DIFFERENCES DUE TO DOUBLING CO2
PRESSURE
100
200
300
400
500
600
700
800
900
1000
80 70 60 50 40 30 20 10 0 -10 -20 -30 -40 -50 -60 -70 -80
LATITUDE

Figure 13(b)

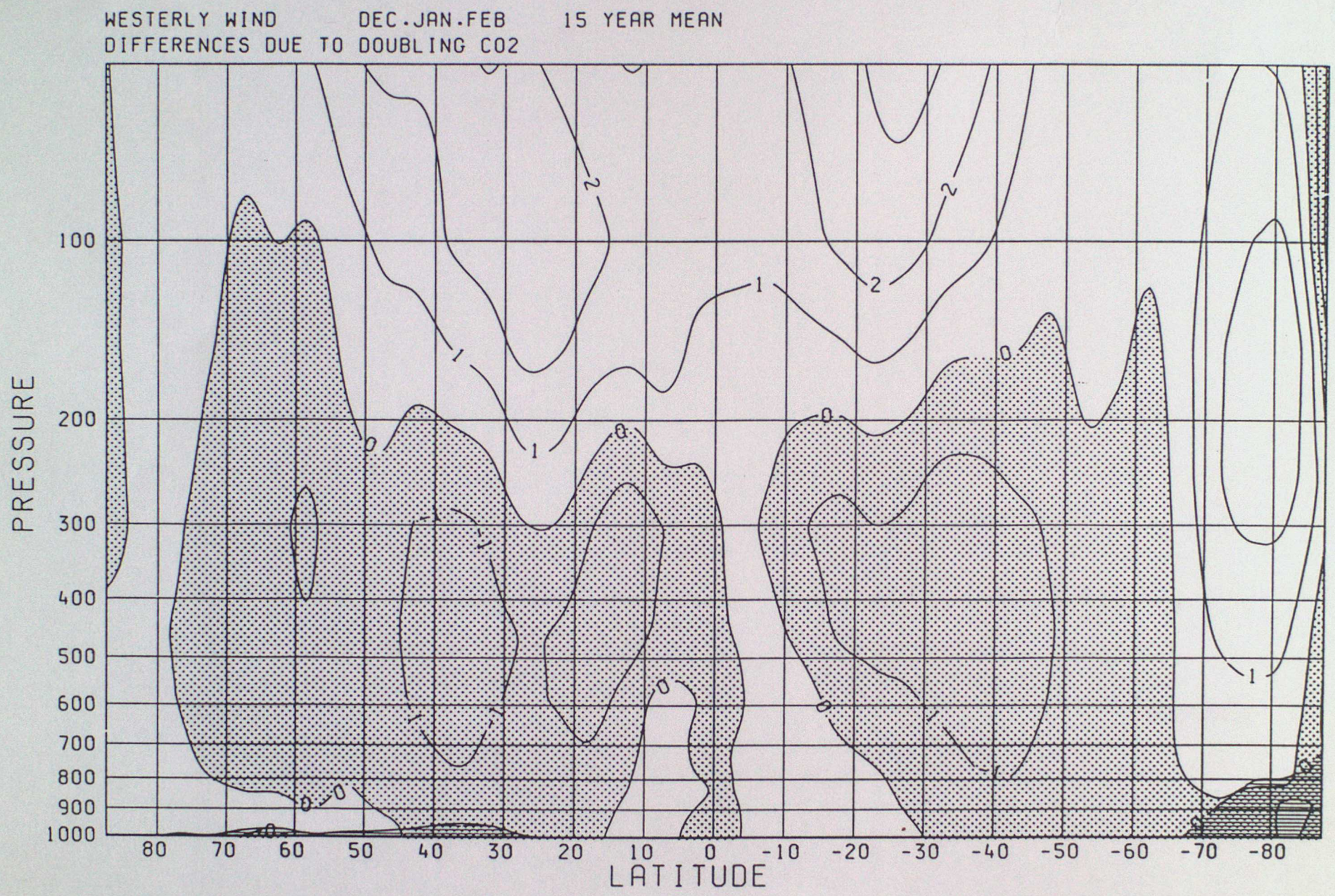
WESTERLY WIND DEC.JAN.FEB 15 YEAR MEAN
DIFFERENCES DUE TO DOUBLING CO2
PRESSURE
100
200
300
400
500
600
700
800
900
1000
80 70 60 50 40 30 20 10 0 -10 -20 -30 -40 -50 -60 -70 -80
LATITUDE

Figure 14(a)

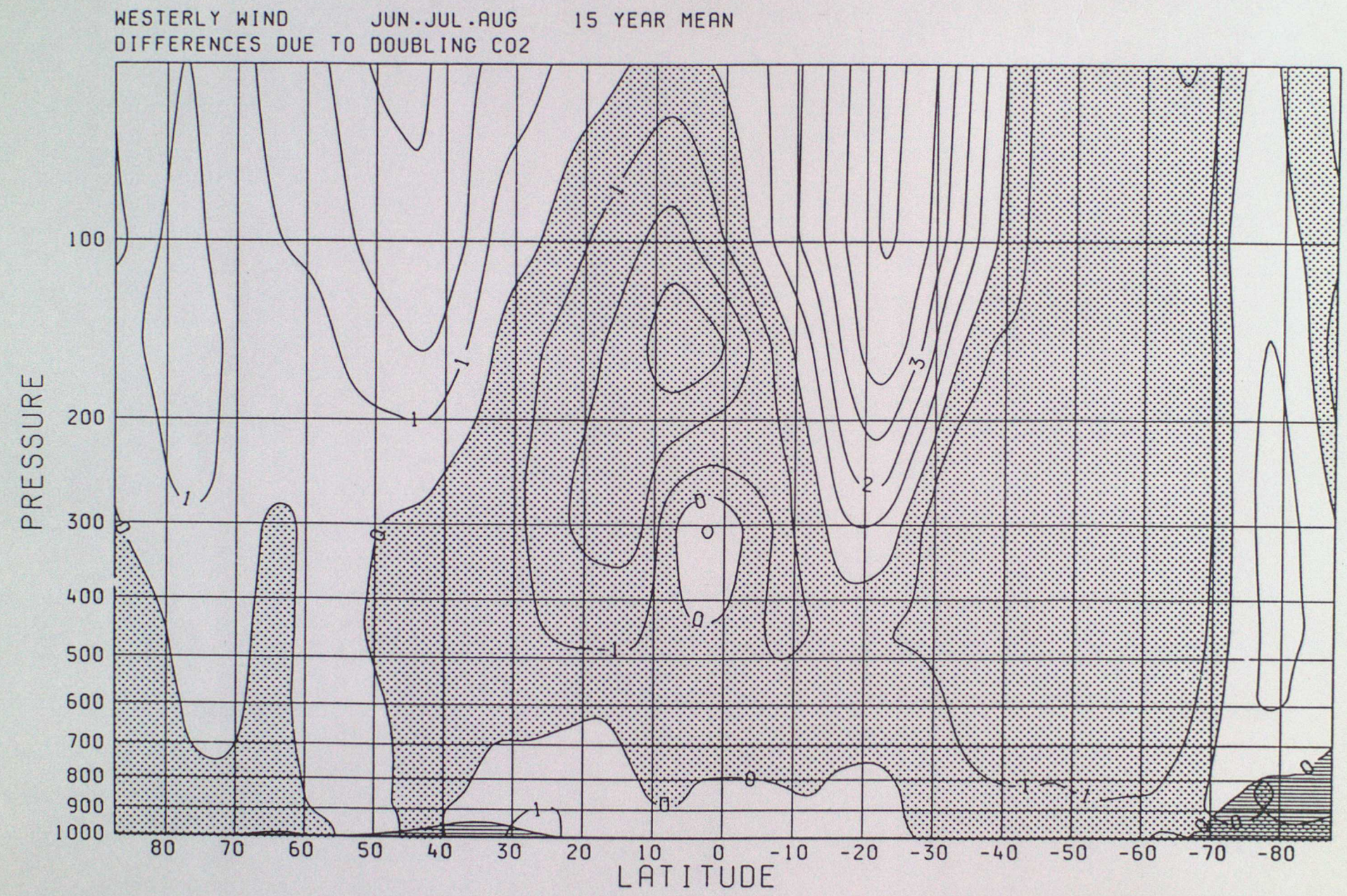
WESTERLY WIND JUN.JUL.AUG 15 YEAR MEAN
DIFFERENCES DUE TO DOUBLING CO2
PRESSURE
100
200
300
400
500
600
700
800
900
1000
80 70 60 50 40 30 20 10 0 -10 -20 -30 -40 -50 -60 -70 -80
LATITUDE

Figure 14(b)

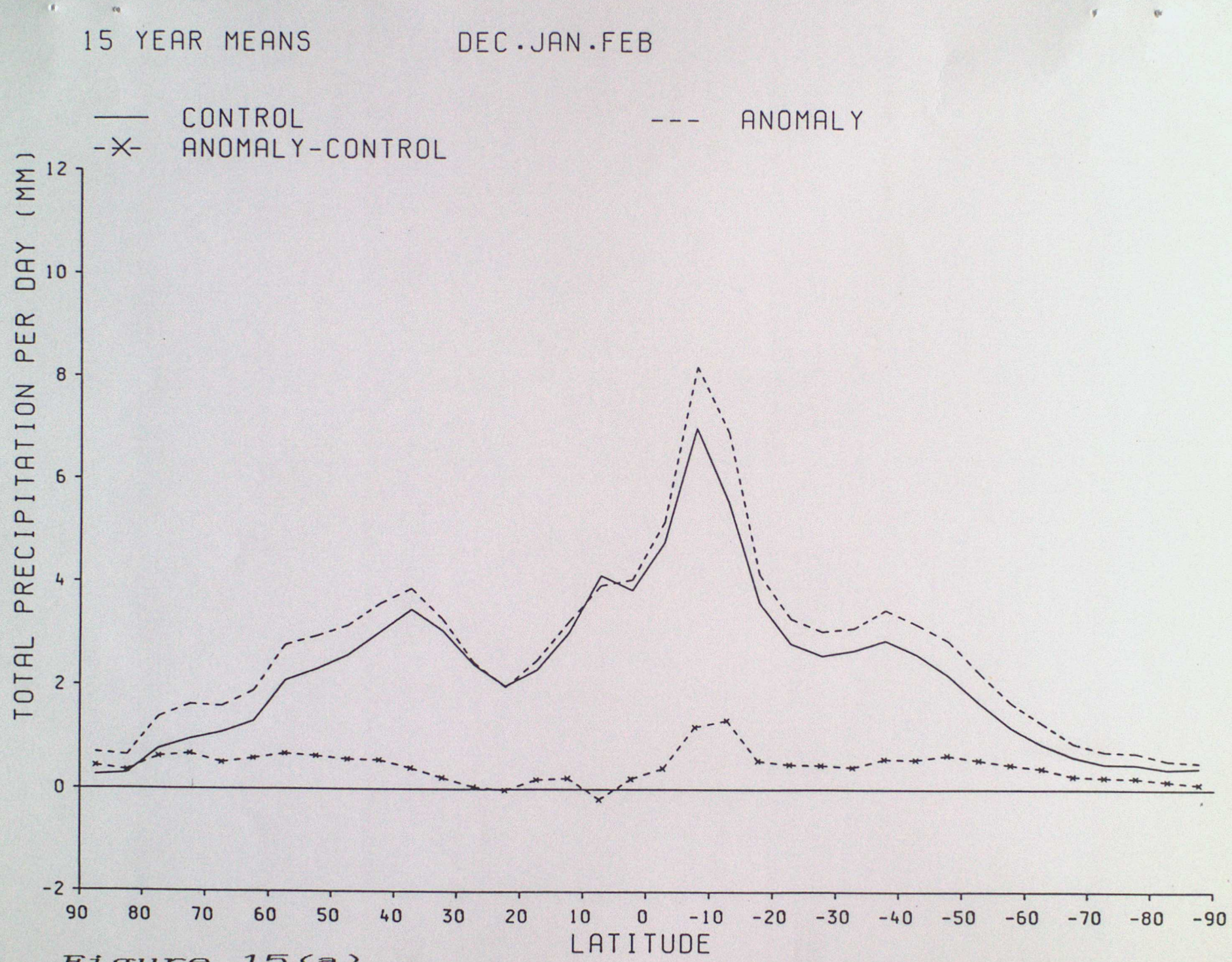
15 YEAR MEANS
DEC.JAN.FEB
CONTROL
ANOMALY
ANOMALY-CONTROL
TOTAL PRECIPITATION PER DAY (MM)
12
10
8
6
4
2
0
-2
90 80 70 60 50 40 30 20 10 0 -10 -20 -30 -40 -50 -60 -70 -80 -90
LATITUDE

Figure 15(a)

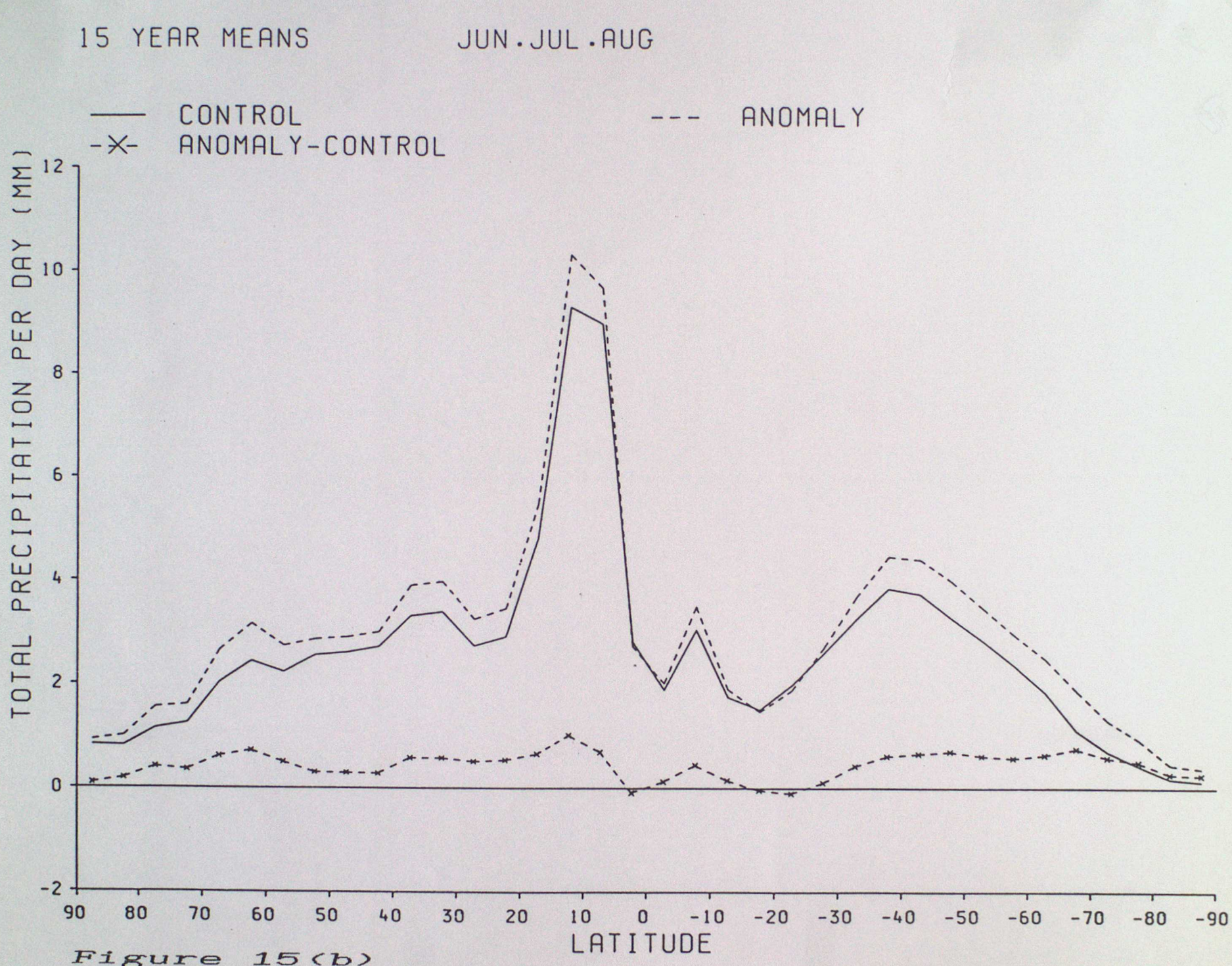
15 YEAR MEANS
JUN.JUL.AUG
CONTROL
ANOMALY
ANOMALY-CONTROL
TOTAL PRECIPITATION PER DAY (MM)
12
10
8
6
4
2
0
-2
90 80 70 60 50 40 30 20 10 0 -10 -20 -30 -40 -50 -60 -70 -80 -90
LATITUDE

Figure 15(b)

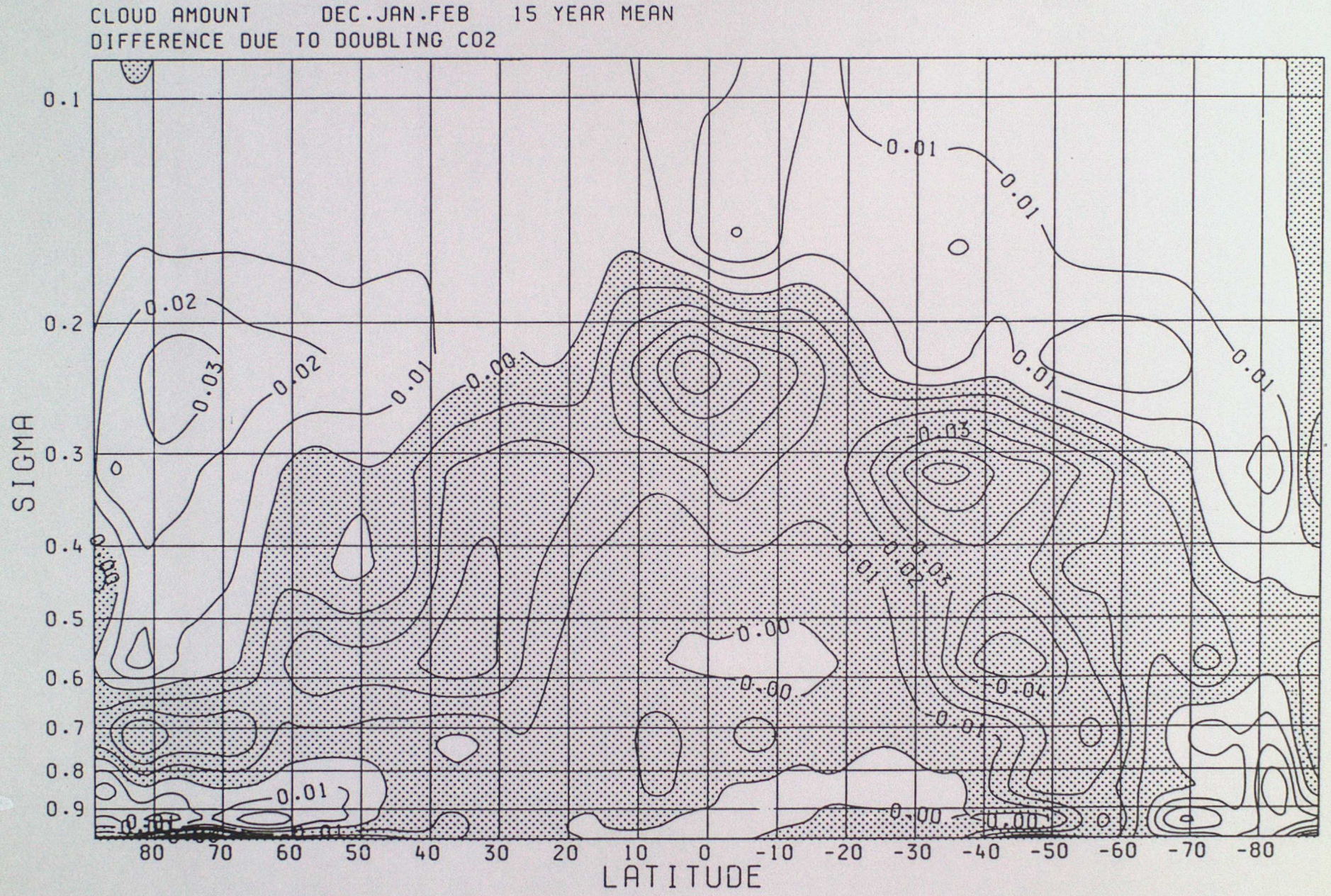
CLOUD AMOUNT DEC.JAN.FEB 15 YEAR MEAN
DIFFERENCE DUE TO DOUBLING CO2
SIGMA
0.1
0.2
0.3
0.4
0.5
0.6
0.7
0.8
0.9
80 70 60 50 40 30 20 10 0 -10 -20 -30 -40 -50 -60 -70 -80
LATITUDE

Figure 16(a)

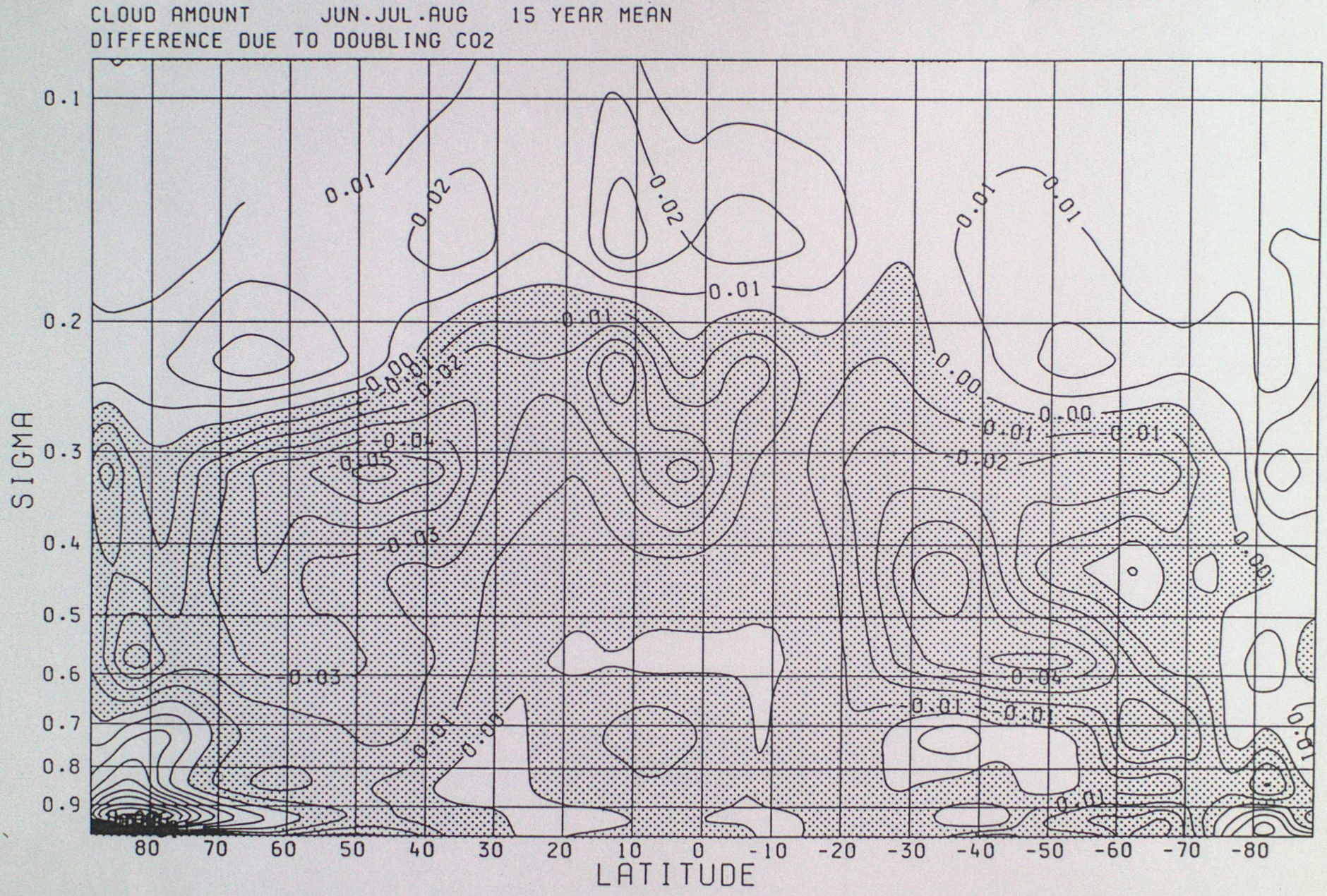
CLOUD AMOUNT JUN.JUL.AUG 15 YEAR MEAN
DIFFERENCE DUE TO DOUBLING CO2
SIGMA
0.1
0.2
0.3
0.4
0.5
0.6
0.7
0.8
0.9
80 70 60 50 40 30 20 10 0 -10 -20 -30 -40 -50 -60 -70 -80
LATITUDE

Figure 16(b)

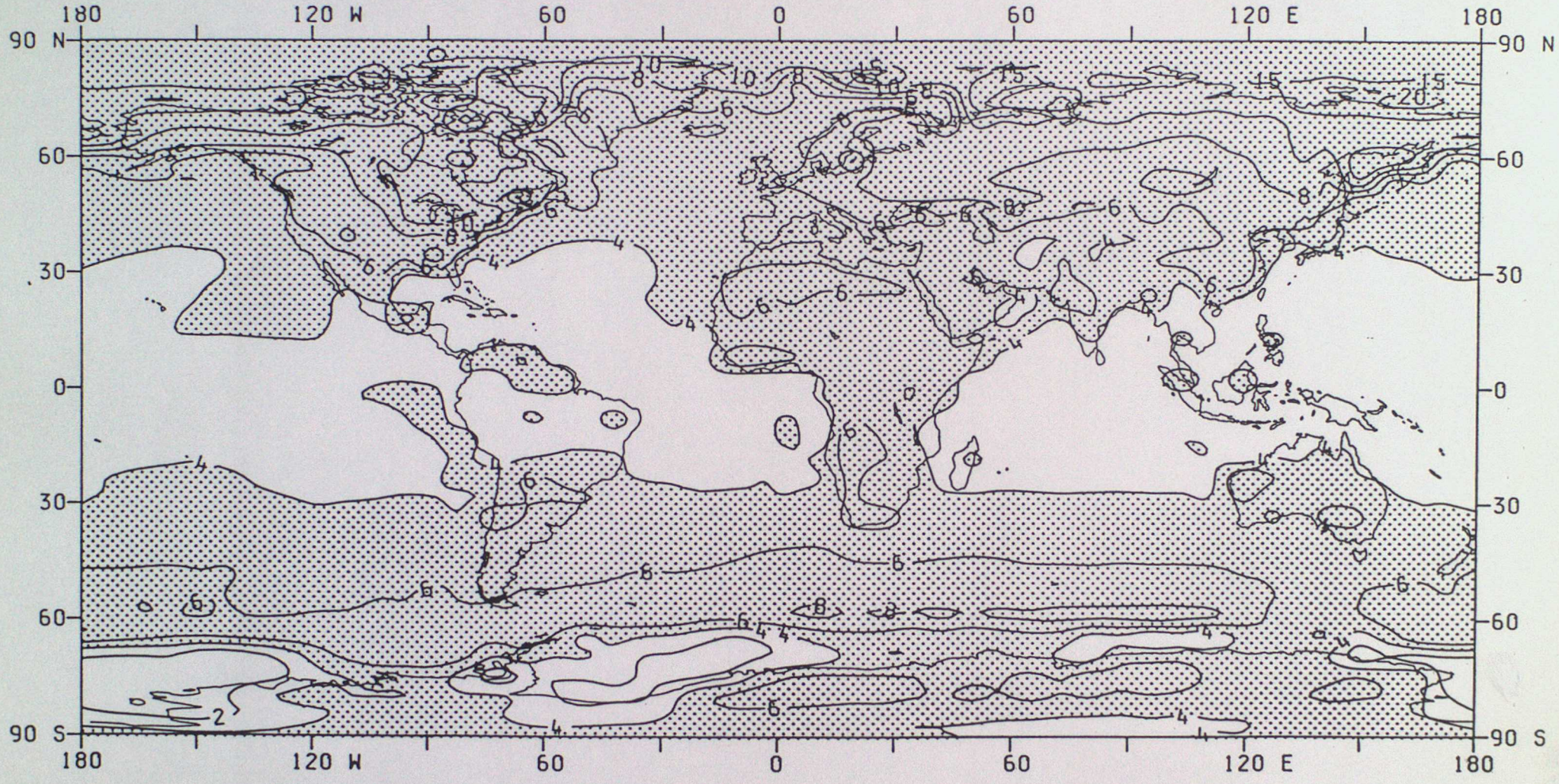

Figure 17(a)

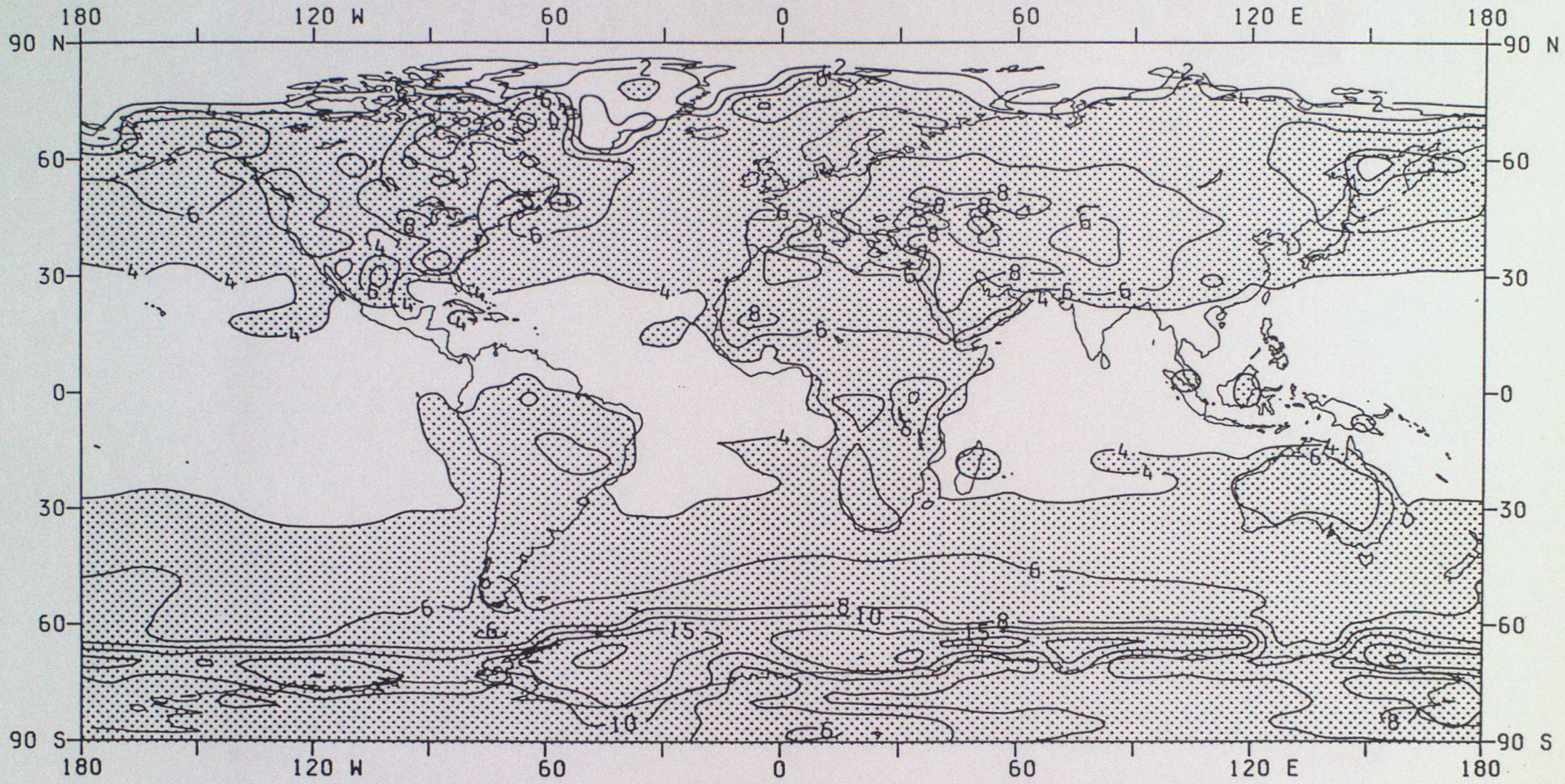

Figure 17(b)

SEA-ICE EXTENTS FEBRUARY
ANOMALY=0. CONTROL=X

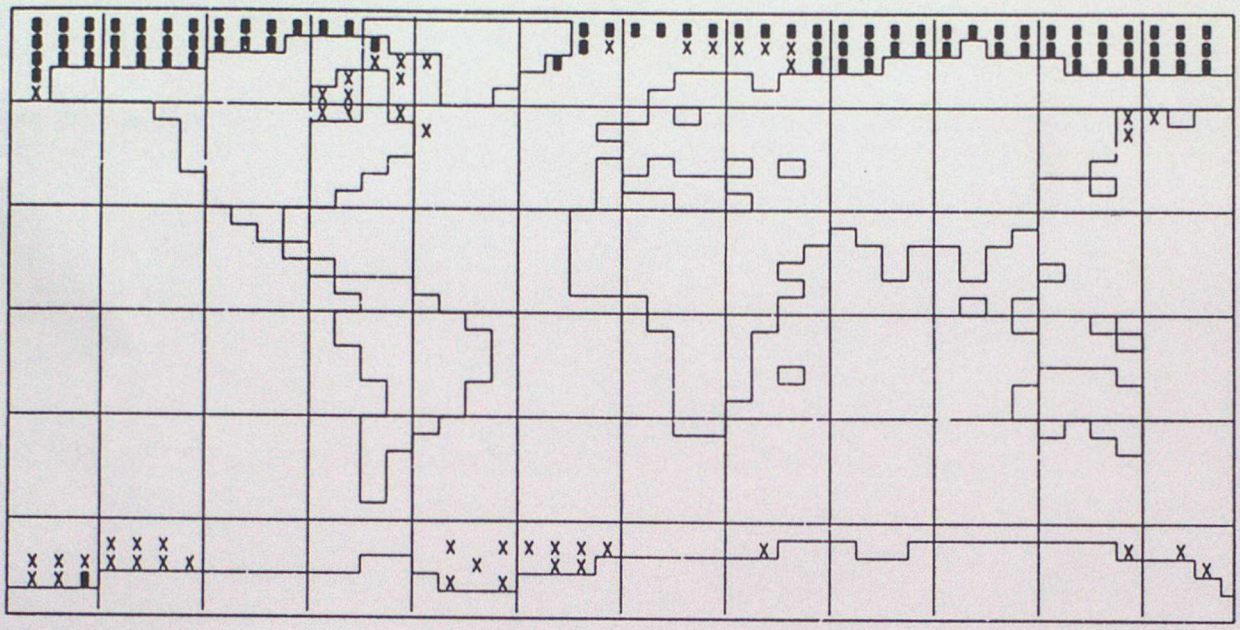

(a)

SEA-ICE EXTENTS AUGUST
ANOMALY=0. CONTROL=X

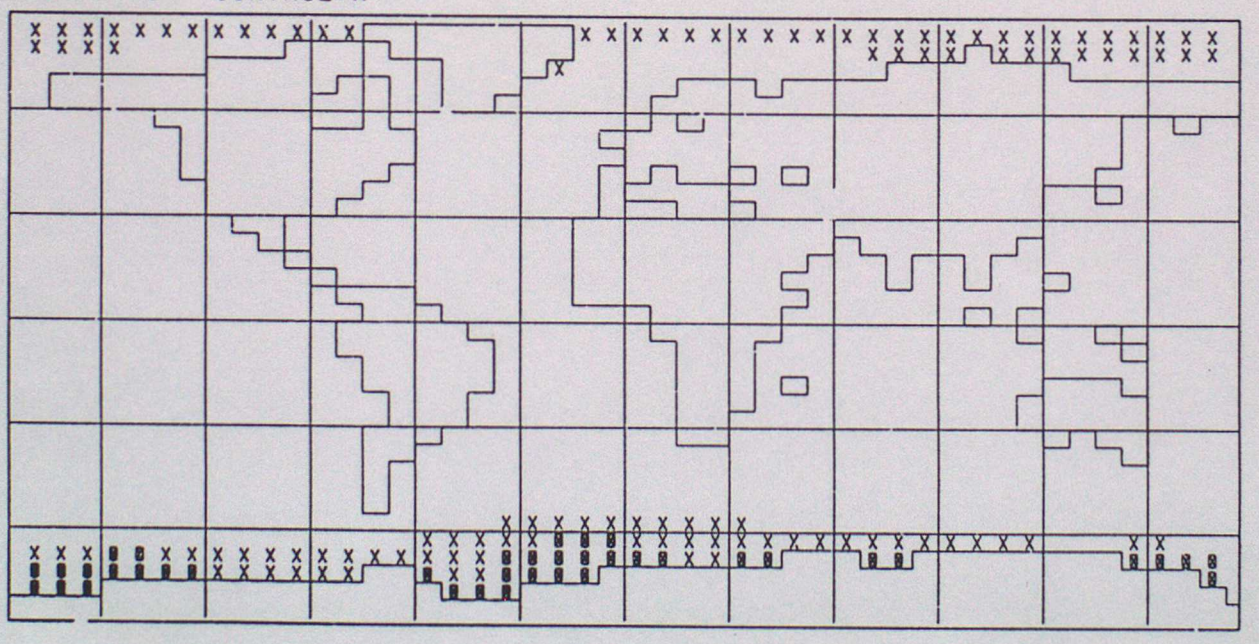

(b)

Figure 18

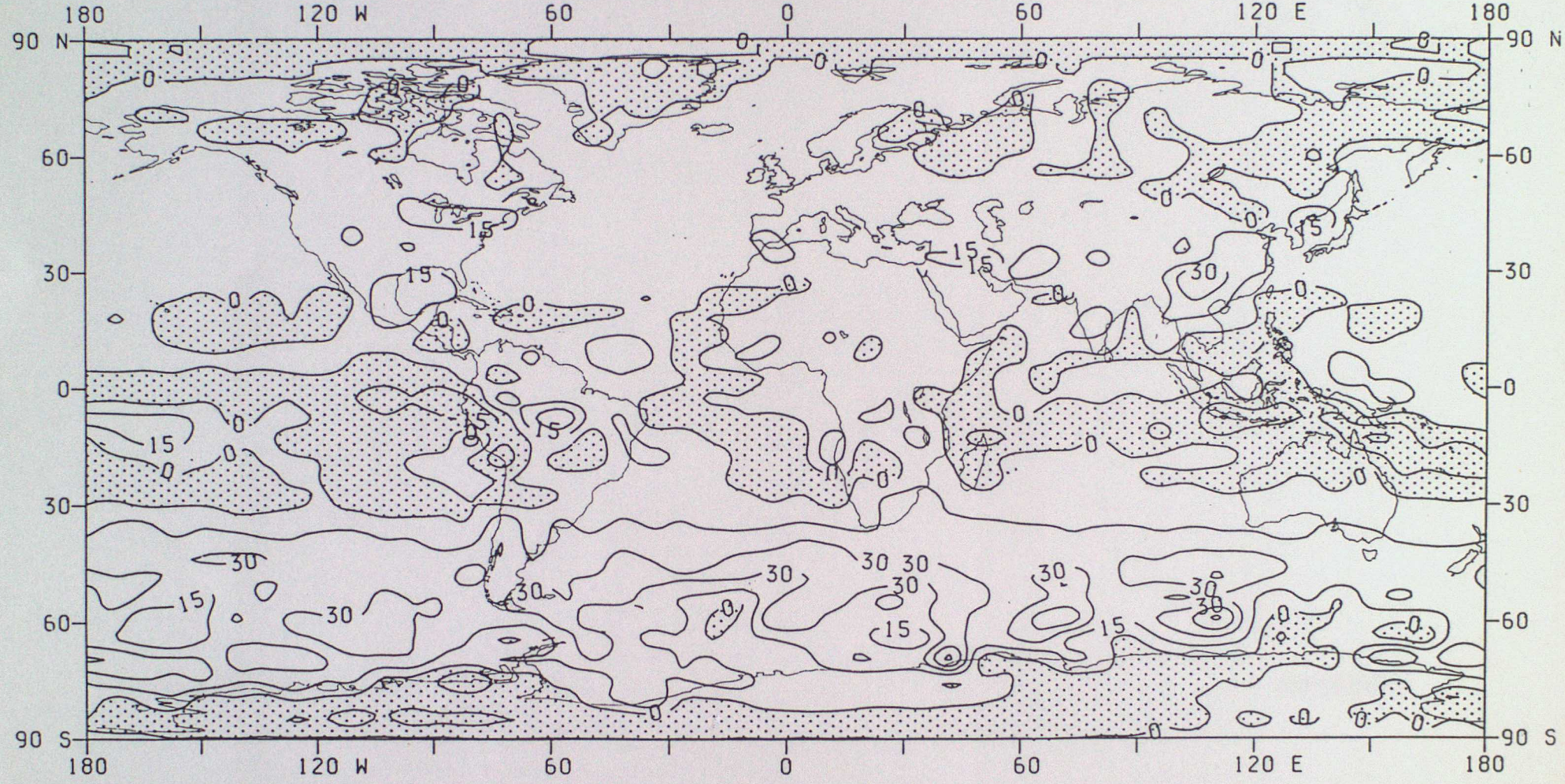

Figure 19(a)

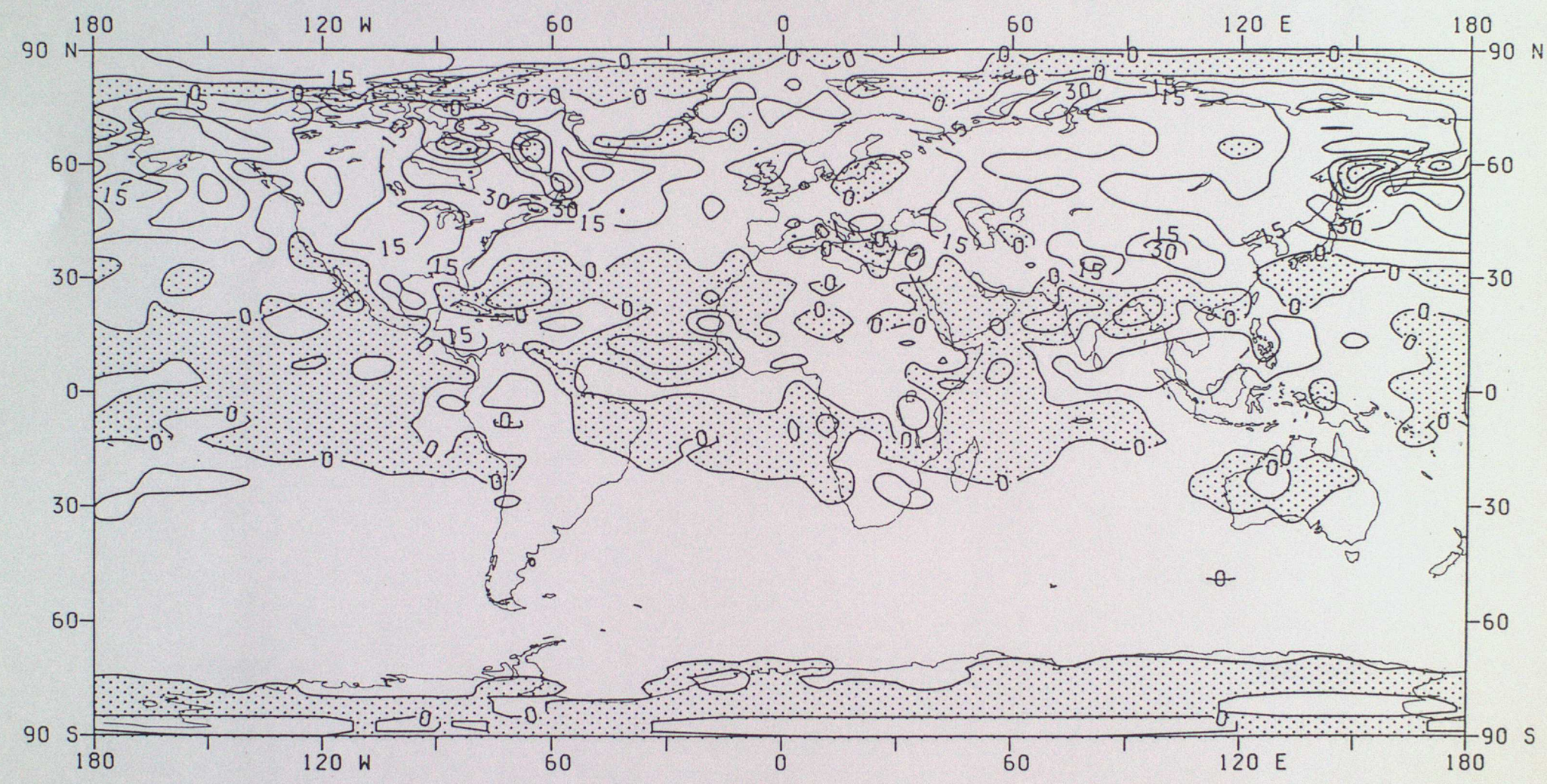

Figure 19(b)

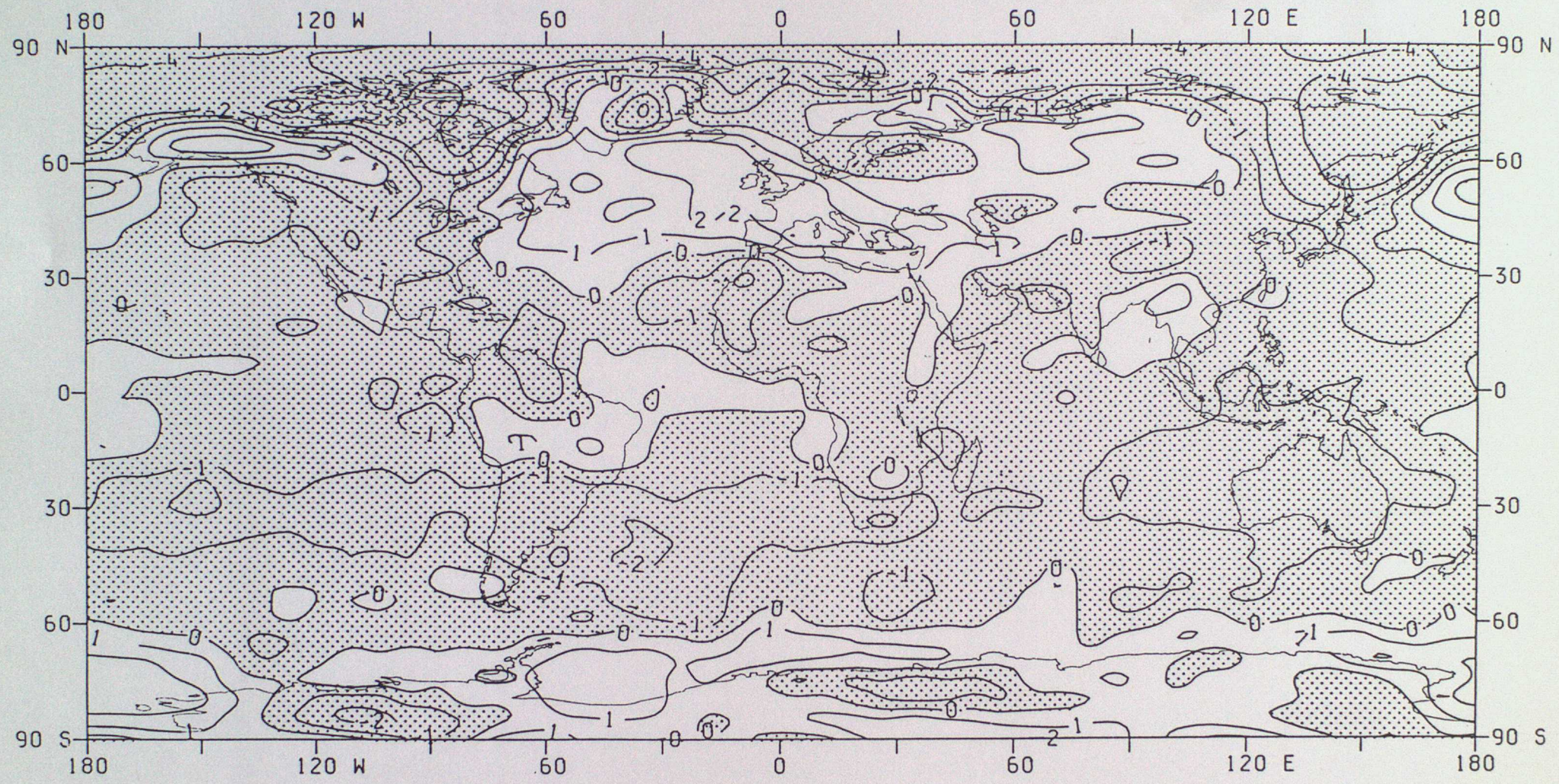

Figure 20(a)

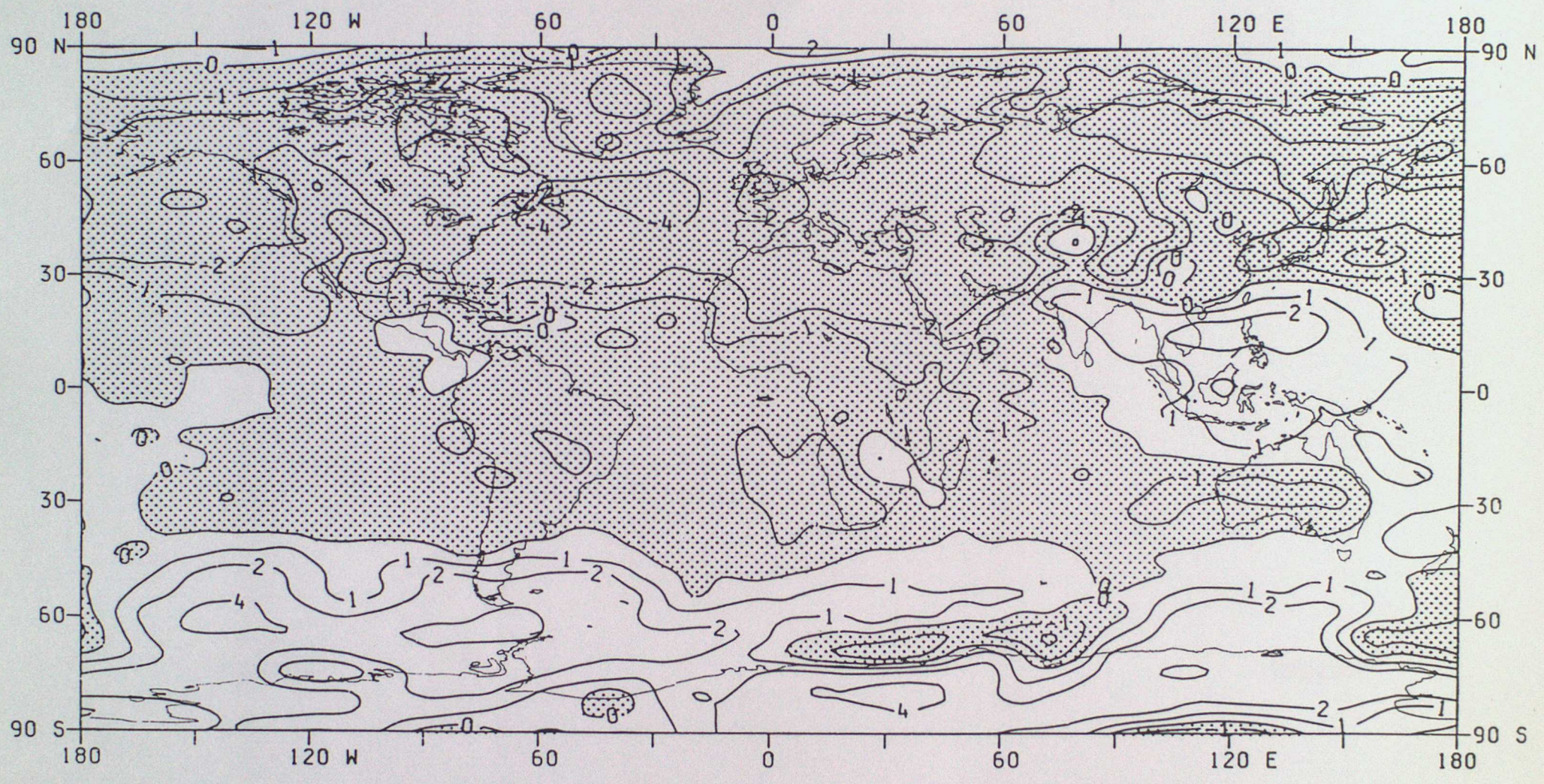

Figure 20(b)

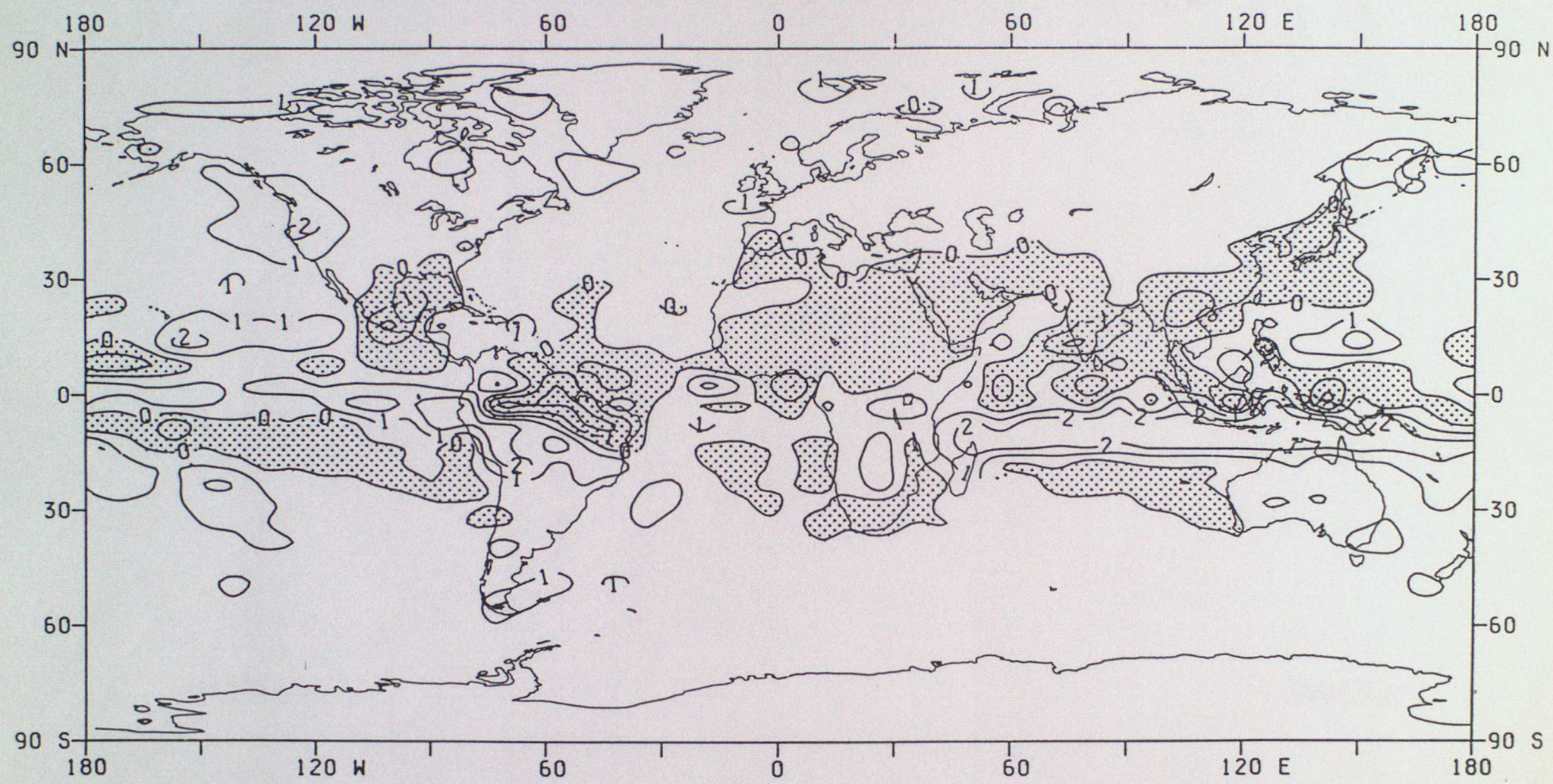

Figure 21(a)

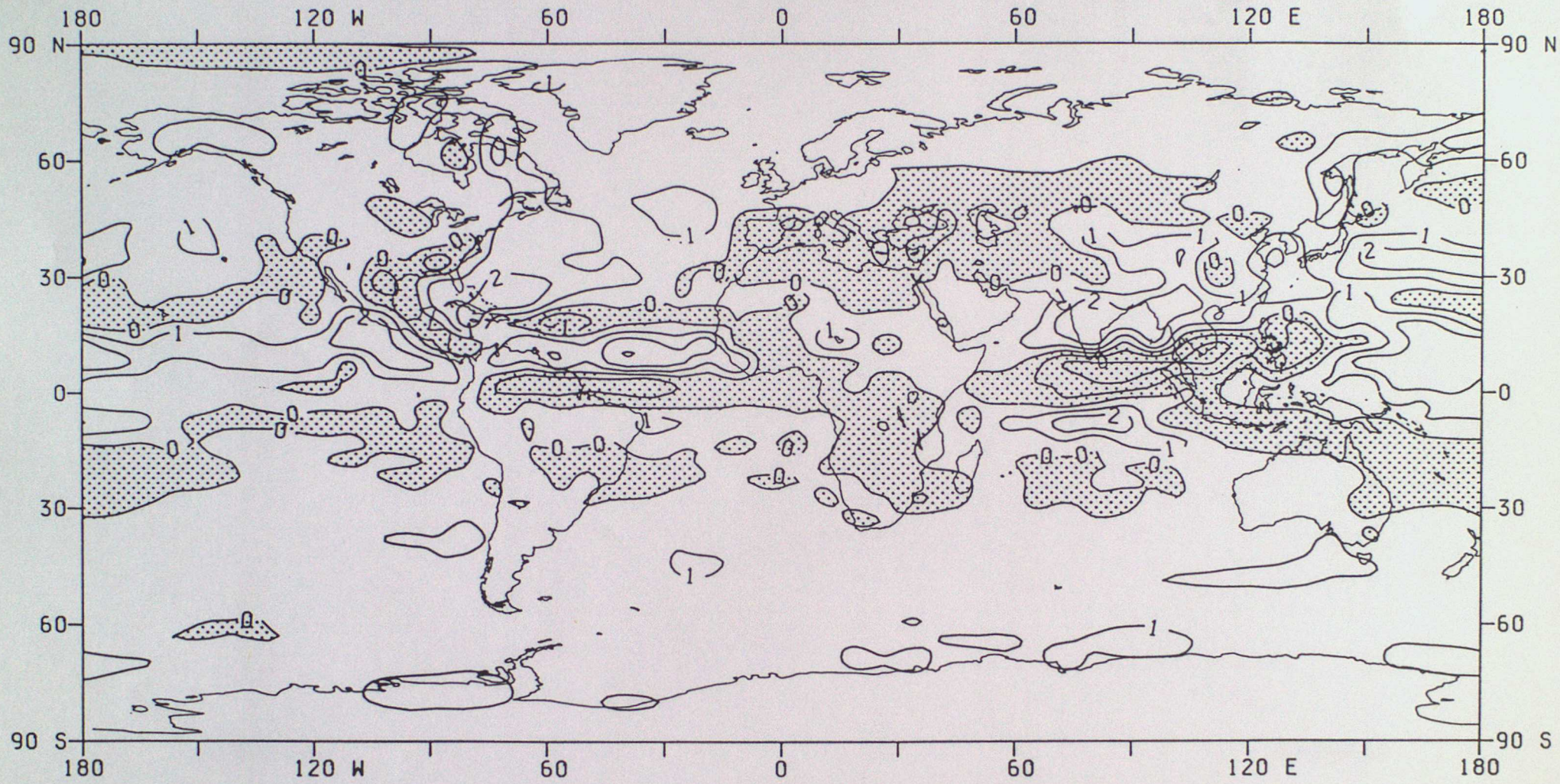

Figure 21(b)

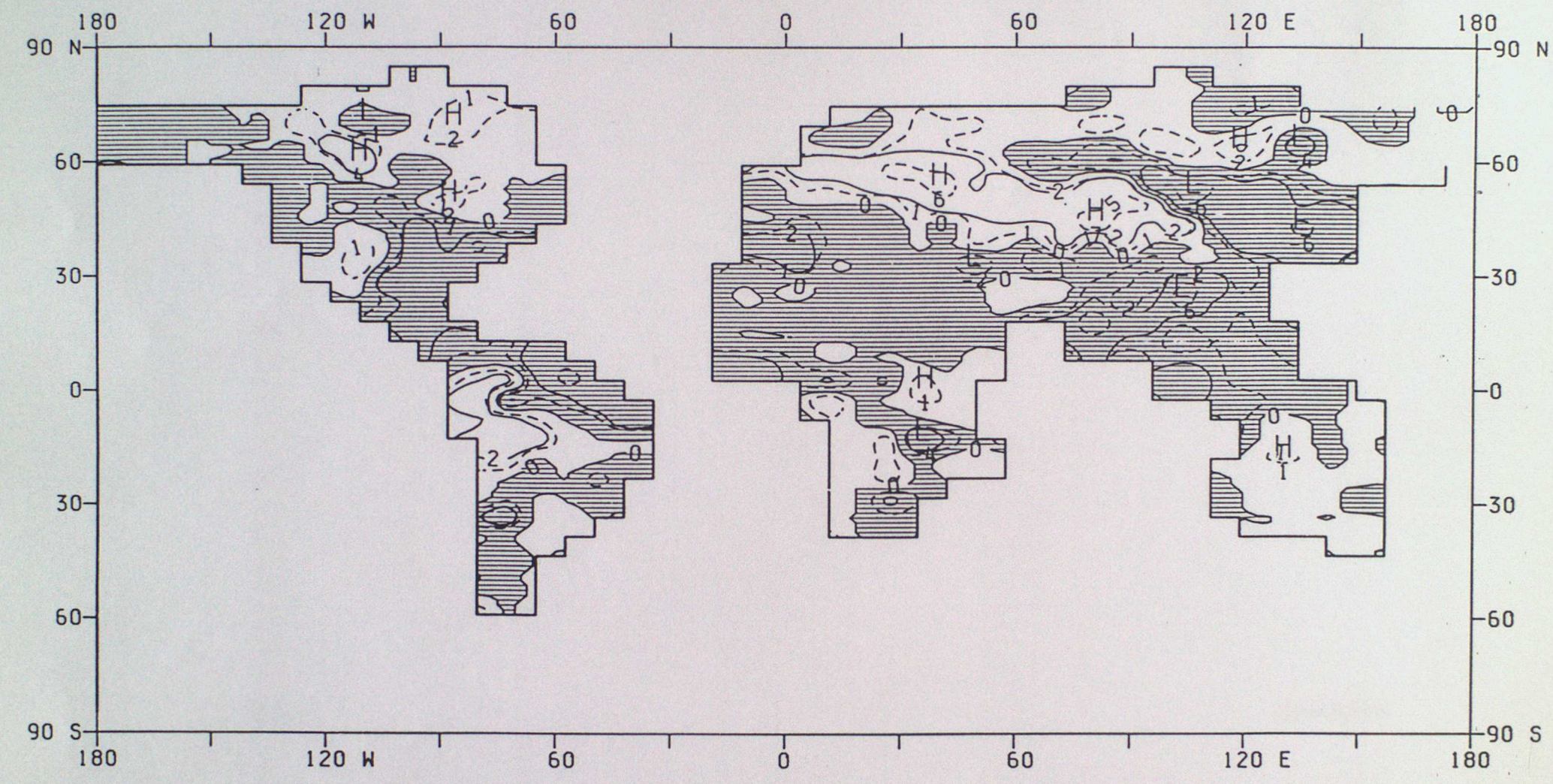

Figure 22(a)

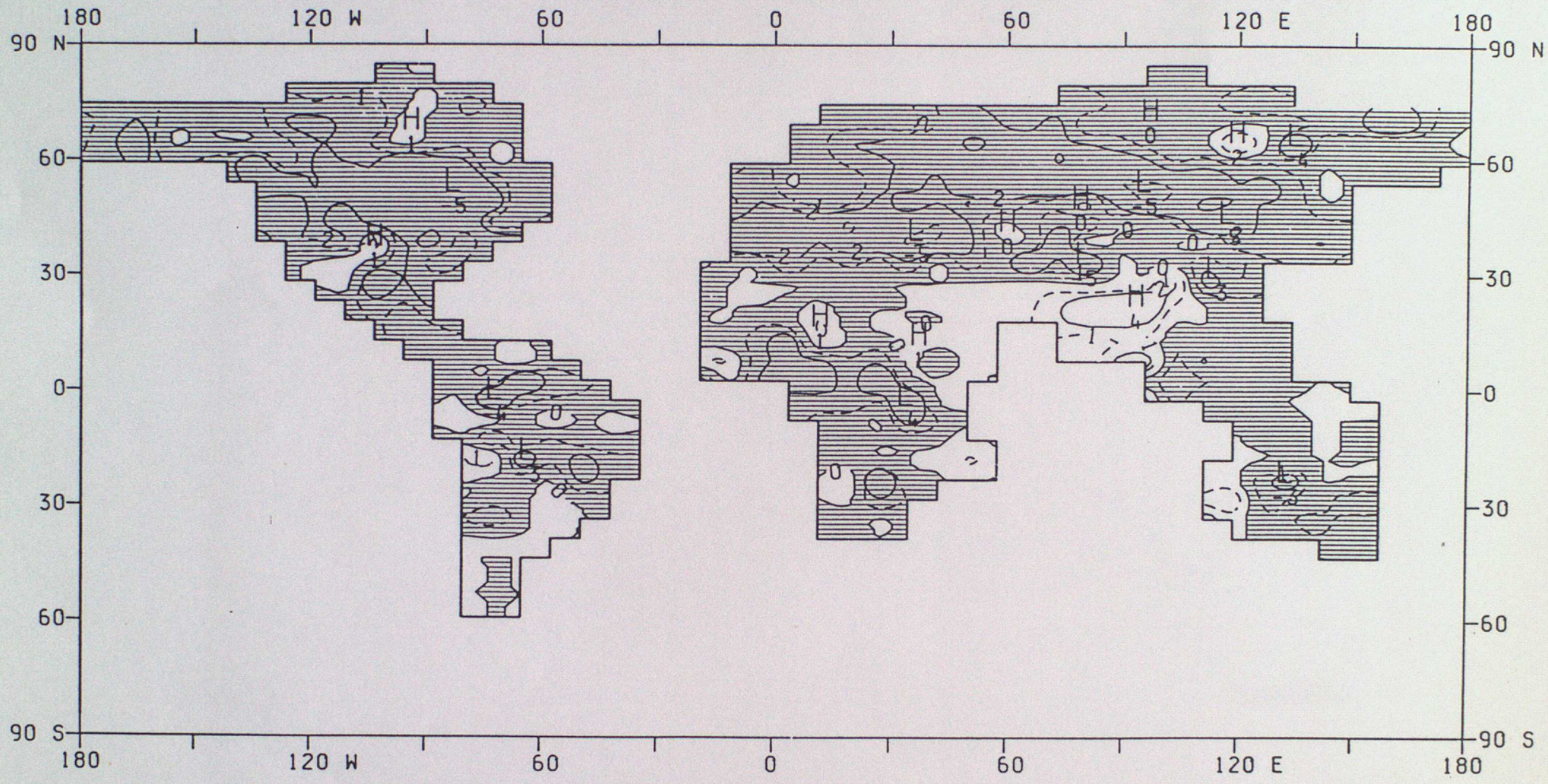

Figure 22(b)

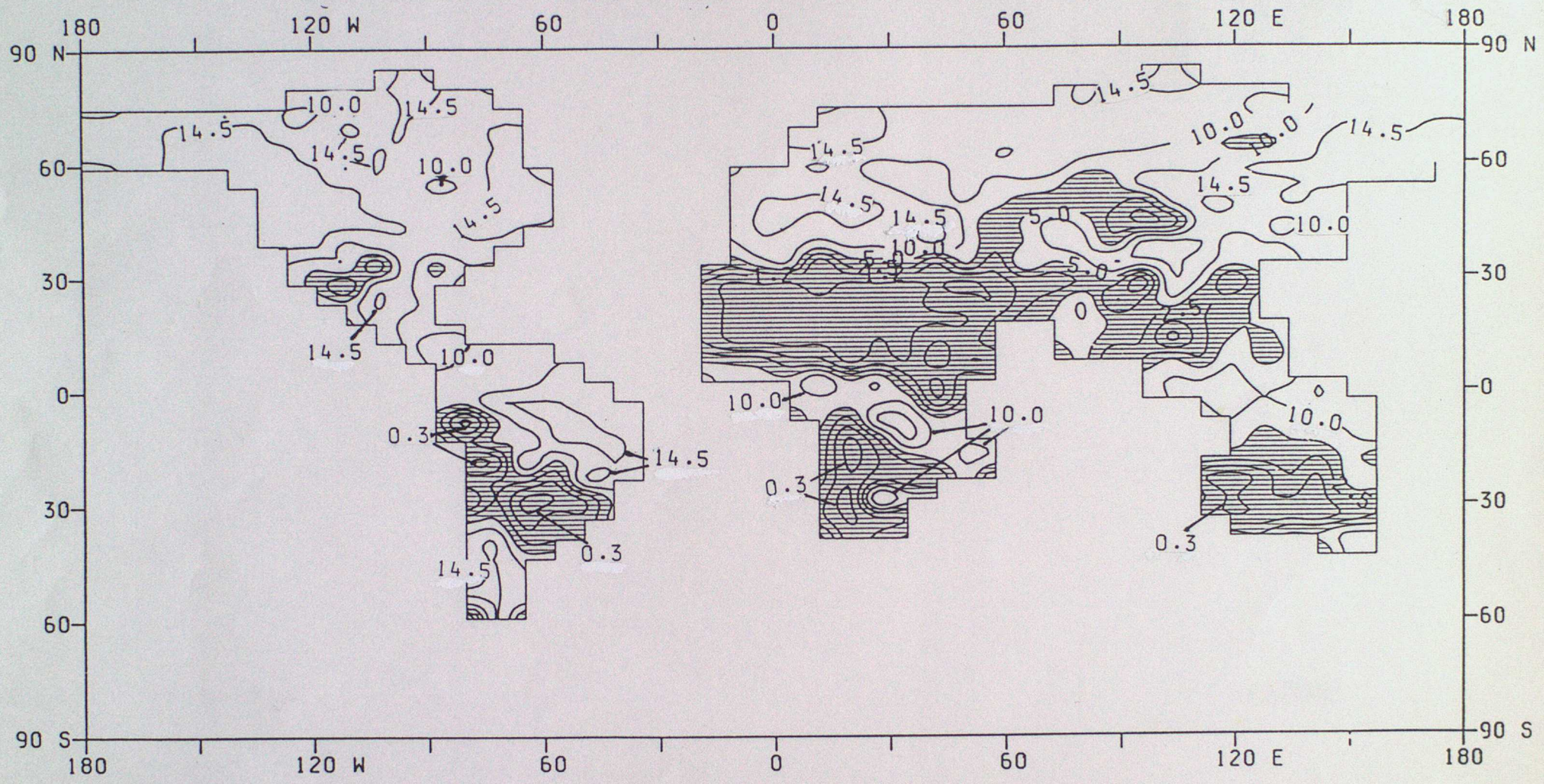

Figure 22(c)

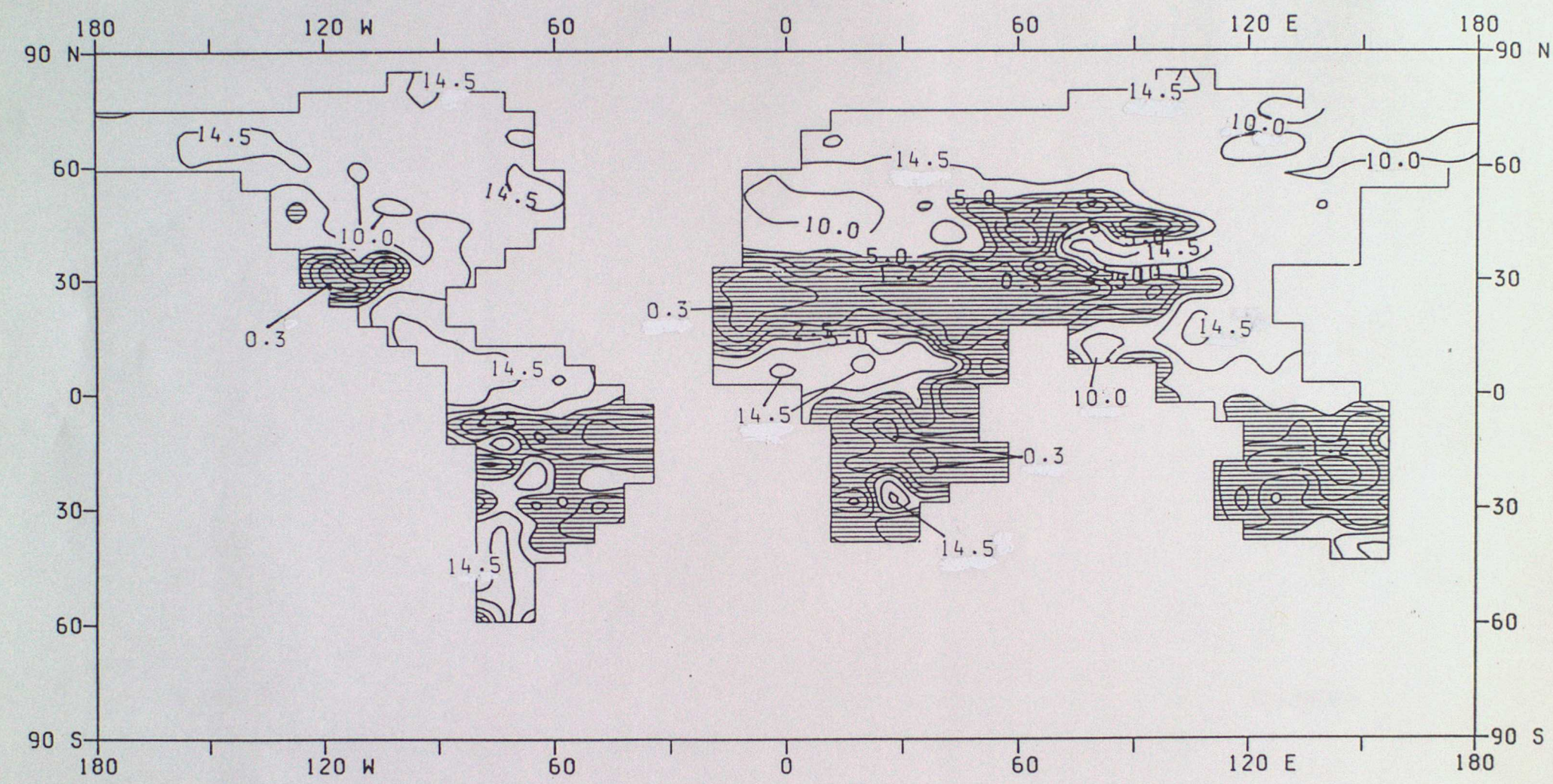

Figure 22(d)

Zonal Mean Differences In Snowmelt (cm)

Averaged Over 15 Years

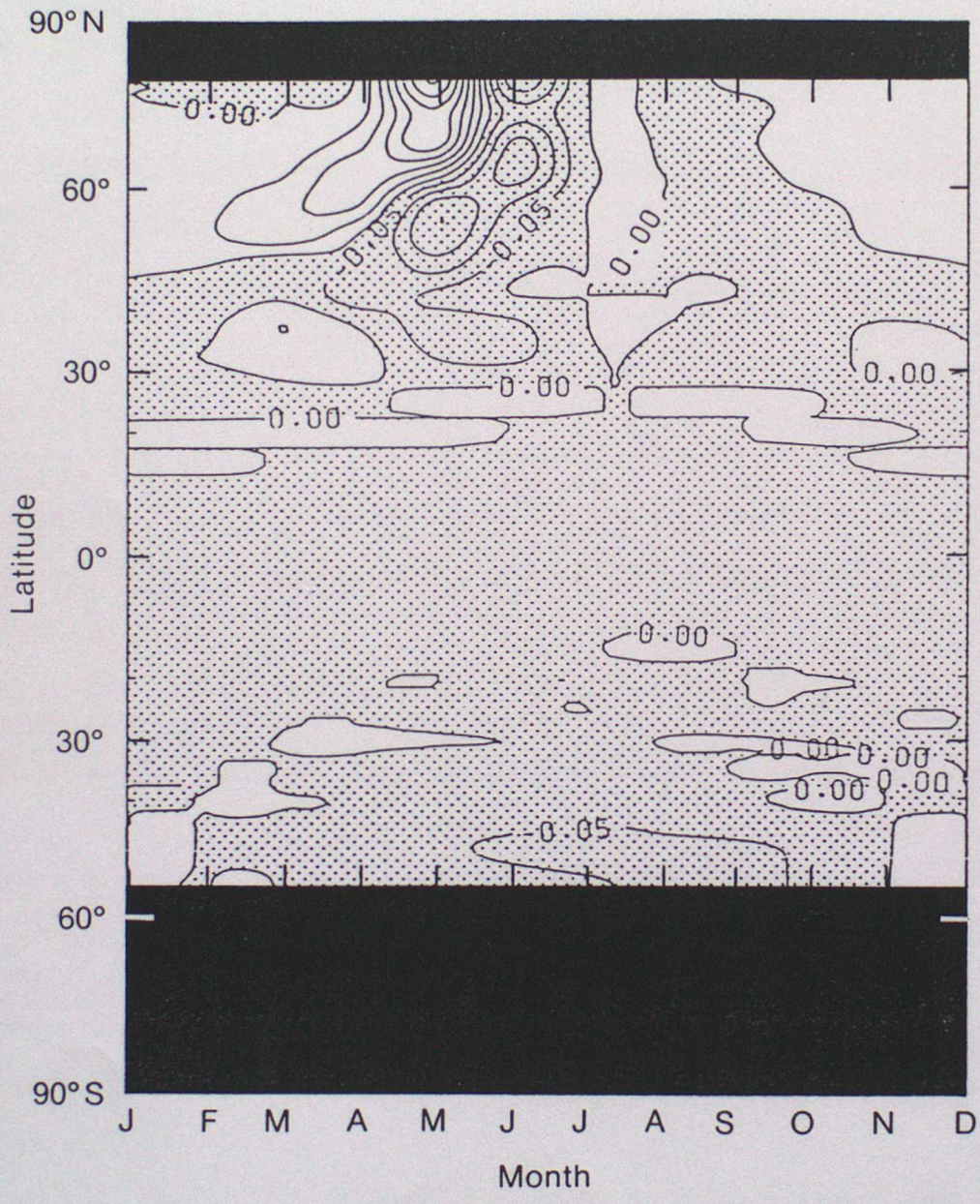

Figure 23(a)

Zonal Mean Differences In Runoff (cm)

Averaged Over 15 Years

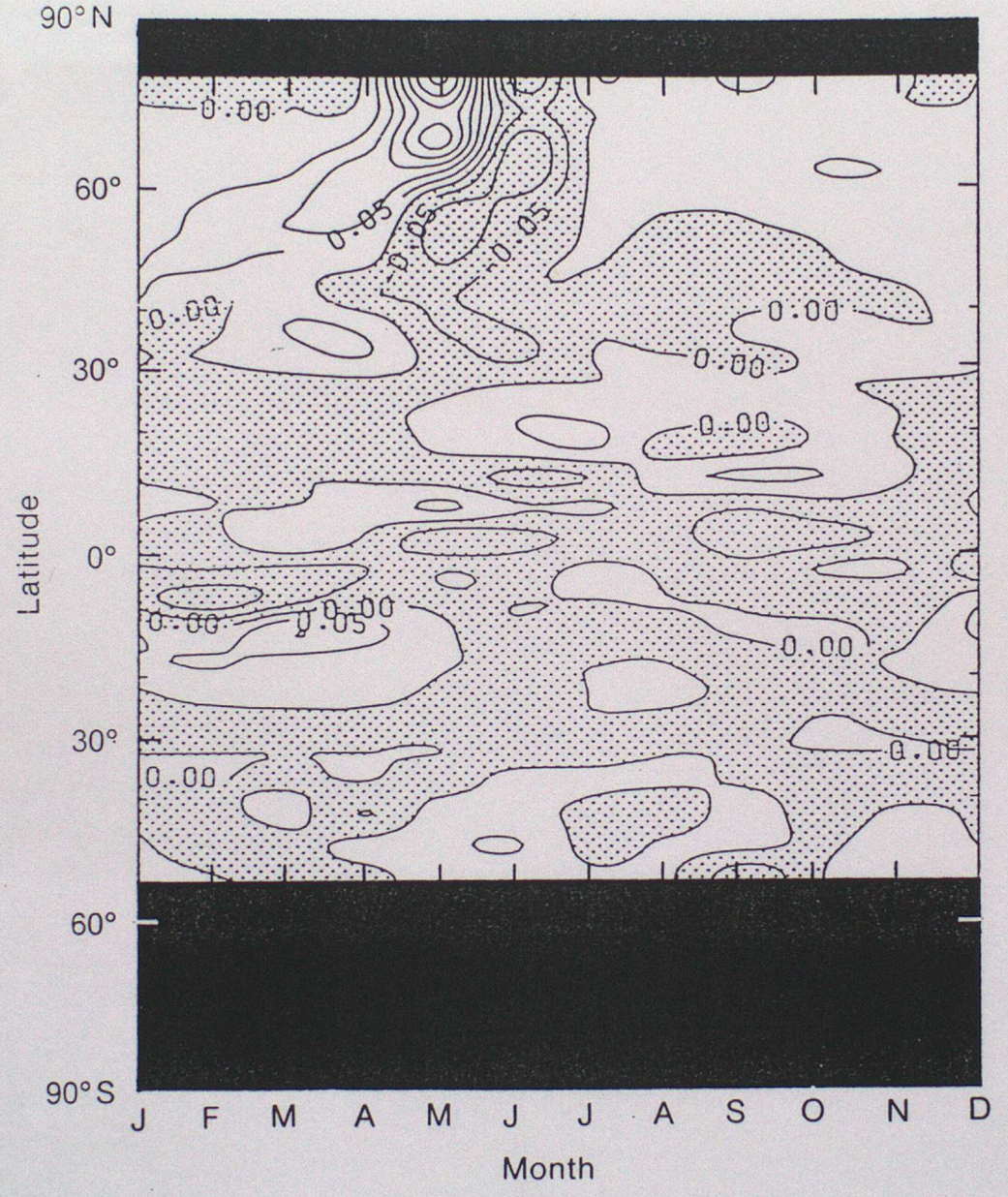

Figure 23(b)

Zonal Mean Differences In Solar Absorption At Surface (wm^{-2})

Averaged Over 15 Years

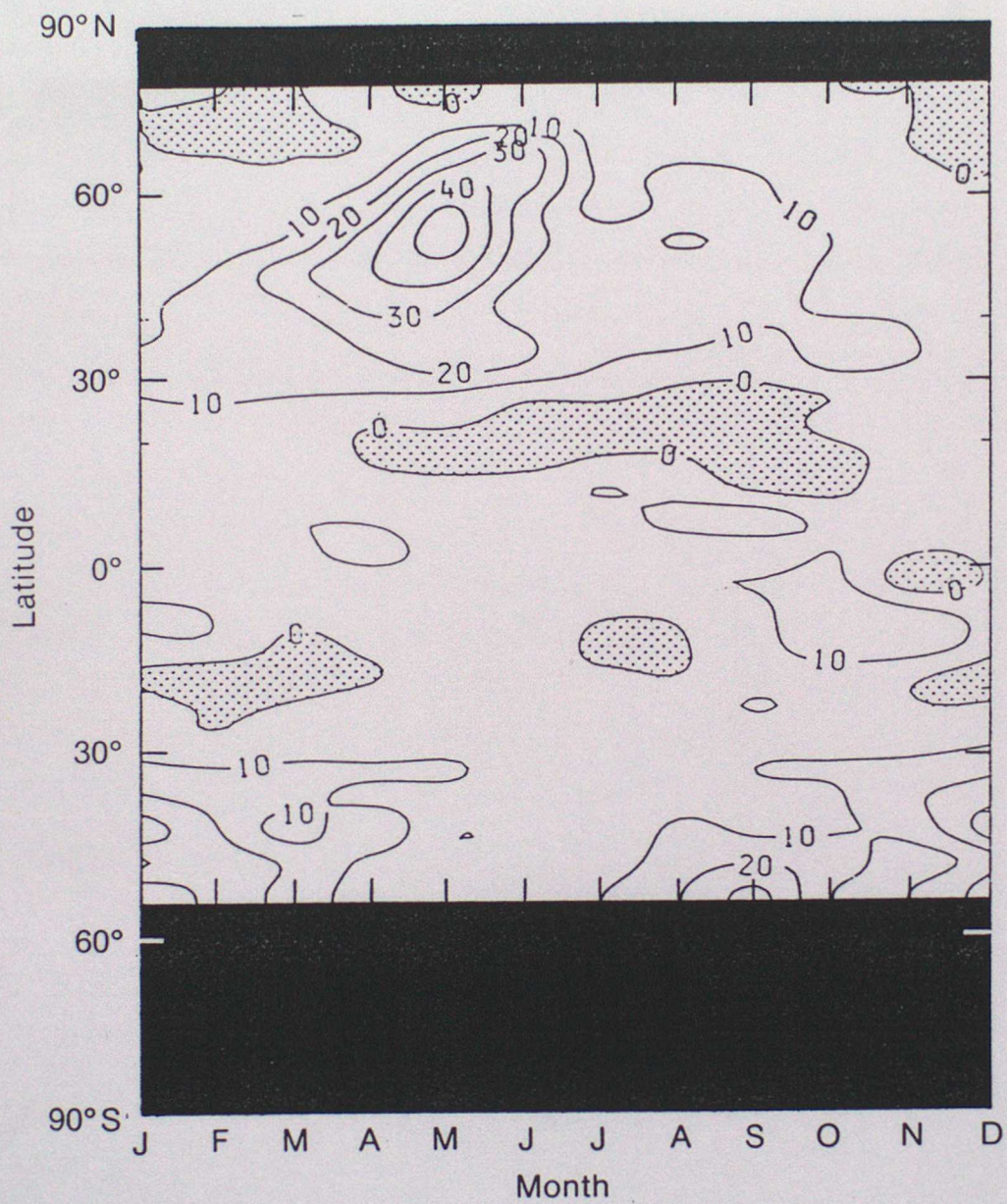

Figure 23(c)

Zonal Mean Differences In Soil Moisture (cm)

Averaged Over 15 Years

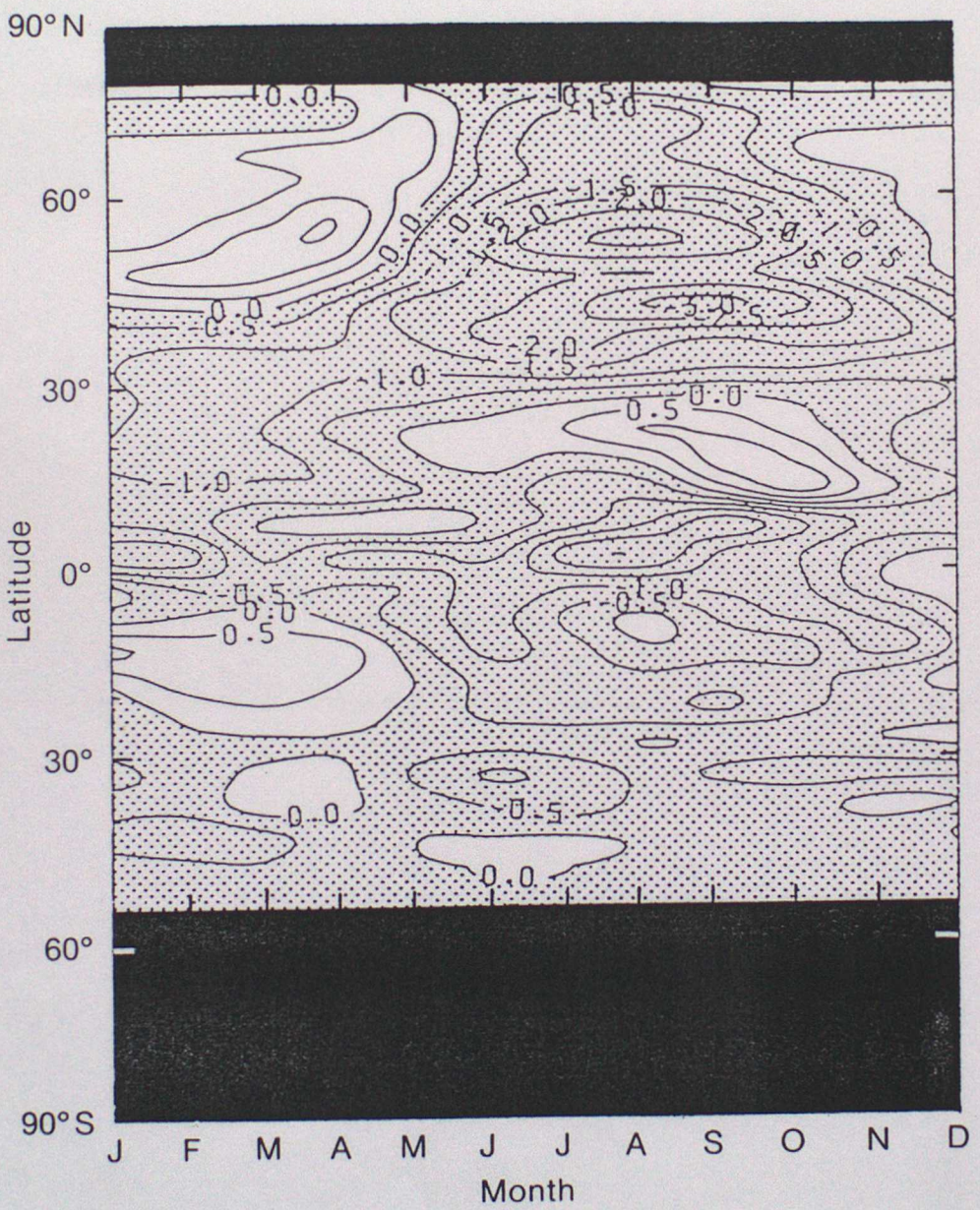

Figure 24

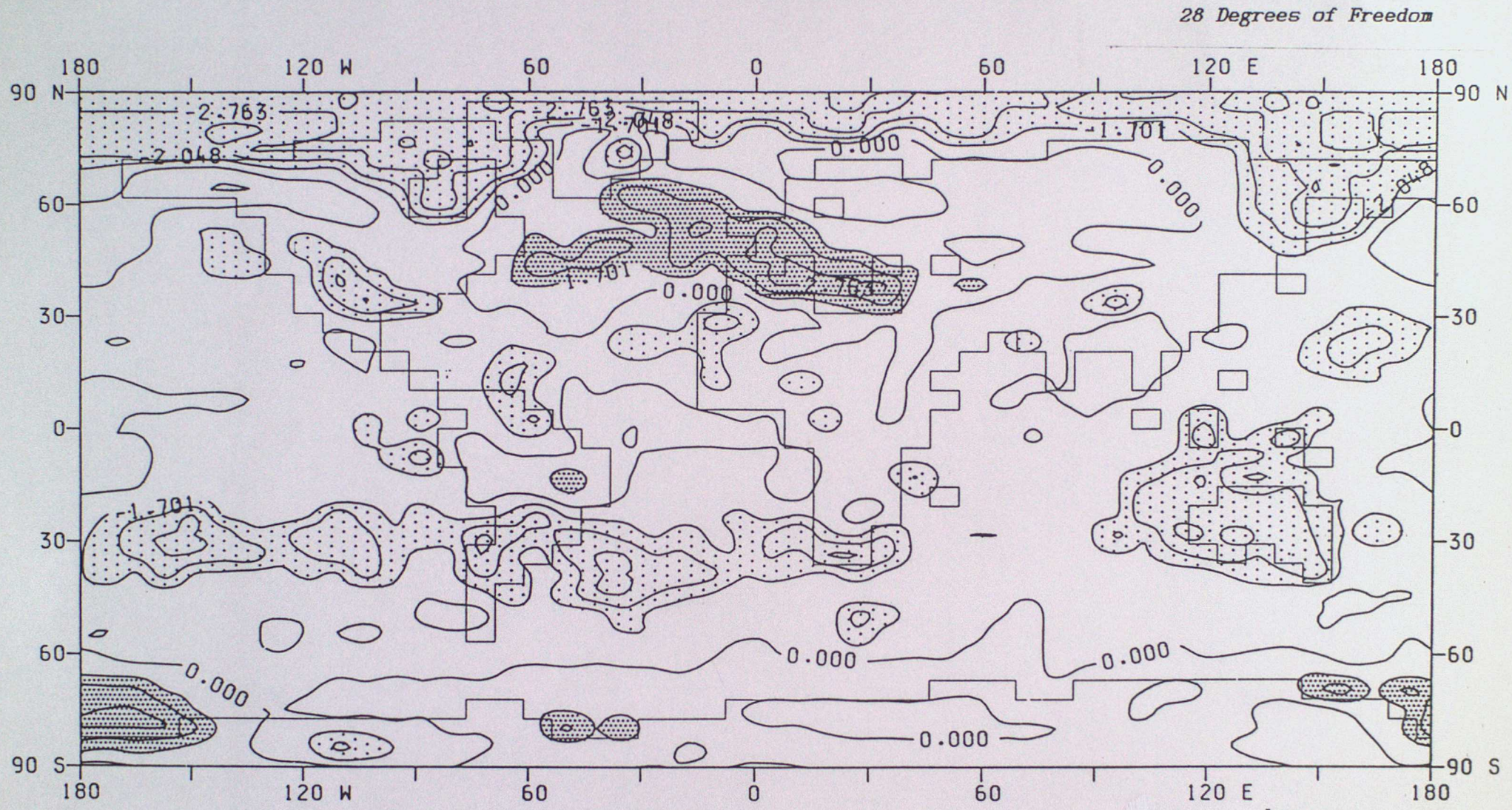
28 Degrees of Freedom
180
120 W
60
0
60
120 E
180
90 N
90 S
60
30
0
30
60
-2.763
-2.048
-1.701
0.000
key
Level
Contour
1%
+ - 2.763
5%
+ - 2.048
10%
+ - 1.701
0.000

Figure 25(a)

28 Degrees of Freedom

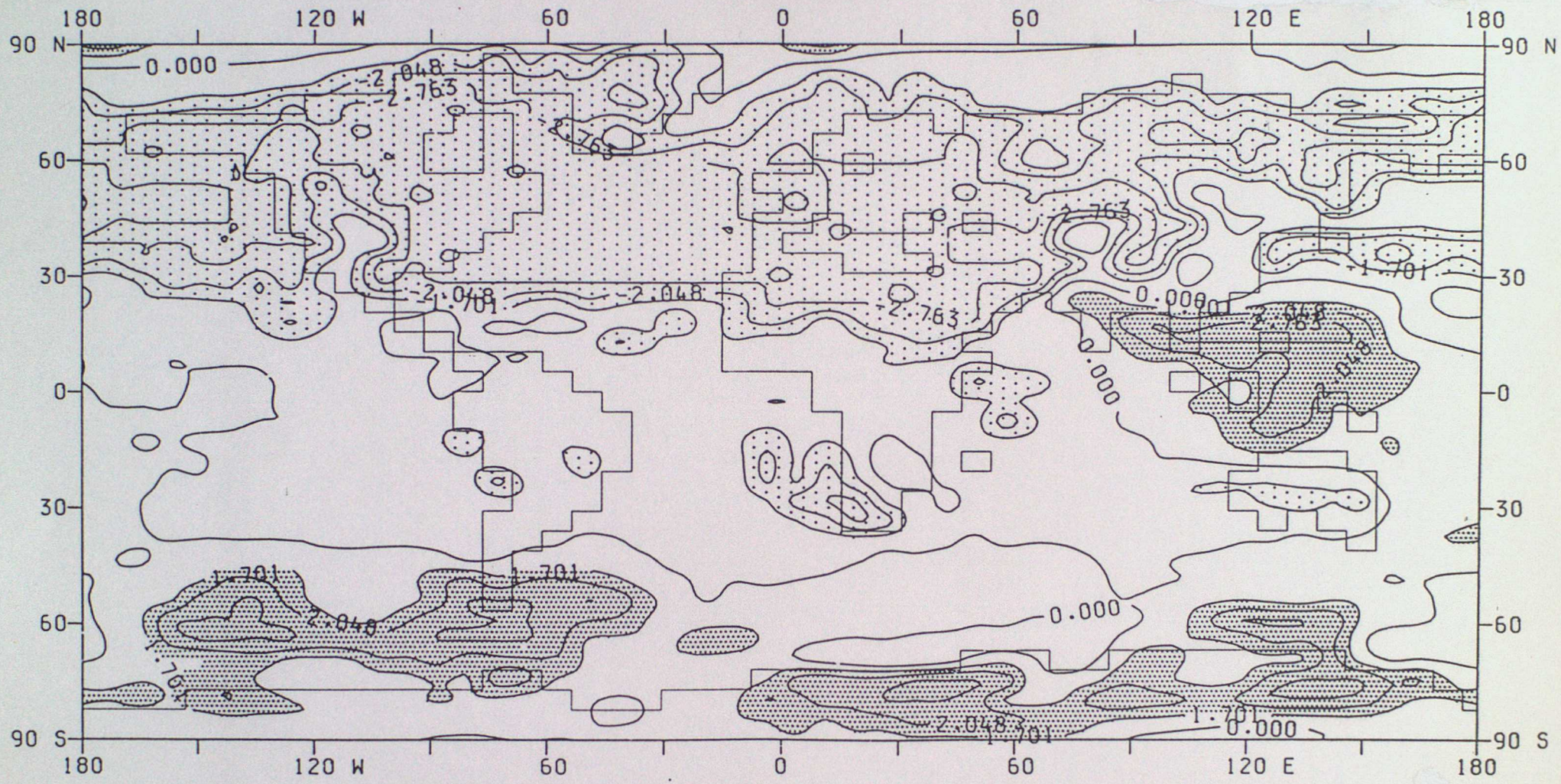

key

Level	Contour
1%	+ - 2.763
5%	+ - 2.048
10%	+ - 1.701
	0.000

Figure 25(b)

28 Degrees of Freedom

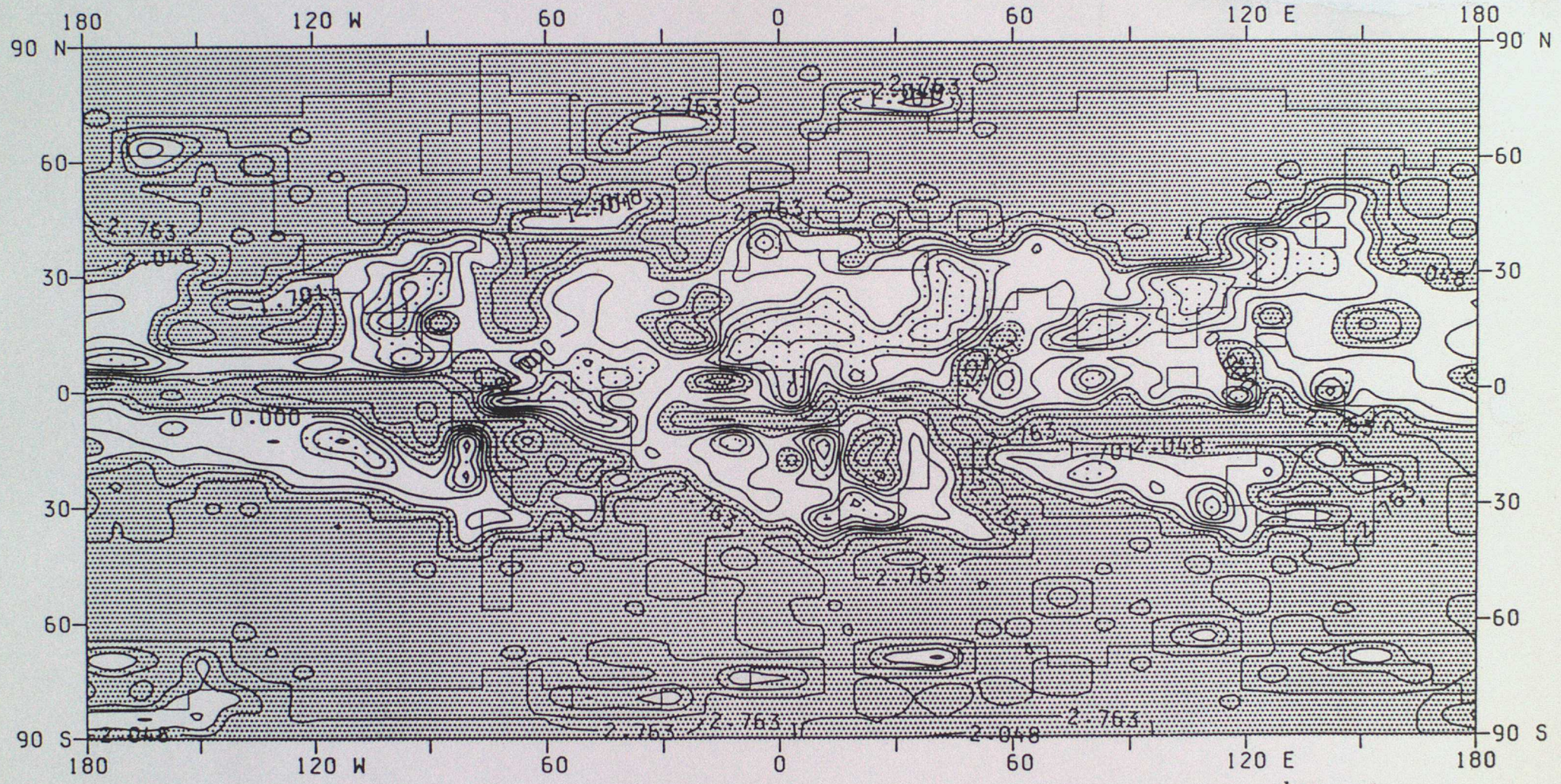

key

Level	*Contour*
1%	*+ - 2.763*
5%	*+ - 2.048*
10%	*+ - 1.701*
	0.000

Figure 26(a)

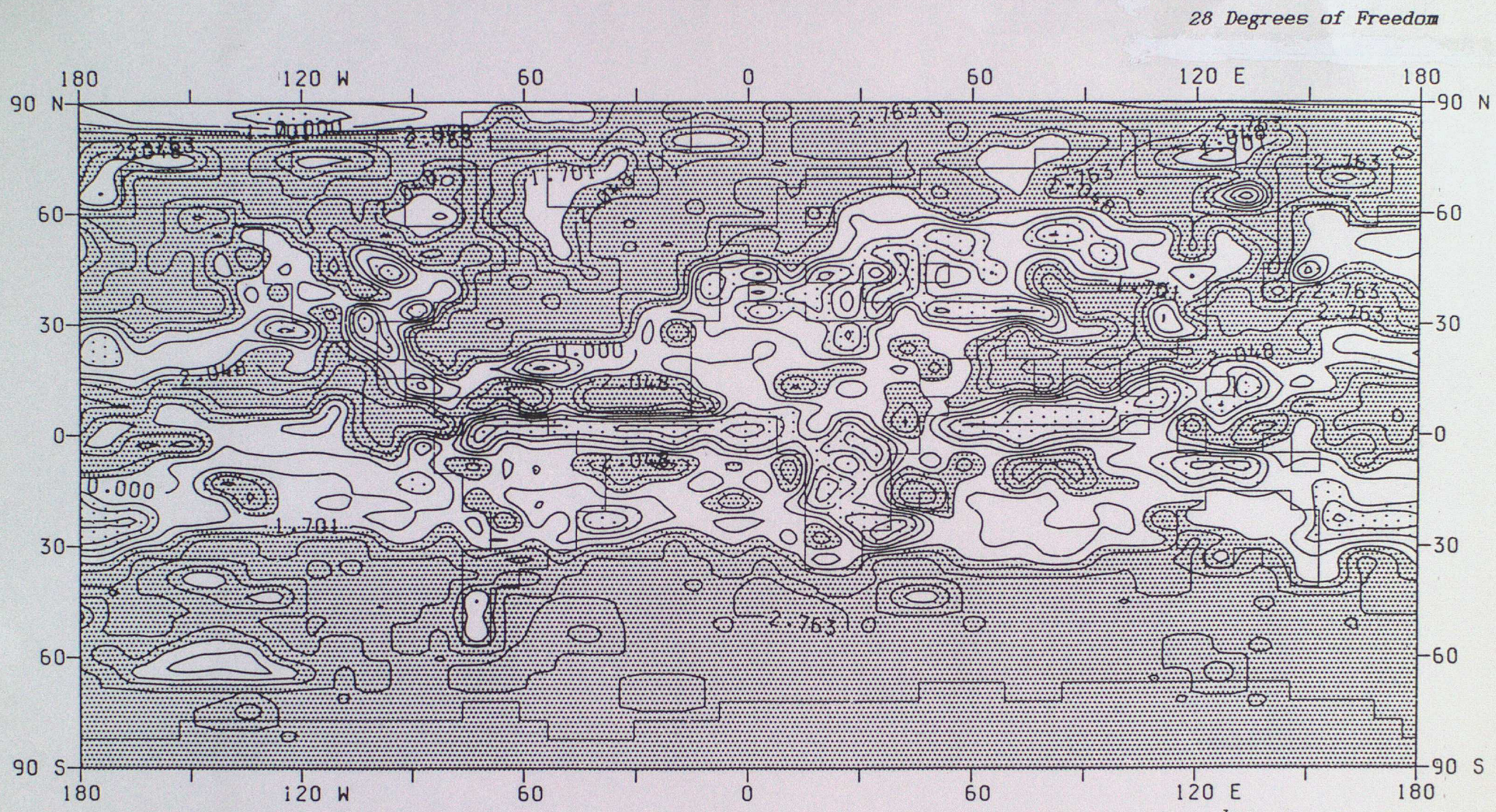
28 Degrees of Freedom
180
120 W
60
0
60
120 E
180
90 N
60
30
0
30
60
90 S
2.763
2.048
1.701
0.000
key
Level
Contour
1%
+ - 2.763
5%
+ - 2.048
10%
+ - 1.701
0.000

Figure 26(b)

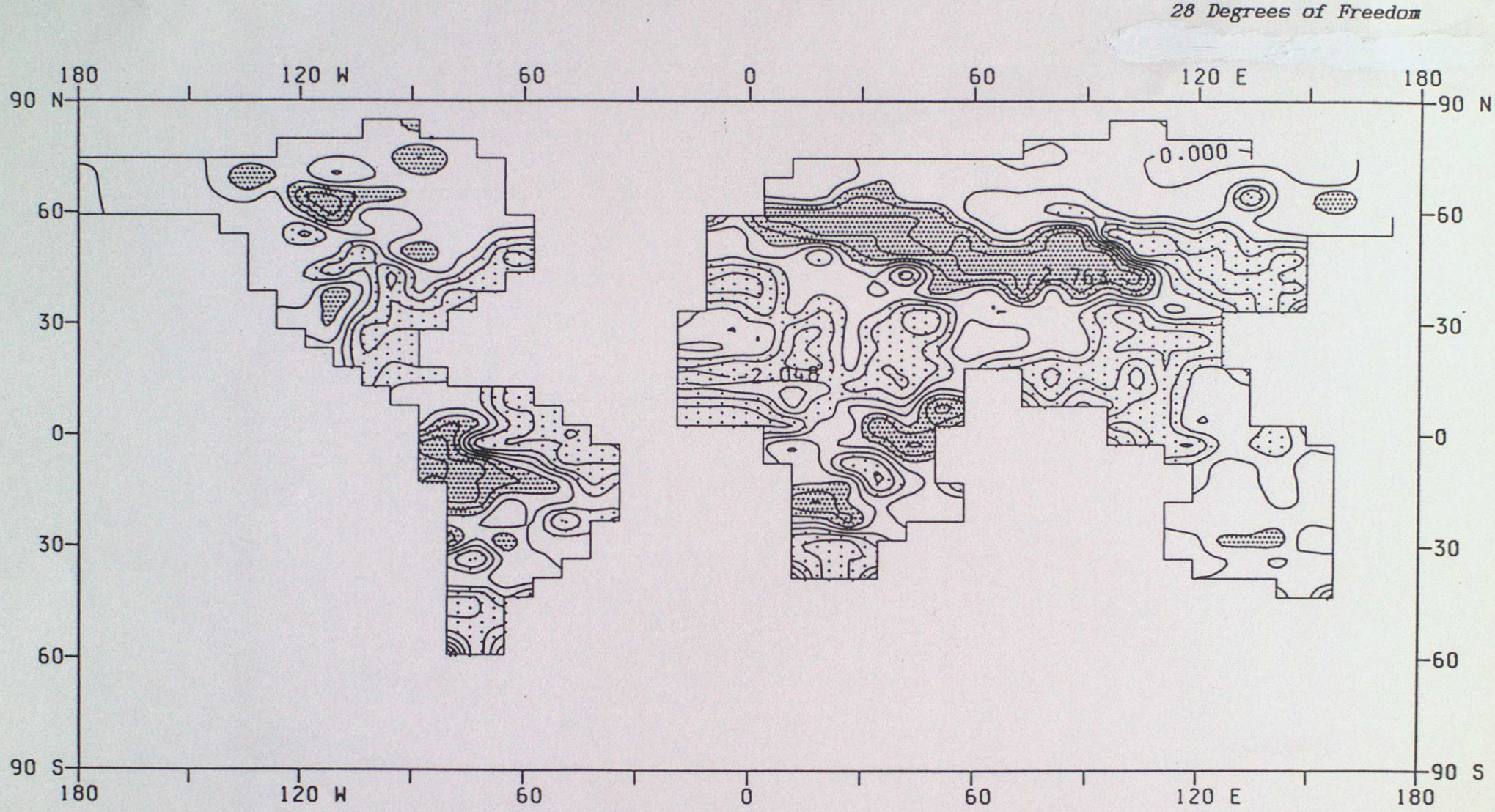
28 Degrees of Freedom
180
120 W
60
0
60
120 E
180
90 N
60
30
0
30
60
90 S
0.000
-2.048
key
Level
Contour
1%
+ - 2.763
5%
+ - 2.048
10%
+ - 1.701
0.000

Figure 27(a)

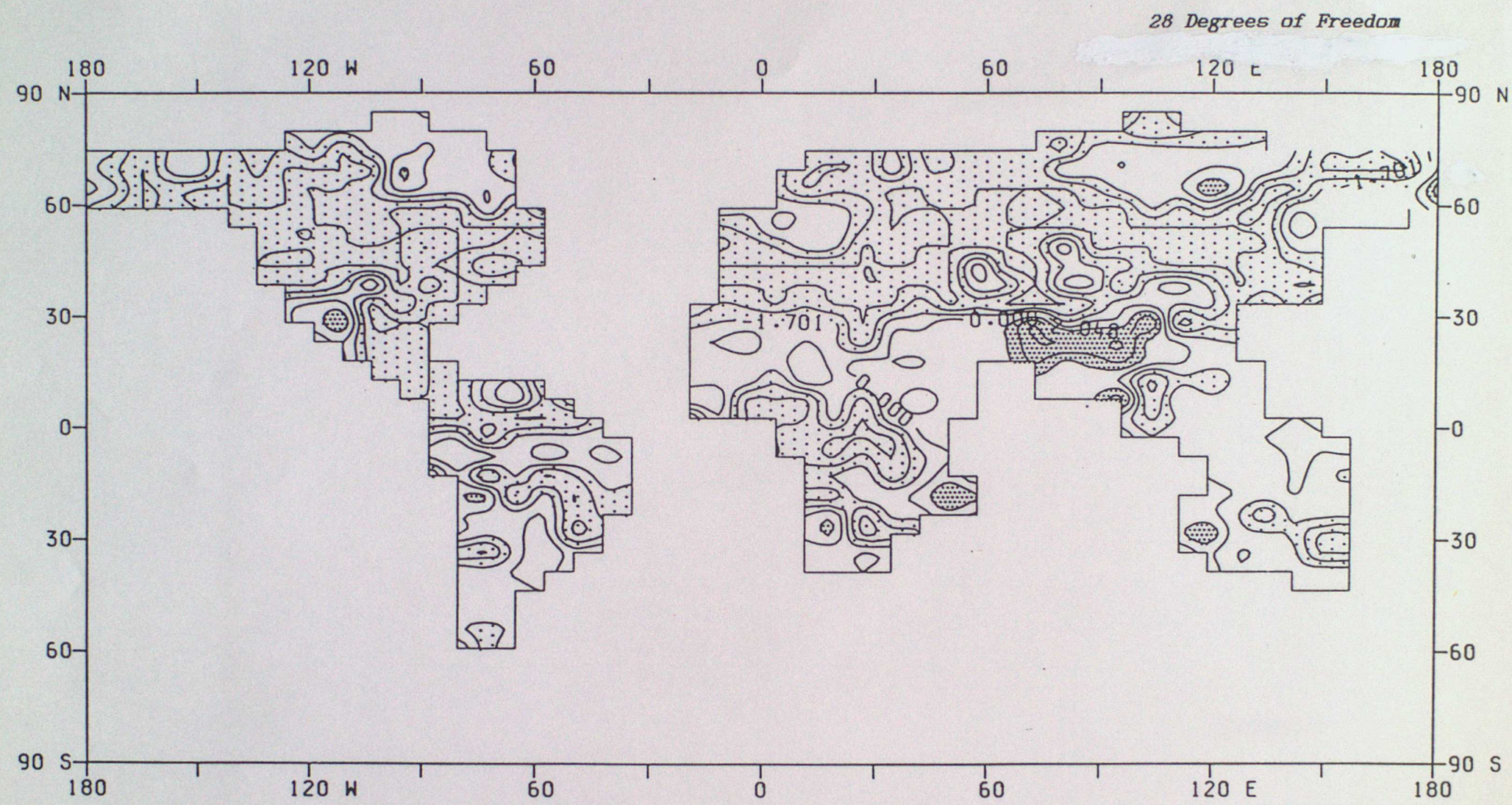

Figure 27(b)

key

Level	Contour
1%	+ - 2.763
5%	+ - 2.048
10%	+ - 1.701
	0.000

DYNAMICAL CLIMATOLOGY TECHNICAL NOTES

DCTN 1	June 1984	A scheme for incorporating the thermodynamic sea-ice model into a coupled ocean-atmosphere model. C Gordon and M Bottomley
DCTN 2	Sept 1984	The parametrization of the upper ocean mixed layer in coupled ocean/atmosphere models. C Gordon and M Bottomley
DCTN 3	Sept 1984	The response of a simple thermodynamic sea-ice model to GCM forcing appropriate for perennial sea-ice. M Bottomley
DCTN 4	Sept 1984	Potential vorticity in the stratosphere derived using data from satellites. S A Clough, N S Grahame and A O'Neill
DCTN 5	Sept 1984	Simulation of the seasonal cycle of SST using globally specified climatological data to force simple ocean models. N S Grahame
DCTN 6	Sept 1984	Development of an improved GCM radiation scheme. A Slingo and R C Wilderspin
DCTN 7	Sept 1984	On the specification of surface fluxes in coupled atmosphere/ocean general circulation models. J F B Mitchell, C A Wilson and C M Price
DCTN 8	Sept 1984	A survey of possible repercussions of the Soviet river reversal programme on Arctic sea-ice. H Cattle
DCTN 9	Oct 1984	A study of a strong stratospheric warming during January 1982 T D A Fairlie
DCTN 10	Nov 1984	An intercomparison of the Met O 11 N45 model and the Met O 20 11-level model on the Cyber 205 J F Dyson
DCTN 11	Nov 1984	Simulation of observed time series of temperature and precipitation over eastern England. D N Reed
DCTN 12	Nov 1984	Forecasts and analyses of the onset of the Southwest monsoon. R Kershaw
DCTN 13	Nov 1984	On modelling the effects of CO_2 on climate. J F B Mitchell
DCTN 14	Dec 1984	Development of a revised longwave radiation scheme for an atmospheric general circulation model. A Slingo and R C Wilderspin
DCTN 15	Jan 1985	Rossby wavetrains in the stratosphere forced by localised disturbances in the troposphere. C J Marks (Oxford), A O'Neill and V D Pope

DYNAMICAL CLIMATOLOGY TECHNICAL NOTES

DCTN 16	Jan 1985	Observing system experiments using the Meteorological Office's 15-level model. R A Bromley
DCTN 17	Feb 1985	Atmospheric general circulation simulation of the climate of the Mediterranean region. H Cattle
DCTN 18	Feb 1985	Diurnal variation and cloud in a general circulation model. C A Wilson and J F B Mitchell
DCTN 19	Feb 1985	The sensitivity of the Saharan region in a general circulation model. W M Cunnington and P R Rowntree
DCTN 20	Mar 1985	The impact of aircraft observations on analyses and forecasts from the operational 15-level model. B R Barwell
DCTN 21	Mar 1985	Non-linear effects on heat-induced circulation of the tropical atmosphere. A E Gill and P J Phlips
DCTN 22	Apr 1985	Simulation of cloudiness with the U.K. Meteorological Office 11-layer AGCM. A Slingo and R C Wilderspin
DCTN 23	Apr 1985	An integrated approach to the representation of cloud processes. R N B Smith
DCTN 24	May 1985	Nuclear Winter: Calculations of the shortwave radiative effects of soot aerosols. A Slingo and P Goldsmith
DCTN 25	Jul 1985	Sea ice and the Antarctic winter circulation: a numerical experiment. J F B Mitchell and T S Hills
DCTN 26	Jul 1985	A Budyko-Sellers model for study of ocean-atmosphere interaction. W J Ingram
DCTN 27	Aug 1985	The effect of a shoaling thermocline on equatorially-trapped Kelvin waves. A E Gill and B A King
DCTN 28	Sept 1985	CO_2 climate sensitivity and model dependence of results. J F B Mitchell, C A Wilson and W M Cunnington
DCTN 29	Sept 1985	Handbook of the Meteorological Office 11-layer atmospheric general circulation model. Volume 1 : Model Description Edited by A Slingo
DCTN 30	Sept 1985	Impact of land surface variations on African rainfall in general circulation models. P R Rowntree, M F Wilson and A B Sangster

DYNAMICAL CLIMATOLOGY TECHNICAL NOTES

DCTN 31 Nov 1985 The annual cycle of sea level in the eastern tropical Pacific.
G R Bigg and A E Gill

DCTN 32 Nov 1985 An analytic model of the heat-induced tropical circulation in the presence of a mean wind.
P J Phlips and A E Gill

DCTN 33 Nov 1985 The effect of resolution and diffusion on the simulated climate.
J F Dyson

DCTN 34 Jan 1986 Rossby adjustment over a step.
M K Davey, A E Gill, E R Johnson and P F Linden

DCTN 35 Jan 1986 Issues concerning the evaluation of effective surface roughness of heterogeneous terrain.
D J Carson

DCTN 36 Mar 1986 Climate sensitivity and past climates : evidence from numerical studies
J F B Mitchell

DCTN 37 Mar 1986 Parametrizations of land-surface processes in Meteorological Office numerical weather prediction and climate models
D J Carson

DCTN 38 Apr 1986 Modelling of land-surface processes and their influence on European Climate
D A Warrilow, A B Sangster and A Slingo

DCTN 39 Apr 1986 Simulation of climatic change due to increased CO_2
J F B Mitchell

DCTN 40 May 1986 On the interpretation of the Eliassen-Palm flux divergence.
Part I : Theory
D G Andrews

DCTN 41 June 1986 Experiments on tropical circulation with a simple moist model.
M K Davey and A E Gill

DCTN 42 Jun 1986 Parameter regimes for studying isolated eddies.
P D Killworth and M K Davey

DCTN 43 Jun 1986 A comparison of the impact of an envelope orography and of a parametrization of orographic gravity-wave drag on model simulations.
A Slingo and D W Pearson

DCTN 44 Jul 1986 The effect of a sea-surface temperature anomaly on a prediction of the onset of the south-west monsoon over India.
R Kershaw

DCTN 45 Jul 1986 An introduction to the parametrization of land-surface processes.
D J Carson

DYNAMICAL CLIMATOLOGY TECHNICAL NOTES

DCTN 46 Sept 1986 Lateral boundaries and the heat-induced flow in the tropical atmosphere.
P J Phlips and A E Gill

DCTN 47 Nov 1986 Simulation of the diurnal cycle of outgoing longwave radiation with an atmospheric GCM.
A Slingo, R C Wilderspin and S J Brentnall

DCTN 48 Feb 1987 A 2 x CO_2 climate sensitivity experiment with a global climate model including a simple ocean
C A Wilson and J F B Mitchell

DCTN 49 Feb 1987 Sensitivity of the Met O 20 11-layer model to increased land surface roughness length
C C Heasman